Marquette University
e-Publications@Marquette

Master's Theses (2009 -) | Dissertations, Theses, and Professional Projects

Synthesis and Characterization of Low Valent Metalloporphyrins

Nagabhushanam Kundakarla
Marquette University

Recommended Citation
Kundakarla, Nagabhushanam, "Synthesis and Characterization of Low Valent Metalloporphyrins" (2015). *Master's Theses (2009 -)*. Paper 316.
http://epublications.marquette.edu/theses_open/316

SYNTHESIS AND CHARACTERIZATION OF LOW VALENT METALLOPORPHYRINS

by

Naga Kundakarla, M.Sc.

A Thesis submitted to the Faculty of the Graduate School,
Marquette University,
in Partial Fulfillment of the Requirements for
the Degree of Master of Science

Milwaukee, Wisconsin

May 2015

ABSTRACT
SYNTHESIS AND CHARACTERIZATION OF LOW VALENT METALLOPORPHYRINS

Naga Kundakarla, M.Sc.

Marquette University, 2015

Metalloporphyrins and metalloporphinones have been seen in a number of enzymes and involved in nitrogen metabolism, photosynthesis, and methanogenesis. The reduction of metalloporphyrins and metalloporphinones are achievable, but the site of reduction in either, the metal center or porphyrin core is still debatable. This prompted us to investigate the position of reduction in order to generate low valent metalloporphyrins and porphinones. The reduced porphyrins were characterized by spectroscopic and X-ray crystallographic methods.

Previous work in our laboratory has generated low valent metalloporphyrins and porphinones by electrochemical reduction. In this work cobalt, manganese, and iron low valent metalloporphyrins were generated via chemical reduction and results were characterized by UV-visible, infrared spectroscopy, and X-ray crystallographic techniques.

ACKNOWLEDGMENTS

Naga Kundakarla, M.Sc.

I would like to gratefully and sincerely thank to my research advisor, Dr. Michael D. Ryan for his guidance, understanding and patience throughout my stay at Marquette University and for his suggestions and corrections of this thesis.

I wish to extend my gratitude the members of my research committee, Dr. James R. Kincaid and Dr. Adam Fiedler for their time in reading my thesis and kindly suggestions. I also would like to thank Dr. Sergey Lindeman for obtaining X-ray crystal data.

I extended my sincere thanks to the faculty and the staff of the Marquette University Chemistry Department for all their help and support during stay here. The financial backing from Marquette University is also gratefully recognize.

Finally, I owe a word of thanks to my parents, friends and colleagues for their help and understanding.

TABLE OF CONTENTS

LIST OF TABLES

LIST OF FIGURES

Chapter One: Introduction

1-1. Porphyrins and their derivatives

The word "porphyrin" has its origins in the classical world of ancient Greece. Originally, the word porphura was used to describe the color of purple, which an important feature of porphyrins. The important functions of porphyrins in the nature is to form metal complexes, which can bind dioxygen, or be involved in electron transfer, catalysis, and photosynthesis[1,2].

Background:

The porphyrin molecule is a highly-conjugated macrocycle which contains 22 π-electrons, but only 18 of them are delocalized according to the Huckel rule of aromaticity (4n+2 delocalized π-electrons, where n = 4). As a result, porphyrins have a planar geometry[3-4]. Figure 1-1 shows the structure of the porphyrin macrocycle whose positions are labeled according to the IUPAC numbering systems[5]. The porphyrin macrocycle consists of four pyrrole rings linked by four methine bridge. From Figure 1-1, positions 5, 10, 15 and 20 are called the meso position while positions 2, 3, 7, 8, 12, 13, 17 and 18, are called the β-pyrrole positions. Positions 1, 4, 6, 9, 11, 14, 16 and 19 are called the α-pyrrole positions. Different groups and side chains can be attached to the β positions of the pyrrole rings or the meso carbons.

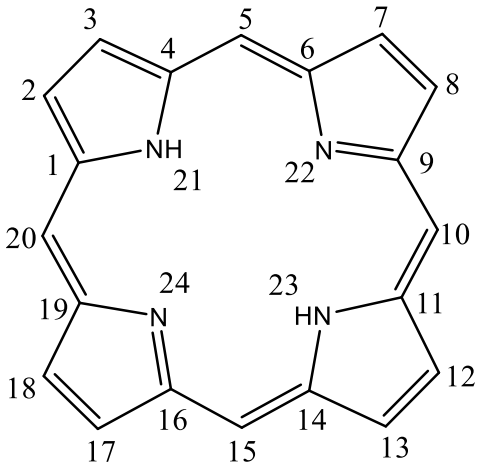

Figure 1-1. Porphyrin numeration

Octaethylporphyrin (OEP) is one of the most commonly synthesized etio-type porphyrin (containing ethyl substituents at the β-pyrrole positions). Another type of porphyrin have substituents at the four meso carbons, and is known as a meso-type porphyrin. The four substituents are usually derivatives of benzene. Tetraphenylporphyrin (TPP) is the most commonly synthesized compound, due to its ease of synthesis. It doesn't occur naturally in nature. Models of different porphyrins, chlorin, and isobacteriochlorin have been examined with regards to the structure of the compounds formed between these metal complexes and intermediates of enzymes found in biological systems[6].

Hydrogenation of one or two pyrrolic double bonds from the parental porphyrin gives rise to new types of porphyrins which are called chlorins, bacteriochlorins, and isobacteriochlorins (Figure 1-2). The reduction of one pyrrole double bond yields a chlorin, while the reduction of two double bonds on two opposite pyrrole gives a bacteriochlorin. An isobacteriochlorin results from the saturation of double bonds on two adjacent pyrroles. These porphyrins are classified as hydroporphyrins. Porphinones,

which contain carbonyl group(s) at the β-carbons, are formed by the oxidation of octaethylporphyrin with osmium tetroxide or hydrogen peroxide (Figure 1-2).

Almost all transition and main group metals can be complexed by the porphyrin macrocycle to form different metalloporphyrins. Metalloporphyrins with no axial ligands attached to the central metal are four-coordinated while five- and six-coordinated metalloporphyrins have one or two ligands attached to the metal center[8], respectively. The specific coordination number depends on several factors such as solvent, type of metal, metal oxidation state and substituents on the metalloporphyrins. The metalloporphyrins ligand coordination compounds found in many biological systems in nature[9,10].

Oxidation and reduction of metalloporphyrins can occur at the porphyrin ring to generate π cation or π anion radicals (the energy of HOMO or LUMO π orbital can be altered) or it may occur at metal center (the change in molecular orbitals involves metal-centered atomic wavefunctions)[11]. Redox reactions can also occur at the axial ligand. The site of oxidation or reduction depends on the porphyrin macrocycle, central metal ion, axial ligand, solvent and supporting electrolyte[12,13].

Metal centered reduction occurs for metalloporphyrins when metal has vacant d-orbitals while porphyrin ring centered reductions frequently occur when the metal has d^8, d^9, and d^{10} configurations. The site of the electron transfer depends on the energy of the HOMO (for oxidation) or LUMO (for reduction). If the reduction occurs at a metal center, the orbital should lie mostly on the metal[14].

The site of electron transfer can be characterized by UV-visible, infrared or EPR spectroscopy[15,16,17,18]. The UV-visible spectra obtained upon oxidation or reduction at

porphyrin metal center will often differ from the spectra obtained after oxidation or reduction at the porphyrin conjugated π system. An oxidation or reduction of the central metal ion will generally shift the absorption bands to a higher or lower wavelength depending on the type of metal ion and axial ligand, but not lead to a substantial decrease in the absorption band. In contrast, an electron transfer involving the porphyrin macrocycle will often be accompanied by a large decrease in the Soret band absorbance and weak broad band may be seen between 600-900 nm; therefore, it is possible to obtain information about the site of electron transfer reaction by observing the absorption spectral changes during the redox process.

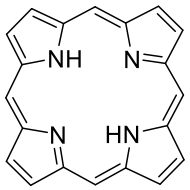

Porphyrin

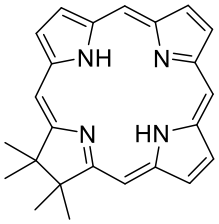

Chlorin

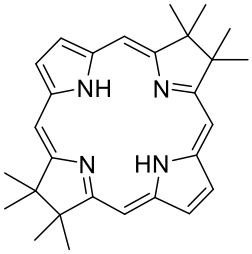

Bacteriochlorin

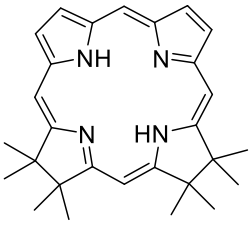

Isobacteriochlorin

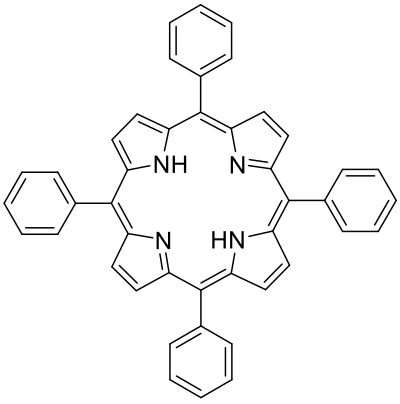

meso-tetraphenylporphyrin

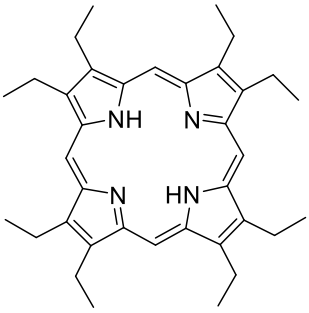

Octaethylporphyrin

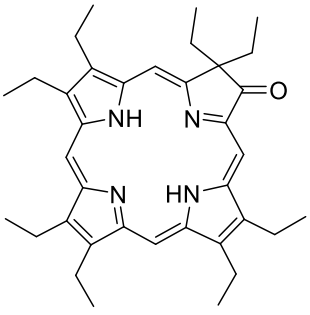

Octaethylporphinone (OEPone)

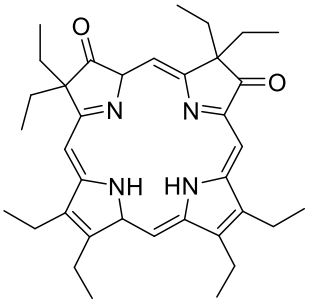

Octaethylporphidione (OEPdione)

Figure 1-2. Structures of porphyrin and porphyrin derivatives

1-2. Metalloporphyrins

Porphyrins can bind with most metals. Buechler reported 55 different metalloporphyrin complexes[20]. In nature we have found eight metals (Mg, V, Mo, Co, Ni, Cu and Zn) that have formed complexes[20]. The major photosynthetic pigments of the plant are chlorophyll-a and –b, which contain Mg as a metal center. The copper complex of uroporphyrin-III was found in the feather of *Turacus indicus*. Nickel was found in the enzyme of Factor F_{430} which catalyzes the reductive cleavage of S-methyl coenzyme M (2-(methylthio)ethanesulfonate) to methane[21].

Ni(OEP) can be reduced to the anion radical while Ni(OEC) and Ni(OEiBC) were reduced to nickel(I) complexes[21]. It was reported that all of the nickel complexes in the tetraphenyl series undergo macrocycle centered reductions[21]. The reduction of Zn(TPiBC) was more difficult than Zn(TPP) and Zn(TPC). Reduction potentials of both cobalt(II) and iron(II) complex of OEiBC appeared at almost same potentials with those metal complexes of OEP and OEC. This is due to the d-electron configurations among these metals. For the Co(II) and Fe(II), which have d^7 and d^6 electron configurations, respectively, either the metal or porphyrin macrocycle can be reduced. Because the d-orbitals of zinc are completely filled, reduction of zinc porphyrins is centered at the porphyrin macrocycles.

1-3. Cobalt porphyrin complexes

Cobalt is one of the commonly studied metalloporphyrin complexes. The biological properties of vitamin B_{12} and its derivatives[25] have made chemical investigation of low valent planar cobalt(I) complexes of considerable interest. Studies of model compounds and synthetic analogues for the active site of cobalt-substituted cytochrome P-450_{CAM} have made chemical and structural investigations of mercaptocobalt porphyrins of interest[26].

In 1965 Bower and coworkers reported the preparation and characterization of cobalt(I) meso-tetraphenylporphyrin[27]. Cobalt(II)TPP is readily reduced by several reducing agents such as sodium amalgam in pyridine or tetrahydrofuran, sodium borohydride in ethanol, acetonitrile or pyridine . After reduction a single air sensitive product, (λ_{max} (pyridine) nm: 362, 427, 511 and 608), was formed. Co(II)TPP is not reduced with ascorbic acid, 1,3-propanedithiol or sodium dithionate in pyridine.

The formation of a diamagnetic cobalt (I) species was obtained by reduction of vitamin B_{12}[28] and cobalt phthalocyanines[29]. Bower and coworkers[27] formulated the reduction product of Co(II) meso-tetraphenylporphyrin as the spin-paired cobalt(I) porphyrin on the basis of NMR spectroscopy and magnetic susceptibility by the Gouy balance method.

In 1971 Youkoh and coworkers[30] prepared cobalt(I) tetraphenylporphyrin by reduction of Co(II) tetraphenylporphyrin with sodium benzophenone ketyl in tetrahydrofuran. Based on the spectral changes, magnetic susceptibility and NMR spectra, the authors concluded that Co(II)TPP leads to Co(I) species. The NMR spectrum of reduced complex Na[Co(I)TPP].5THF is shown in Figure 1-3.

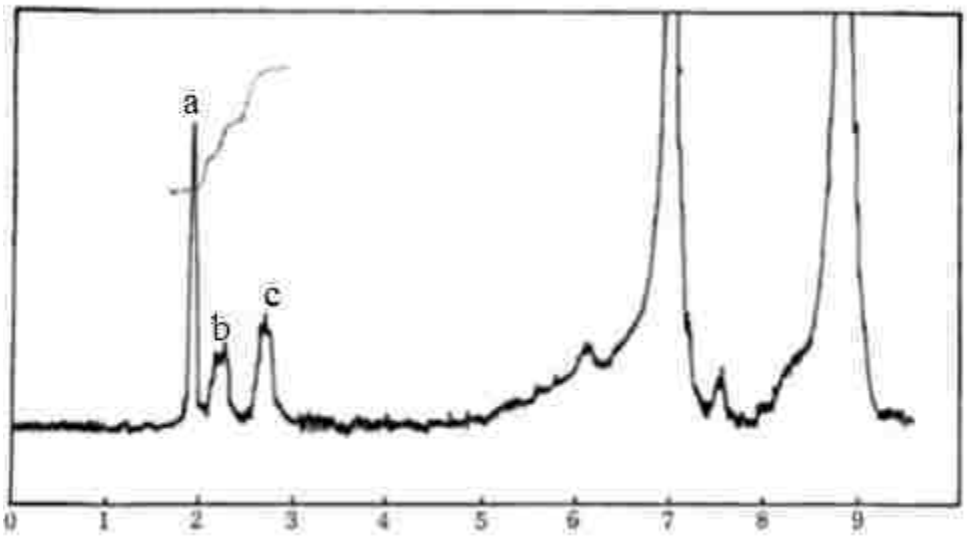

Figure 1-3.[1]H-NMR spectrum (chemical shift in τ) of Na[Co(I)TPP].5THF in THF [30]

Table 1-1

Complex	a (δ)	b (δ)	c (δ)	Solvent	Reference
TPP	8.95	8.3	7.8	$CDCl_3$	47
TPPMg.2Pyridine	8.95	8.3	7.8	$CDCl_3$	47
TPPCo(III)Cl	8.97	8.02	7.65	THF	46
Na[Co(I)TPP].5THF	8.05	7.9	7.45	THF	46

From Figure 1-3, a singlet peak at 8.05 δ (band a) was assigned as a pyrrole ring protons, the multiplet at 7.90 δ (band b) was assigned to the o-protons of phenyl groups and the one at 7.45 δ (band c), to m- and p-protons. The chemical shift values of different porphyrin complexes showed in Table 1-1 (chemical shift in δ). As seen in the case of Co(III)TPPCl , the chemical shift of pyrrole protons are influenced by the central metal ion which is less dπ-donating. In the case of $[Co(I)TPP]^-$ the NMR signal of pyrrole ring protons is shifted to higher field . This high-field shift is attributed to an increase of electron density at the pyrrole ring protons which arises from a back-donation of dπ electron to the lowest vacant π molecular orbital of porphyrin. By seeing these changes in

NMR spectrum we can conclude that reduction occurred at the metal center lead to formation of the product $[Co(I)TPP]^-$.

Reduction of Co(III)TPPCl in chlorobenzene by an excess of 222 cryptated potassium 2-methyl-2-propanethiolate yielded Co(I)TPP derivative $[Co^I(TPP)]$ $[K\cap222]_4C1_3.H_2O$[31]. Weiss and coworkers reported X-ray crystal structure of the Co^I complex.

The UV-visible spectra and X-ray crystal structure of $[Co(I)TPP]^-$ are shown in Figure 1-4 and 1-5. The visible spectrum of $[Co(I)TPP]^-$ are shown in both solution and solid state. The UV-visible spectrum of reduced complexes is very similar to those reported by previous studies[27,33]. Figure 1-5 shows the structure of the centrosymmetric $[Co(I)TPP]^-$ anion. The average bond distances between cobalt and the four pyrrole nitrogens is 1.942 Å and average bond angle between (C_p-Co-N_p) is 89.9 ˚. The deviations found from the 24-atom core mean plane showed that the porphyrin skeleton is slightly puckered. Despite the slight puckering of the ring, the individual pyrrole rings are planar and dihedral angle between the adjacent pyrroles was only 4.2˚. Planar porphyrins have angle between adjacent pyrrole lying between 3 and 5˚[34]. No ruffling of the 24-atom core appeared in $[Co(I)TPP]^-$. Instead of the ruffling, a large puckering of the ring appeared when compared to the quasi-planar triclinic form of Ni(OEP)[34] in which the average bond distance between Ni and pyrrole nitrogens of 1.96 Å. It is not significantly different from Hoards[35] value of 1.96 Å. The $(C_\alpha\text{-}C_\beta)_{av}$ and (C_β- C_β) bond lengths are slightly shortened and (N- C_α) distances are somewhat lengthened when compared to Ni(OEP). These small changes occurred probably due to enhanced back-donation of the electron-rich cobalt(I) center toward porphyrin π system.

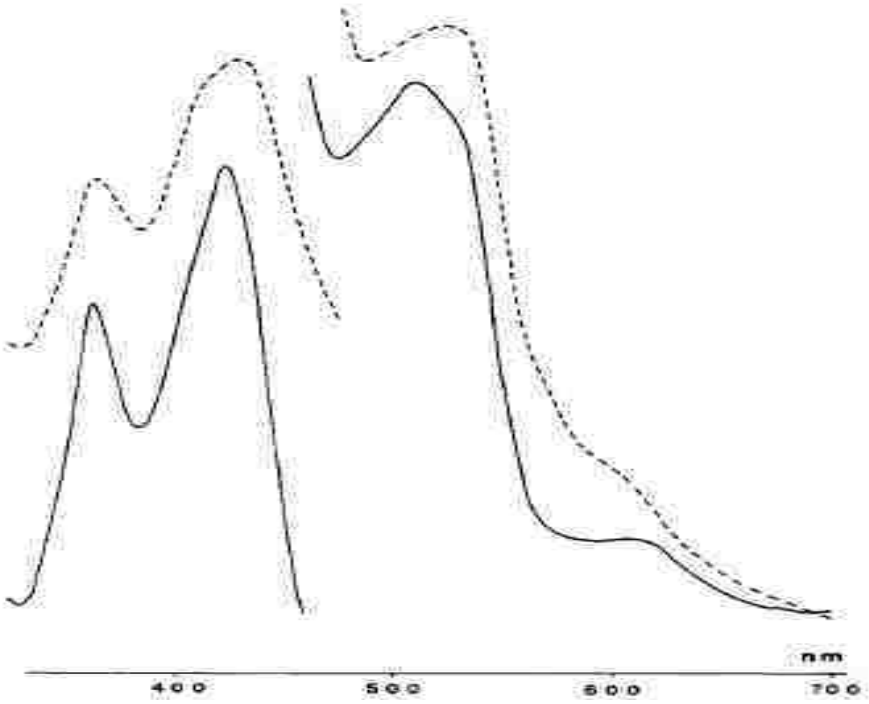

Figure 1-4. $[Co^{I}(TPP)]$ $[K\cap222]_4C1_3.H_2O$: solid (broken line), solution in C_6H_5Cl (solid line)[31]

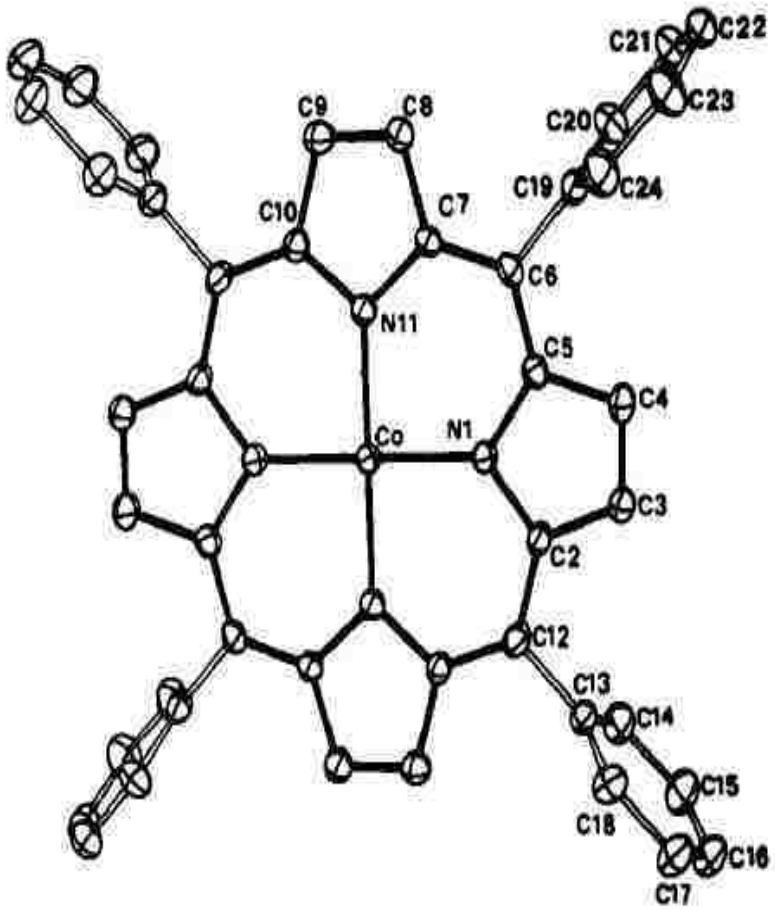

Figure 1-5. ORTEP plot of the $[Co(I)TPP]^{-}$ [31]

Electrochemical studies of cobalt porphyrins:

The electrochemical, UV-visible and infrared spectroelectrochemical studies on cobalt porphinone and cobalt porphinedione complexes carried out by Tutunea and Ryan[36]. Dioxygen porphyrin complexes are seen in enzyme contain a heme d_1, which is an iron porphinonedione, heme d1 binds NO[19]. The authors focused on the study of low valance cobalt porphyrins by monitoring carbonyl frequencies in the infrared spectrum and compared results with DFT calculations[36]. Because the carbonyl band absorbs strongly in

the infrared region, the interaction between the central metal and porphyrin ring, as well as reduction in the ring can be monitored by the shift in carbonyl band.

Cobalt(II) porphinones are reduced by one-electron and oxidized by two-electron steps within the potential range studied[41]. The half-wave potentials ($E_{1/2}$) of Co(II)OEPone was -1.36 V as compared to a value of -1.15 V for Co(II)OEPdione. The reduction process was reversible. The reduction potentials of Co(II)OEP and Co(II)OEPone showed that the carbonyl group significantly decreased potentials (240 mV). This shift was much larger than that observed for Fe(II)OEP versus Fe(II)OEPone , where a smaller 30 mV shift was observed[37]. The addition of a second carbonyl group on ring [Co(II)OEPdione] had a much smaller effect (a decrease of 80 mV compared to Co(II)OEPone. This was similar to the shift observed between Fe(II)OEPone and Fe(II)OEPdione (80 mV decrease)[38]. The electroreduction of Co(II)OEPone and Co(II)OEPdione was analyzed by UV-visible spectroelectrochemistry[36], the reduction of Co(II)OEPone resulted a split Soret band being observed. The Q band and the Soret band at 374 nm are blue shifted to 354 nm. Isobestic points were observed at 382, 426, 624 nm which indicated that no intermediates were formed during electrolysis. The lack of band broadening in the 450-550 and 700-900 nm region suggested that reduction process occurred at the metal centered[39]. The reduction of Co(II)OEPdione resulted single Soret band. The Soret and the Q bands decreased in absorbance and were blue shifted. The UV-visible spectral values of Co(II)OEPone and Co(II)OEPdione and their reduction products were summarized in Table 1-2.

Table 1-2. Visible spectra data of cobalt porphinones 0.08 mM in THF, with 0.10 M TBAP[36]

Compounds	Solvent	B bands (nm)	Q bands (nm)	Ref
Co^{II}(OEPone)	THF	374, 412	606	36
Co^{I}(OEPone)$^-$	THF	354, 412	510, 606	36
Co^{II}(OEPdione)	THF	384, 432	620	36
Co^{I}(OEPdione)$^-$	THF	382	544, 620	36

Infrared spectroelectrochemistry for Co(II)OEPone and Co(II)OEPdione was carried out by Tutunea and Ryan[36], The carbonyl band for Co(II)OEPone was observed at 1709 cm^{-1}. Upon a one electron reduction, the carbonyl band shifted to 1676 cm^{-1}, a decrease of 33 cm^{-1}. In addition to the shifts of the carbonyl band, new bands were observed at 1616, 1593, 1580 and 1556 cm^{-1}. The original spectrum of Co(II)OEPone was obtained upon reoxidation. From the DFT calculations, the carbonyl band for Co(II)OEPone observed at 1700 cm^{-1} and for Co^{I}(OEPone)$^-$ carbonyl band was observed at 1661 cm^{-1}. The carbonyl shift in Co(II)OEPone (33 cm^{-1}) was similar to the shift observed for Fe(II)OEPone (32 cm^{-1})[40]. These results indicated that the carbonyl vibration was weakened due to the electron density on the porphyrin ring caused by back-donation of the reduced metal dπ orbital to the porphyrin π^* orbital. The Co(II)OEPone reduction results were similar reduction results of Fe(II)OEPone. This indicated ring delocalization as shown by IR results where the carbonyl band shifted to lower frequency. By considering all these spectral changes the authors concluded that Co^{I}(OEPone)$^-$ species as similar to Fe^{I}(OEPone)$^-$, DFT calculations have indicated considerable Fe(I) and Co(I) character,

with significant metal d_π back bonding to the ring. Infrared spectrum of Co(II)OEPone and its reduction products are shown in Fig 1-6.

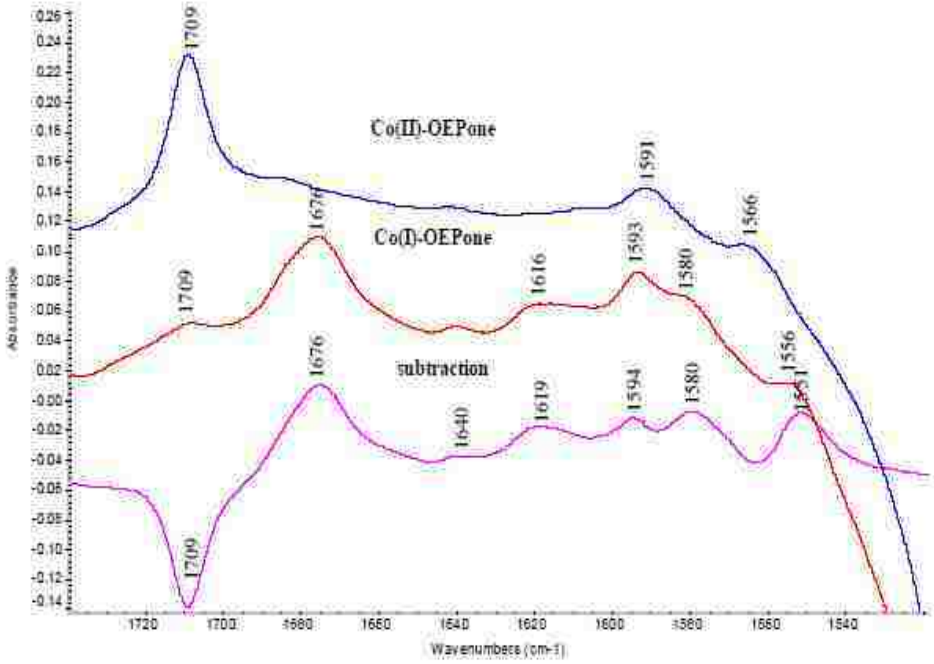

Figure 1-6. FTIR spectra of Co(II)-OEPone reduction 3.0 mM, in THF, 0.10 M TBAP, at -1.5 V by OTTLE spectroelectrochemistry, 32 scans[41]

The carbonyl band for Co(II)(OEPdione)[41] was observed at 1709 cm^{-1} and additional bands was observed at 1606 and 1583 cm^{-1}. Upon a one electron reduction by electrolysis, the carbonyl band shifted and was split into two bands at 1681 and 1667 cm^{-1}. These spectra changes were similar to the iron porphinediones[40]. The carbonyl band split in two peaks with same absorbance although with a slightly higher wavenumber than the iron porphinedione. The porphyrin region peak shifted from 1583 to 1579 cm^{-1}. The split in two bands due to the presence of the two non-equivalent carbonyls in the molecule. According to previous studies[40] , the changes of these shifts was due to

increased electron density on the porphyrin ring caused by back bonding of d_π electron from the metal to vacant molecular orbital of porphyrin[41].

1-4. Manganese porphyrin complexes

Manganese porphyrin complexes have a significant importance because of their unique absorption spectra and mostly for their utility as model compounds for a general understanding of more complex metalloporphyrin spectra and structure. Previous studies of the reduction of manganese porphyrin complexes have indicated that manganese(III) complexes are reduced to manganese(II), and then to manganese(II) anion radical[42,43]. The properties and preparation of some manganese porphyrins have been previously reported. Zaleski[44] prepared the first manganese(III) porphyrins, which were not studied fully until Taylor examined its redox properties and represented electronic absorption spectra for the first time[32,45].

The physical and spectral properties and elemental analyses of manganese protoporphyrin IX dimethyl ester complexes were first investigated by Boucher[46]. Boucher also explained the UV-visible absorption spectra analyzed with Gouterman molecular orbital of metalloporphyrins.

There are few studies on manganese metalloporphyrin reductions and most of them referred to the process that takes place at manganese metal. Kadish's[47] work revealed that, when metal ions with an oxidation number of +3 or +4 are introduced into the porphyrin cavity, the extra positive charge has a great influence on the porphyrin π

system and its redox properties. The reduction potential values for Mn(II)/Mn(II)$^-$ is -1.61 V and -0.42 V for Mn(III)/Mn(II) reduction[47].

Additional information about Mn(II)P$^-$ anion formation is shown by a study performed on redox reactions of manganese porphyrins in aqueous solution by pulse radiolysis[48]. The absorption spectra recorded upon radiolytic reduction of Mn(II)TPPS (tetrakis(4-sulfonato- phenyl)porphyrin) and Mn(II)TMPyP (tetrakis(N-methyl- 4-pyridyl)porphyrin) exhibited a broad absorption around 770 nm which was characteristic of π-radical anions.

Electrochemical reduction of Mn(TPP)Cl in THF was reported by Boucher[46]. Figure 1-7 illustrates acquired spectra for the spectroelectrochemical reduction of Mn(III) tetraphenylporphyrin chloride in THF containing 0.1 M Bu_4NBF_4. The spectrum of the Mn(III) complex, shows the characteristic split Soret band and Q bands in visible region, while the Mn(II) complex displays a normal absorption spectrum.

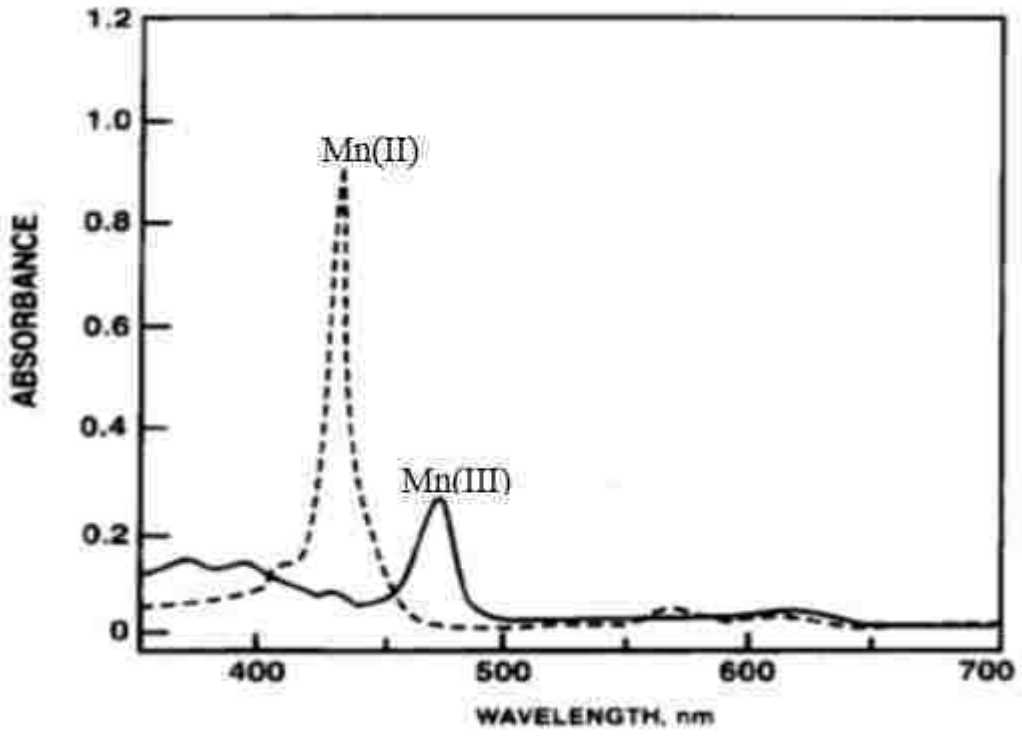

Figure 1-7. Thin-layer visible spectroelectrochemical reduction of Mn(III)/Mn(II)TP in chloroform: Mn(II)-----, Mn(III)____[46]

The X-ray crystal structure of the potassium cryptate $[K(K222)]^+$ salt of the chloro(tetraphenyl-porphinato) manganese(II) anion was reported by Valanetine[49]. This complex was prepared in THF by reaction of $Mn^{III}TPPCl$ with zinc amalgam followed by excess amount of potassium cryptand. The X-ray crystal structure of [K(K222)] [MnTPPCl] is shown Figure 1-8.

In $Mn^{II}TPP(Cl)^-$ complex, the average bond distance between Mn-N_p is 2.160 Å and manganese out-of-plane displacement is 0.641 Å. For comparison, $Mn^{II}TPP$(1-methylimidazole)[50] has an average Mn-N bond length of 2.128 Å a manganese displacement of 0.512 Å and the average Mn-N distance and Mn out-of-plane displacement for $Mn^{III}TPPCl$[51] are 2.009 Å and 0.27 Å which are a little longer in $[Mn^{II}TPPCl]^-$. The longer metal-nitrogen bond length and metal out-of –plane

displacement of $[Mn^{II}TPPCl]^-$ presumably reflects the larger ionic radius of Mn(II) relative to Mn(III).

The Mn-Cl distance in $[Mn^{II}TPPCl]^-$ is 2.364 Å, and the Mn-Cl bond is slightly tilted (3.7˚) from the pyrrole nitrogen plane toward N2. Even though $[Mn^{II}TPPCl]^-$ differs in its formal oxidation state from Mn^{III}, the Mn-Cl distance is almost exactly the same (2.363 Å) as that of $Mn^{III}TPPCl$[51]. These observations can be explained if the additional electron in $Mn^{II}TPPCl]^-$ is assumed to occupy the d_{x2-y2} orbital. That orbital has little direct interaction with the axial ligand. Interestingly, the Mn-Cl distance is substantially shorter (2.295 Å) for $Mn(NCH_3TPP)Cl$[52] than for $Mn^{II}TPPCl]^-$. The may be due to differences in the bonding of the N-methylated porphyrin to manganese which leads to increased interaction with the axial ligand.

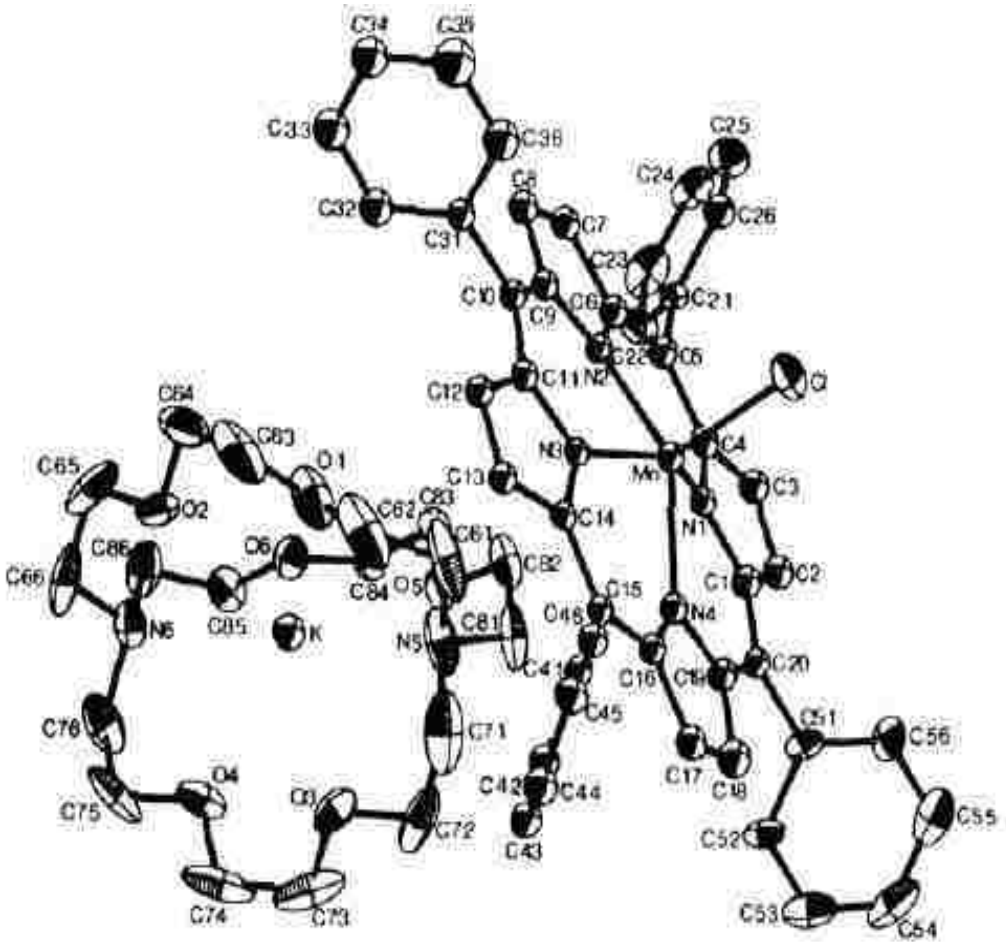

Figure 1-8. ORTEP plot of [K(K222)] [MnTPPCl] showing bath the porphyrin anion and potassium cryptate cation. Hydrogen atoms have been omitted for clarity[49]

The UV-visible and infrared spectroelectrochemistry studies on manganese porphinone and porphinedione has been carried out by Tutunea[41]. The UV-visible spectrum of manganese octaethylporphinone showed a split Soret band at 364 nm and 478 nm and a Q band a 642 nm. The split Soret band, characteristic for manganese complex, decreased during electrolysis. Upon one electron reduction (Figure 1-19), a peak at 440 nm appeared in Soret band region and the Q band at 642 nm shifted to lower wavelength. Isobestic points were observed, indicating that there was direct conversion to the

manganous complex without any intermediates. According to previous studies[53], the Kadish group concluded that resulting spectrum indicated Mn(III)/Mn(II) reduction. The second electron reduction of Mn(III)OEPone (Figure 1-10) resulted in a red shift of the Soret band from 440 to 488 nm and the Q band at 624 nm became featureless. Band broadening observed within the visible region 600-700 nm suggested formation of π radical anion of $Mn^{II}(OEPone)^{-}$.

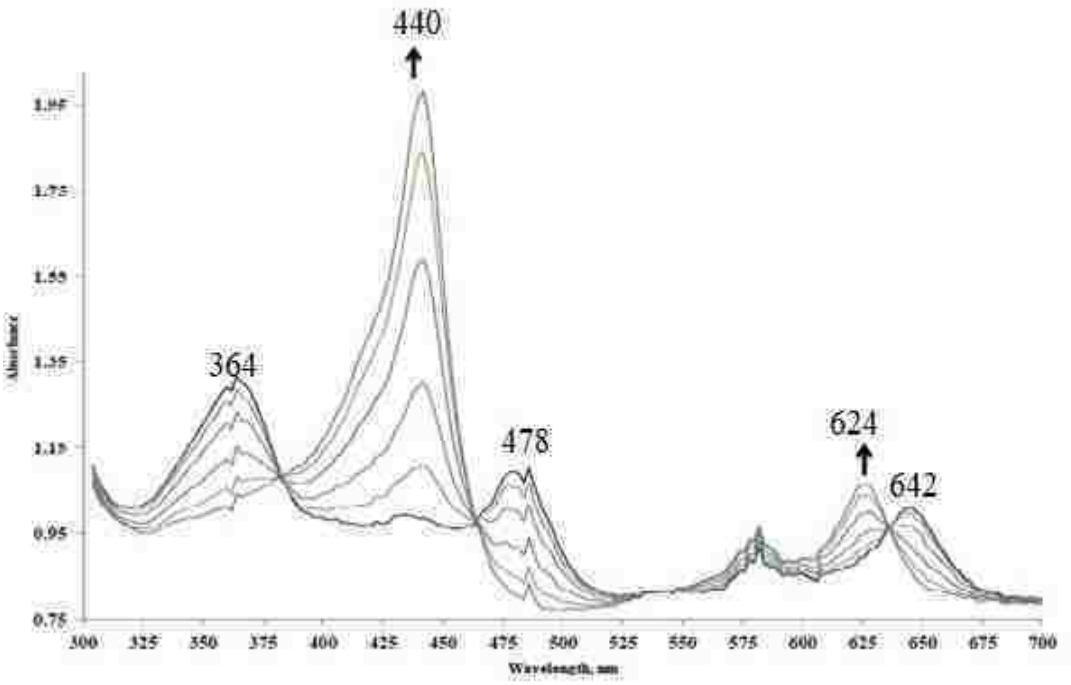

Figure 1-9. Thin-layer visible spectroelectrochemistry obtained during the reduction of Mn(III)OEPoneCl 0.80 mM in THF, with 0.10 M TBAP, potential region 0.4 V to -0.6 V (THF as solvent)[41]

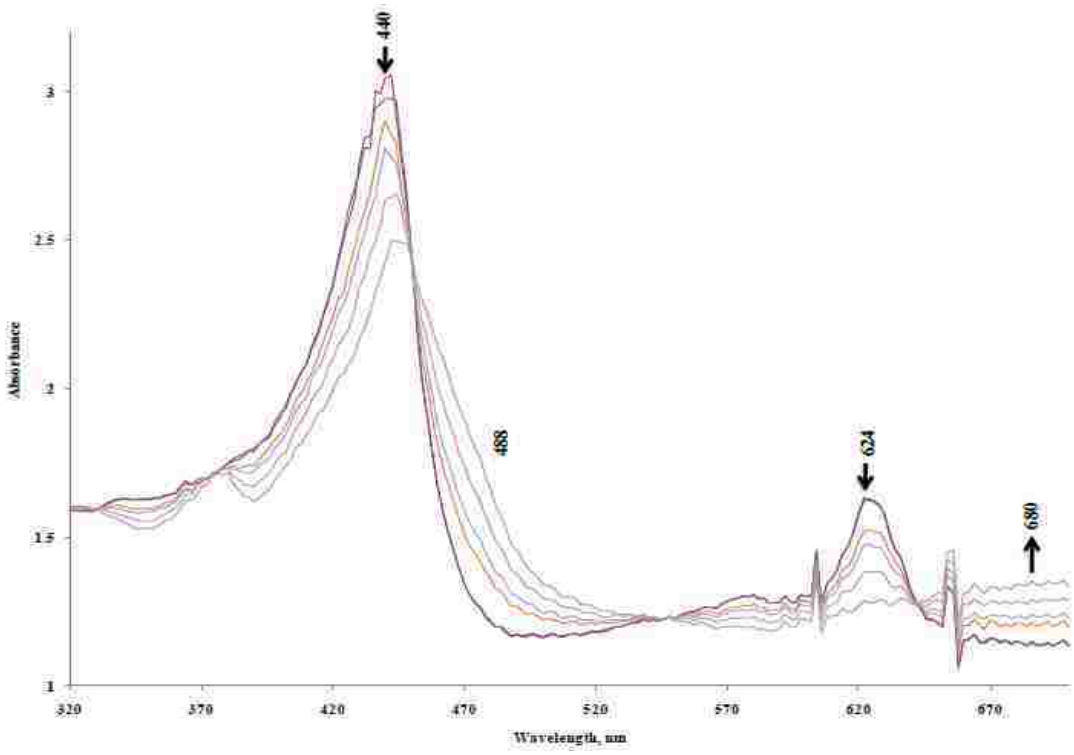

Figure 1-10. Thin-layer visible spectroelectrochemistry obtained during the reduction of Mn(II)OEPone 0.80 mM in THF, with 0.10 M TBAP, potential region -0.6 V to -1.5 V [41]

The infrared spectrum of Mn^{III}(OEPone)[41] showed the carbonyl vibration band at 1721 cm^{-1}. Upon a one electron reduction, the carbonyl C=O band shifted to 1706 cm^{-1} (Figure 1-11), a shift of 15 cm^{-1}. The shift in carbonyl is similar to the shift observed for Fe^{III}(OEPone) reduction (16 cm^{-1})[40]. The carbonyl vibration was weakened due to back-bonding from metal to porphinone. For the second electron reduction of Mn^{III}(OEPone)Cl , the carbonyl band shifted from 1706 cm^{-1} to 1657 cm^{-1} (Figure 1-12), an observed shift of 49 cm^{-1}. This was than the shift observed for the first electron reduction process of Mn^{III}(OEPone)Cl. This shift is larger than that observed for carbonyl band when Fe^{II}(OEPone)[40] was reduced (31 cm^{-1})[41].

The shift in the carbonyl band for Mn^{II}(OEPone) (49 cm^{-1}) is similar to the shift of Zn^{II}(OEPone) (47 cm^{-1})[41] but larger than Co^{II}(OEPone) (33 cm^{-1})[36]. In addition, the

reduced species of Mn^{II}(OEPone) displayed two peaks in the porphyrin region at 1538 and 1530 cm^{-1} which are observed in Zn^{II}(OEPone) as well at 1550 and 1540 cm^{-1}. Therefore the reduction site in these compounds is same.

By seeing the changes in Mn^{III}(OEPone)Cl from UV-visible and infrared spectrum the authors concluded that first electron reduction process occurred at metal center, lead to formation of Mn^{II}(OEPone) and second electron reduction occurred at porphyrin ring lead to the formation $Mn^{II}(OEPone)^{-}$ radical anion[41].

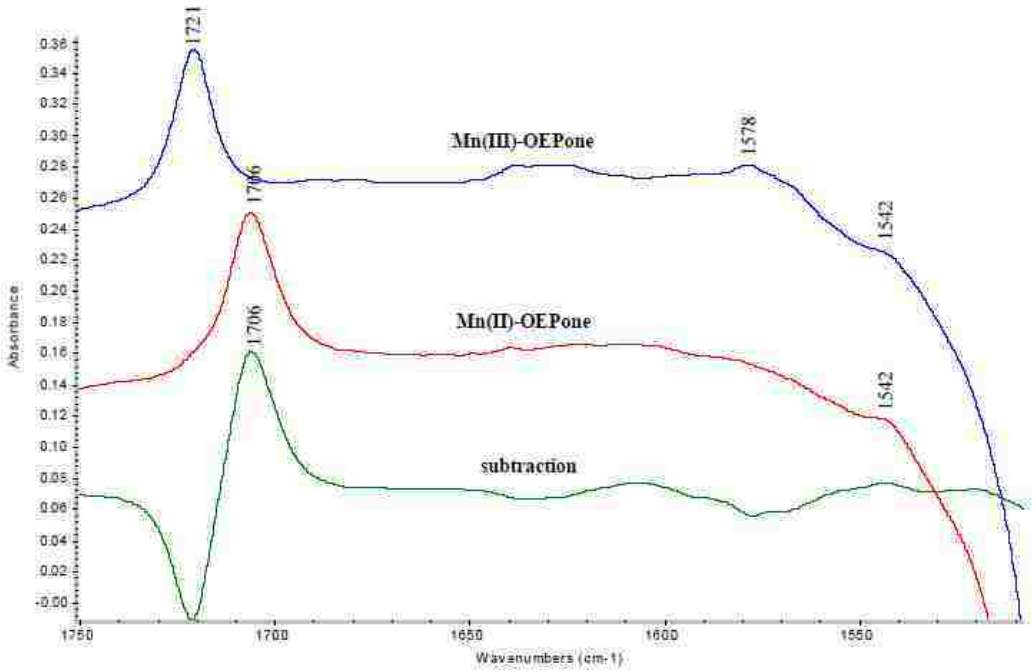

Figure 1-11. FT-IR reduction spectra of Mn^{III}(OEPone)Cl 3.0 mM, In THF, 0.01 M TBAP by OTTLE spectroelectrochemistry, 32 scans[41]

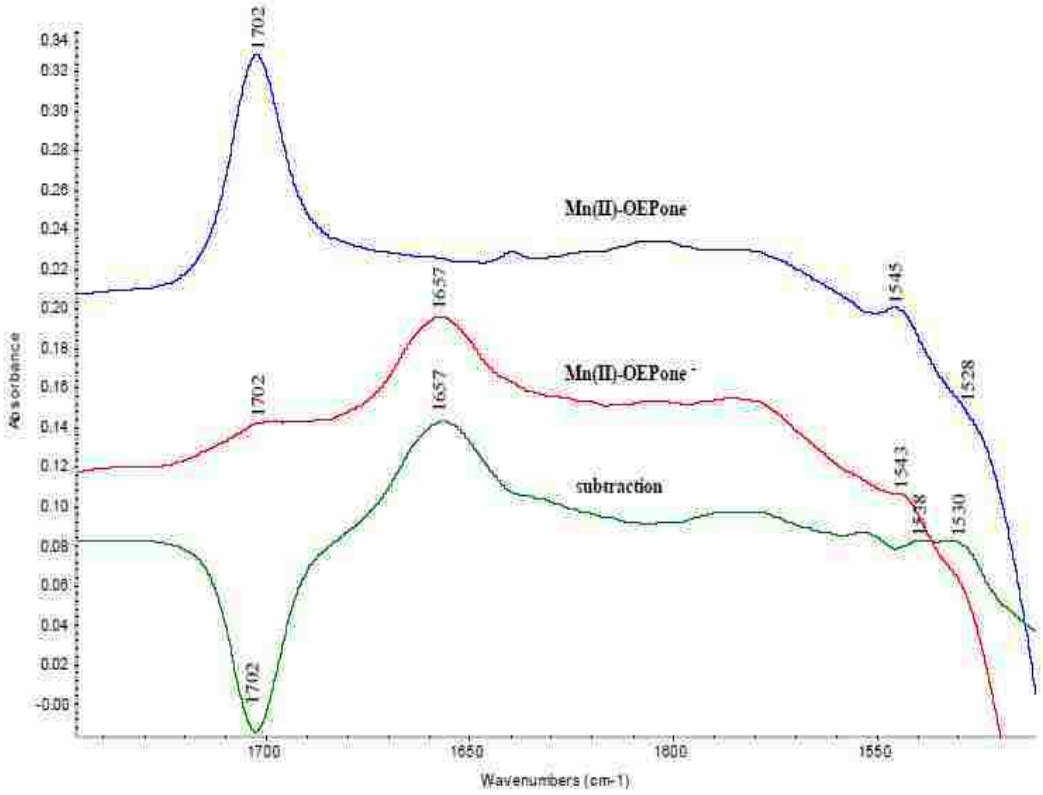

Figure 1-12. FT-IR reduction spectra of Mn^{II}(OEPone) 3.0 mM, In THF, 0.01 M TBAP by OTTLE spectroelectrochemistry, 32 scans[41]

1-5. Iron porphyrin complexes

Many studies have been done on iron porphyrin complexes with different techniques which include resonance Raman spectroscopy, X-ray crystallography and NMR spectroscopy. Resonance Raman spectroscopy is an important tool for to determine structure and bonding in porphyrin complexes. By using this technique we can get information such as the oxidation state and spin state of the metal in the porphyrin complex[54,55,56].

Iron tetraphenylporphyrin (FeTPP) has been used broadly to study the structure, redox potentials, spin state and spectroscopic properties for various oxidation states. Little work

has been done for the iron tetraphenyl series of chlorin and isobacteriochlorin complexes. Fe(OEP), Fe(OEC) and Fe(OEiBC) have been synthesized and the physicochemical properties of these complex have been examined[57,58].

The electronic structure of $Fe(TPP)^-$ is still uncertain. The one electron reduction of product of Fe(II) porphyrin was studied with NMR spectroscopy[59] and X-ray crystallography[60]. The formulation of $[Fe^I\text{-}P]^-$ supported by NMR spectroscopy while X-ray crystal data support the $[Fe^{II}\text{-}P^-]$ species.

The iron(I) porphyrin complexes tend to be more nucleophilic when compared to ferric and ferrous states. Generally the ferrous and ferric states are electrophilic. The increased nucleophilicity of low valent metalloporphyrins may be important for their use as catalysts[61].

The amount of molecular dinitrogen, nitrous oxide, ammonia, nitrite and nitrate on the global earth is regulated by nitrogen cycle[62]. The most important steps in this nitrogen cycle is the synthesis of ammonia from the reduction of nitrite, which is catalyzed by the enzyme assimilatory nitrite reductase. The prosthetic group in assimilatory nitrite reductase has been identified as an iron isobacteriochlorin, siroheme. The second type of enzyme is called a dissimilatory nitrite reductase, which have either iron or copper as their prosthetic group, it reduces nitrite to nitric or nitrous oxide[65].

Assimilatory nitrite reductase process

$$NO_2^- \dashrightarrow NO \dashrightarrow NOH \dashrightarrow NH_2OH \dashrightarrow NH_4^+$$

Dissimilatory nitrite reductase process

$$NO_3^- \dashrightarrow NO_2^- \dashrightarrow NO \dashrightarrow N_2O \dashrightarrow N_2$$

In the above assimilatory nitrite reductase process, nitrite initially reacts with the siroheme to form a nitrite complex that is reduced to an iron nitrosyl, hydroxylamine and then ammonia[63]. Among these intermediates only the enzyme bound nitrosyl has been observed experimentally, and has been found to the major species present during turnover[64]. While hydroxylamine has been proposed as a possible intermediate, experimental evidence is lacking.

In the dissimilatory reduction process the reduction of nitrite is catalyzed by dissimilatory nitrite reductase which has a prosthetic group heme c and an unusual heme d_1 which contain 2,4-porphinedione.The nitrosyl complex, which is an important intermediate in dissimilatory nitrite reduction has been experimentally observed[66]. The further reduction of NO to N_2O is catalyzed by another enzyme called a nitric oxide reductase.

1-6. Iron porphyrin nitrosyl complexes

Iron nitrosyl porphyrin complexes have been studied by electrochemistry[67], X-ray crystal structure[68], infrared spectroscopy[67], electron paramagnetic resonance spectroscopy[67] and resonance Raman spectroscopy[70]. The X-ray crystal structure study showed that the Fe-N-O moiety is bent in Fe^{II}(TPP)(NO) with an angle of 149.2˚, while it is linear in the case of Fe^{III}(TPP)(NO)ClO_4. The displacement of the iron atom from the mean plane of porphyrin core is 0.21 Å in Fe^{II} (TPP)NO and 0.29 Å in Fe^{III} (TPP)(NO)ClO_4. In both Fe(OEP)(NO) and Fe(TPP)NO the iron has low spin , is pentacocordinated in methylene chloride, and the spin state of the complex is 1/2[69].

Iron porphyrin nitrosyls are reduced in three electron steps in non-aqueous solvents[71].

The visible spectra of different nitrosyl complexes Fe(P)(NO) (where P= TPP, OEP,

OEC and OEiBC), and their reduction products were obtained by using thin-layer spectroelectrochemistry[71]. The reduction products $Fe(P)(NO)^{-}$, were stable in butryonitrile or THF. The visible spectra of two electron reduction product $Fe(P)(NO)^{-2}$ was reported by Choi at al[70].

The possible reduction site for Fe(P)(NO) complexes are the NO ligand, the porphyrin, or the metal. The reduction must be centered on the NO ligand in order to lead to more reduced nitrogen species. Figure 1-13 illustrates the one and two electron reduction of Fe(TPP)(NO) in THF by control-potential electrolysis by spectroelectrochemistry. The first-electron reduction of Fe(TPP)(NO) led to a new band which appeared at 512 nm, while only small changes were observed in the Soret region[71]. Two isobestic points were observed at 454 and 495 nm, indicating that only two species were present in solution during electrolysis. Upon reversal of the applied potential, visible spectra showed complete regeneration of Fe(TPP)(NO). These results indicated that the coordinated NO was not lost after one electron was added. The small changes in the Soret band with addition of electron suggest that the reduction occurs at the Fe-NO moiety, rather than the porphyrin ring.

When a second electron was added to $Fe(TPP)(NO)^{-}$, the resulted UV-visible spectra is show in Figure 1-13. In contrast to the small spectral changes observed during the first-electron reduction, second-electron reduction indicated in a dramatic change in visible spectrum. During the reduction, the Soret band (408 nm) decreased and shifted to 452 nm, and isobestic point was observed at 431 nm. The bands for $Fe(TPP)(NO)^{-2}$ in both Soret and visible region were broad. When the potential was reversed, the visible spectra of $Fe(TPP)(NO)^{-}$ and Fe(TPP)(NO) were regenerated, suggesting that NO ligand was not

lost even after the second-electron reduction. The weak and broad absorbance bands of $Fe(TPP)(NO)^{-2}$ suggest that second electron is more likely added to the porphyrin[71]. The vibrational spectra for Fe(P)(NO) and its reduction product $Fe(P)(NO)^{-}$ have been obtained[71]. Vibrations for both porphyrin species were consistent with low-spin ferrous complex. The NO frequencies for Fe(TPP)(NO) and $Fe(TPP)(NO)^{-}$ are 1681 cm^{-1} and 1496 cm^{-1} respectively, while the $\nu_{Fe\text{-}NO}$ frequencies increased from 525 cm^{-1} to 549 cm^{-1} up on reduction. These results indicated that addition of one electron, strengthened the Fe-N bond and weakened the N-O bond. These results are contrary to the mechanism that postulate the release of a nitrosyl moiety during the dissimilatory reduction process.

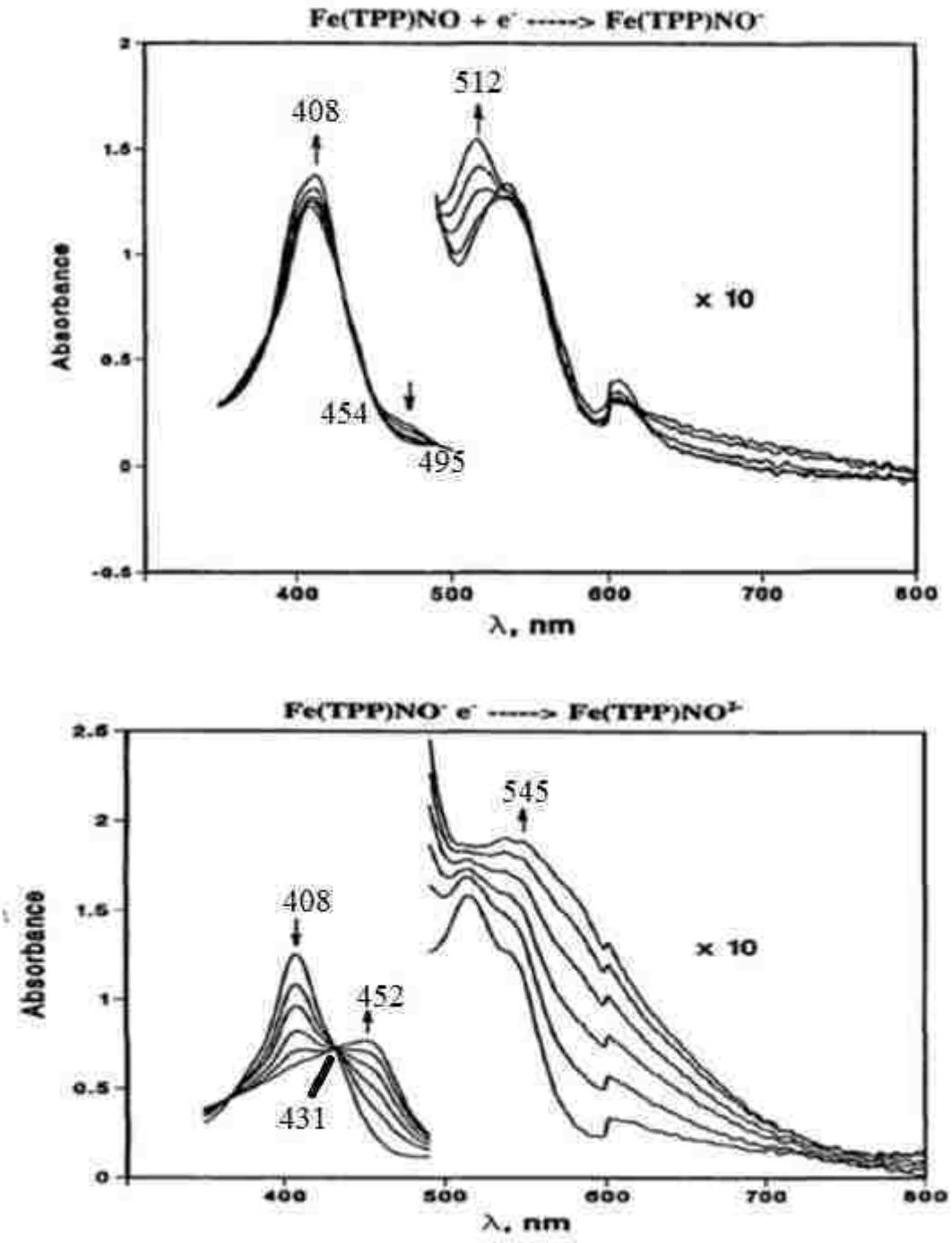

Figure 1-13. Visible spectra recorded during the first and second electron reduction of Fe(TPP)(NO) in THF by controlled-potential electrolysis in an OTTLE cell[71]

1-7. Aim of this work

The goal of this research is the investigation of X-ray crystal structure of low valent metalloporphyrin complexes (metals: Fe, Mn, Co), iron nitrosyl porphyrin complexes ($Fe(P)(NO)^{-}$) and metalloporphinone complexes (M(II) and M(I) porphinones). Initially, those three types of porphyrin complexes will be synthesized and their low valent metalloporphyrins and metalloporphinones will be generated via chemical reduction. Secondly, the reduced products will be characterized by using UV-visble and infrared spectroscopy. Eventually X-ray quality crystal structures of those reduced complexes will be generated using layering technique.

According to the previous studies most of highly reduced metalloporphyrins have been prepared by electrochemical reduction. In this work chemical reduction methods will be utilized over the electrolytic reduction in order to gain the X-ray quality crystals. This chemical reduction is leads to the isolation of products through precipitation. The tetrabutylammonium borohydride, 222 cryptated potassium 2-methyl-2-propanethiolate, sodium anthracenide, and potassium anthracenide will be used as chemical reducing agents for the reduction of following metalloporphyrins and porphinones; Mn(P)(P: tetraphenylporphyrin, octaethylporphyrin, octaethylporphinone), Co(P) (P: tetraphenylporphyrin, octaethylporphinone) and Fe(P) (P: tetraphenylporphyrin nitrosyl, octaethylporphyrin nitrosyl).

The UV-visible spectral studies give primary information about the results of redox process. The infrared spectroscopic analysis also important tool for study of particular complexes like porphinones and nitrosyl porphyrins due to the presence of carbonyl (C=O) and nitrosyls (NO) functional groups. These functional groups shows strong

absorbance in infrared spectrum and they are well separated from porphyrin bands region. Additionally, X-ray crystallography also opens an avenue for studying the atomic and molecular structure of metal porphyrins.

The reduction of iron porphyrins results are still ambiguous due to the electron accepting capability of both metal and porphyrin ring. The presence of both Fe(I) and Fe(II) porphyrin radical anion have been proposed in the reduction process of ferrous porphyrin complex. The electrochemical studies of the reduced Fe(II)porphyrin data is not well characterized. This gave an insight to identify the reduced products via spectroscopic and X-ray crystallographic techniques.

Chapter Two: Experimental

2-1. Instrument

UV-visible spectra: The UV-visible spectra were recorded on a Hewlett-Packard 8452A diode array spectrophotometer. The spectrophotometer is controlled from a computer equipped with the software of Olis Global Works running on Windows XP.

Infrared spectroscopy: The infrared spectroscopy data were produced with a Thermo Nicolet Nexus 670 Fourier-transform infrared spectrophotometer. Spectra were measured from 4000 to 400 cm^{-1} with the sample mixed in the matrix of potassium bromide (KBr, Aldrich).

Proton-NMR: The Proton-NMR data were obtained on a Varian Mercury-400 MHz spectrometer. Spectra were analyzed with Spinwork3. Spectra were taken with the sample mixed in the DMSO-d_6 or $CDCl_3$ (Cambridge Isotopes) matrix in the NMR tubes.

X-ray diffraction: X-ray crystal structures were obtained with Oxford SuperNova diffractometer using Cu(Kα) radiation.

2-2. Chemicals

Free base octaethylporphyrin (H_2-OEP), free base octaethylporphinone (H_2-OEPone), iron (III) tetraphenylporphyrin chloride [Fe^{III} (TPP)Cl], iron(III) octaethylporphyrin chloride [Fe^{III}(OEP)Cl] were purchased from Frontier Scientific Chemical Company. Tetrabutylammonium borohydride, 4,7,13,16,21,24-hexaoxa-1,10-diazobicyclo [8-8-8] hexacosane (2.2.2-crypatand), manganese(III) tetraphenylporphyrin chloride [Mn^{III}(TPP)Cl], cobalt(II) tetraphenylporphyrin [Co^{II}TPP], manganese acetate tetrahydrate were purchased from Sigma Aldrich Chemical Company . All the solvents were anhydrous unless noted separately.

Anhydrous tetrahydrofuran THF was refluxed in the presence of sodium and benzophenone under a nitrogen atmosphere until the dark blue benzophenone anion color was formed, and then stored in the glove box. All other solvents were spectrophotometric grade and were used without further purification.

2-3. Synthesis of metalloporphyrins and metalloporphinones

Mn(III)OEPCl Synthesis[41]: 25 mg of octaethylporhyrin (H_2OEP), 50 mg of manganese acetate tetrahydrate, 25 mg of sodium chloride and 40 mg of sodium acetate were added to 15 mL glacial acetic acid in 3-necked round bottom flask and were refluxed for 24 h under a nitrogen atmosphere. After 24 h, another 50 mg amount of manganese acetate tetrahydrate as added to the reaction mixture and the reaction was allowed to continue for another 24 hours .

The reaction progress was monitored by UV-visible spectra. The resulting solution was cooled to room temperature, and the reaction mixture was taken into a 1000 mL separatory funnel. 50 mL of dichloromethane was added, washed with 5%$NaHCO_3$ solution (5 ▪ 150 mL), then the combined organic phases were successively washed with water (3▪150 mL) , dried over anhydrous Na_2SO_4 , and concentrated. The Mn(III)OEPCl product was characterized by UV-visible (THF), λ_{max}, nm: 356, 396, 424, 470, 556 and 586.

Mn(III)(OEP)($OClO_3$) Synthesis[72]: 20 mg of Mn(III)OEPCl was dissolved in dichloromethane (10 mL) , resultant solution was transferred to 1000 mL separatory funnel and extracted with (2%) aqueous perchloric acid (100 mL) . The separatory funnel was shaken several times. The organic layer was dried over anhydrous Na_2SO_4, and concentrated. The Mn(III)(OEP)($OClO_3$) product was characterized by UV-visible ((THF), λ_{max}, nm: 374, 396, 434, 474, 554 and 586.

Mn(III)OEPoneCl Synthesis[41]: 25 mg of free base octaethylporphinone (H_2-OEPone), 50 mg of manganese acetate tetrahydrate, 25 mg of sodium chloride and 40 mg of sodium acetate were added to 15 mL glacial acetic acid in 3-necked round bottom flask and were refluxed for 24 h under a nitrogen atmosphere. After 24 h, another 50 mg amount of manganese acetate tetrahydrate were added to the reaction mixture and the reaction was allowed to continue for 24 hours. At that point, 25 mg of manganese acetate tetrahydrate, and 15 mg NaCl were added to the reaction mixture and reaction was allowed to continue for another 24 hours.

The reaction completion was monitored by UV-visible spectra. The resulting solution was cooled to room temperature, the reaction mixture were taken into a 1000 mL separatory funnel, 50 mL of dichloromethane was added, washed with 5%$NaHCO_3$ solution (5 ▪ 150 mL), then the combined organic phases were successively washed with water (3▪150 mL) , dried over anhydrous Na_2SO_4 , and concentrated. The Mn(III)OEPoneCl product was characterized by UV-visible (THF), λ_{max}, nm: 360, 402, 428, 468 and 644.

Co(II)OEPone synthesis[41]: 20 mg of porphinone H_2OEPone was allowed to react with 100 mg of cobalt acetate tetrahydrate in 10 mL chloroform and 5 mL methanol at reflux for 24 hours. The reaction completion was checked by UV-visible spectra. The resulting solution was cooled to room temperature, reaction mixture was taken in to a 1000 mL separatory funnel, 15 mL of chloroform was added, washed with water (4▪100 mL), and the combined organic phases were dried over anhydrous Na_2SO_4, and concentrated. The Co(II)OEPone product was characterized by UV-visible (THF), λ_{max}, nm: 370, 418, 566 and 616.

Potassium 2-methyl-2-propanethiolate synthesis[31]: 0.25 mL of 2-methyl-2-propanethiol was dissolved in 15 mL anhydrous ethanol, the solution was stirred for 15 minutes. A solution was prepared with 115 mg of potassium hydroxide, which was dissolved in 5 mL ethanol. This solution was stirred until all the potassium hydroxide was dissolved. At that point of time, the prepared potassium hydroxide solution was transferred to the 2-methyl-2-propanethiol solution by using a cannula and refluxed for 2 hours. The solution was cooled to room temperature. The product was precipitated by addition of 30 mL of anhydrous diethyl ether. The resultant white precipitate was washed with pentane and dried under vacuum. The product was stored in a glove box. The above experiment was carried out under a nitrogen atmosphere.

222 cryptand potassium 2-metyl-2-propanethiolate was prepared by addition of equivalent amounts of 2-methyl-2-propanethiolate and 222-cryptand in chlorobenzene solution.

Sodium anthracenide[73] was prepared by accurately weighing 0.30 (54 mg) mmol anthracene into a 50 mL round bottom flask which was placed in the glove box for 24 hours. An excess amount of freshly cut sodium metal was added into 10 mL of double distilled THF. The solution was stirred for about 5 minutes and was followed by an addition of 0.30 mmol anthracene. The solution was allowed to react for 4 hours, until the solution was dark blue color.

Potassium anthracenide was prepared by accurately weighing 0.30 (54 mg) mmol anthracene into a 50 mL round bottom flask which was placed in the glove box for 24 hours. An excess amount of freshly cut potassium metal was added into 10 mL of double

distilled THF. The solution was stirred for about 5 minutes and was followed by an addition of 0.30 mmol anthracene. The solution was allowed to react for 3 hours, until the solution was dark blue color.

2% Hydroxylamine Solution, 2% ^{15}N-labeled Hydroxylamine Solution, FeTPP^{15}NO and FeOEP^{15}NO were synthesized by literature methods[74].

2-4. Reduction of metalloporphyrin and metalloporphinone complexes

Reduction of Mn^{III}TPPCl, Mn^{III}TPPOClO$_3$, Mn^{III}OEPCl, Mn^{III}OEPOClO$_3$, Mn^{III}OEPoneCl, Fe^{II}TPPNO and Fe^{II}TPP^{15}NO: 0.035 mmol Mn^{III}TPPCl (Mn^{III}OEPCl, Mn^{III}OEPOClO$_3$, Mn^{III}OEPoneCl, Fe^{II}TPPNO and Fe^{II}TPP^{15}NO) and 0.09 mmol of tetrabutylammonium borohydride was dissolved into a 25 mL Erlenmeyer flask with 10 mL of THF solution. The resultant solution was stirred for 5-10 minutes at 75 ˚C. After 5 minutes the solution was filtered and 25 mL anhydrous heptane was added into a 100 mL round bottom flask. The solution was set aside until it formed a precipitate. It was then filtered to obtain the final product. All the above experiments were carried out, under an inert atmosphere in a Vacuum atmosphere glove box.

Dark-violet single crystals suitable for X-ray analysis were obtained by slow diffusion of heptane into a chloroform solution of [Mn(TPP)Cl$^-$][NBu$_4$] at room temperature. Dark-red single crystals suitable for X-ray analysis were obtained by slow diffusion of heptane into a dichloromethane solution of [Mn(OEP)Cl] at room temperature. In both cases crystals were formed after several days.

Reduction of Fe(OEP)(NO): 0.04 (50 mg) mmol Fe(OEP)(NO) was dissolved into a 25 mL Erlenmeyer flask with 4 mL of distilled THF. 4 mL of the dark blue potassium anthracenide solution was added to the stirred Fe(OEP)(NO) solution above. The resultant solution was stirred for 5 minutes.

Reduction of Co^{II}TPP and Co^{II}TPPone: 0.030 mmol of Co^{II}TPP (Co^{II}TPPone) was dissolved into a 0.15 mmol 222 cryptand potassium 2-methyl-2-propanethiolate in 20 mL of chlorobenzene. The resultant solution was stirred for 1 h. After 1 h the solution was filtered and 50 mL anhydrous heptane was added. The solution was aside for until it formed a precipitate. The final product was isolated by filtration.

Dark-brown single crystals suitable for X-ray studies were obtained by slow diffusion of a heptane layer into a chlorobenzene solution of [Co(TPP)][K.222.cryptand] at room temperature, crystal was obtained after several days.

All the above experiments were carried out under an inert atmosphere in a Vacuum atmosphere glove box.

Chapter Three: Results and Discussion

3-1. UV-visible and infrared spectrum of one electron reduction cobalt tetraphenyl porphyrin complex

Reduction of Co(II) meso-tetraphenylporphyrin was done with excess amount of 222 cryptated potassium-2-methyl-2-propanethiolate in chlorobenzene yielded the Co(I) meso-tetraphenylporphyrin salt, [Co(TPP)] [K-222 cryptand]. The reaction is shown in Figure 3-1.

The UV-visible absorption spectrum of the reduction product $[Co^{I}(TPP)]^{-}$ is shown in Figure 3-2. The absorption spectrum was compared to that obtained by Weiss[31]. The absorption spectrum was consistent with the work done by Weiss[31] and Bower[27] with λ_{max} values of 366, 426 and 518 nm. The Soret band of the Co(II) complex was split into two bands at 366 and 426 nm from the value of 416 nm for $Co^{II}TPP$. The Q- band shifted from 532 nm to 518 nm.

The UV-visible spectrum of reduction product $[Co^{I}(TPP)]^{-}$ is a type of the d-hyperporphyrin, which is atypical for a cobalt complex[75]. This is due to back donation of the cobalt dπ electron toward the porphyrin π conjugated system.

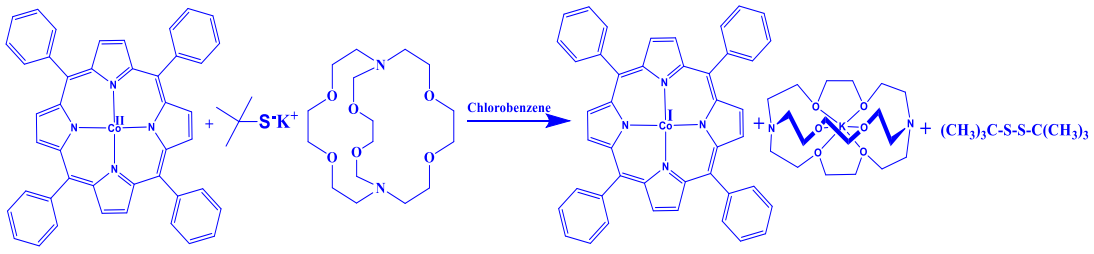

Figure 3-1. Scheme of the reduction of $Co^{II}TPP$ with 222 cryptated potassium thiolate

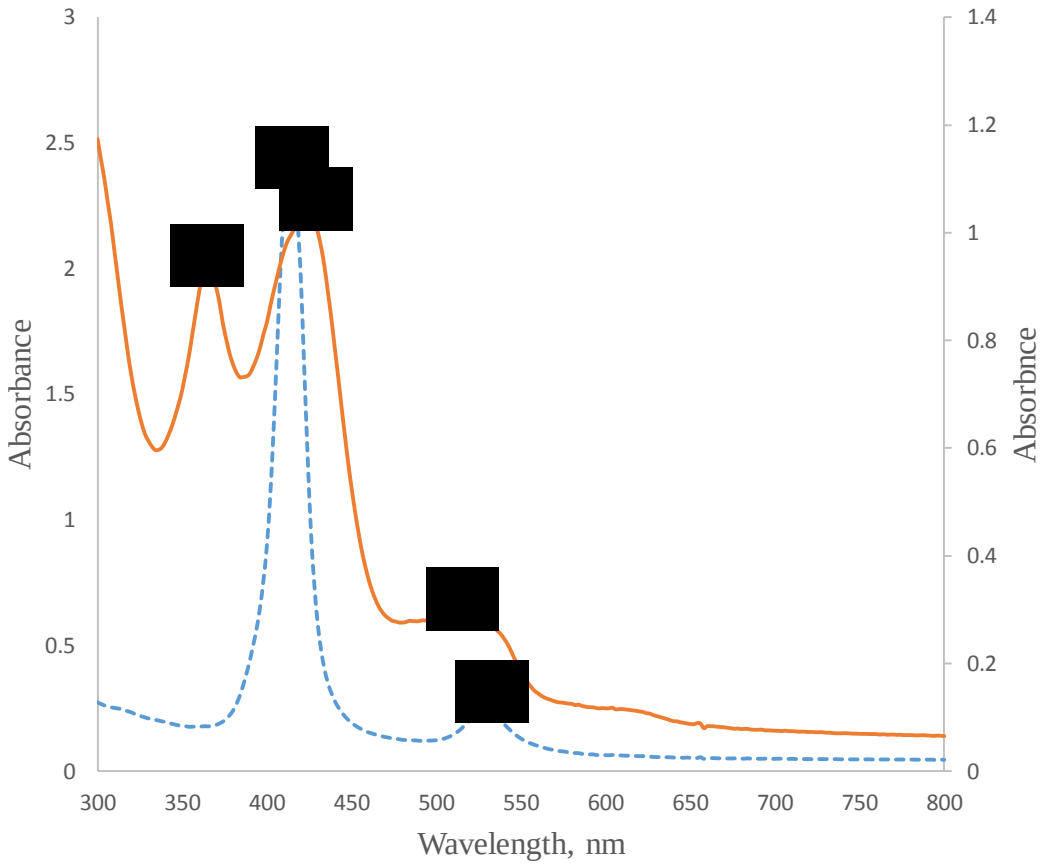

Figure 3-2. UV-visible spectra of the $Co^{II}TPP$ (dash line) and reduction product $[Co^{I}TPP]^{-}$ (solid line) in a chlorobenzene solution

$Co^{II}TPP$ is a paramagnetic complex where cobalt (II) ion has one unpaired electron with a configuration of $(d\pi)^6(dz^2)$, the calculated magnetic moment is somewhat more than the expected value of S=1/2 due to the mixing of the excited state by spin orbit coupling perturbation[30.] From the measurement of the magnetic susceptibility, the reduction of Co(I) complex forms a diamagnetic complex with a low spin d^8 configuration. The spectroscopic properties of the reduction product of the diamagnetic complex indicated that the reduction occurred mainly on the cobalt atom.

3-2. X- ray crystallographic studies of $[Co^{I}(TPP)]^{-}$

X-ray crystal structure analysis of reduction product $[Co^{I}(TPP)]^{-}$ was performed and crystallographic parameters like bond angles and bond lengths were summarized in Table 3-3.

The $[Co^{I}(TPP)]^{-}$ crystals were dark-brown prisms and good diffraction was observed. The X-ray structure of $[Co^{I}(TPP)]^{-}$ is shown in Figure 3-5. The Co(I) porphyrin exhibits some deviations from planarity (with the opposite pyrrole rings twisted by ~18°) but the Co ion is positioned almost exactly in the geometric center of the ligand. Co(I) ion has a square planar coordination with four pyrrole nitrogens.

Potassium [2.2.2] cryptand complex counter ion has a usual, ordered structure, with gauche conformation for all ethylene bridges in Figure 3-4. The average bond distance between K and oxygen atoms is 2.837 Å, where in the case of K and N is 3.03 Å, these values are similar to those found elsewhere[76]. Potassium ion is completely surrounded by the macrocyclic ligand.

Table 3-1. Average Bond Lengths (Å) of various metalloporphyrins

Atom-Atom	$[Co^{I}(TPP)]^{-}$ P	$[Ni^{II}(OEP)]$[34]	$[Co^{II}(pip)_2(TPP)]$[77]	$[Co^{I}(TPP)]^{-}$ [31]	$[Fe^{I}(TPP)]^{-}$[61]	$Co^{II}(TPP)$[78]	$[Fe^{II}(pip)_2(TPP)]$[79]
M-N	1.951	1.958	1.987	1.942	1.98	1.949	2.002
N-Cα	1.393	1.376	1.38	1.397	1.401	1.379	1.385
Cα-Cβ	1.434	1.443	1.444	1.434	1.429	1.433	1.438
Cβ-Cβ	1.351	1.346	1.344	1.337	1.338	1.354	1.34
Cα-Cm	1.387	1.371	1.393	1.38	1.385	1.386	1.397

P: Present work

Average bond angles in $[Co^{I}(TPP)]^{-}$

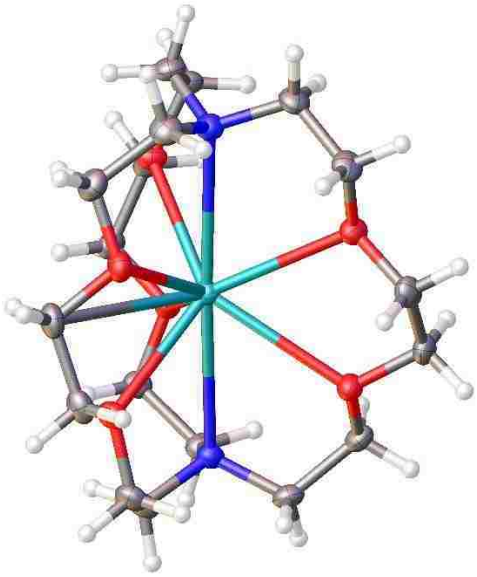

Atoms	Angles (deg)
$(Co\text{-}N\text{-}C\alpha)_{avg}$	127.9
$(C\alpha\text{-}N\text{-}C\alpha)_{avg}$	104.15
$(N\text{-}C\alpha\text{-}Cm)_{avg}$	125.22
$(C\alpha\text{-}N\text{-}C\alpha)_{avg}$	122.58

Figure 3-4. Potassium [2.2.2] cryptand cation

.

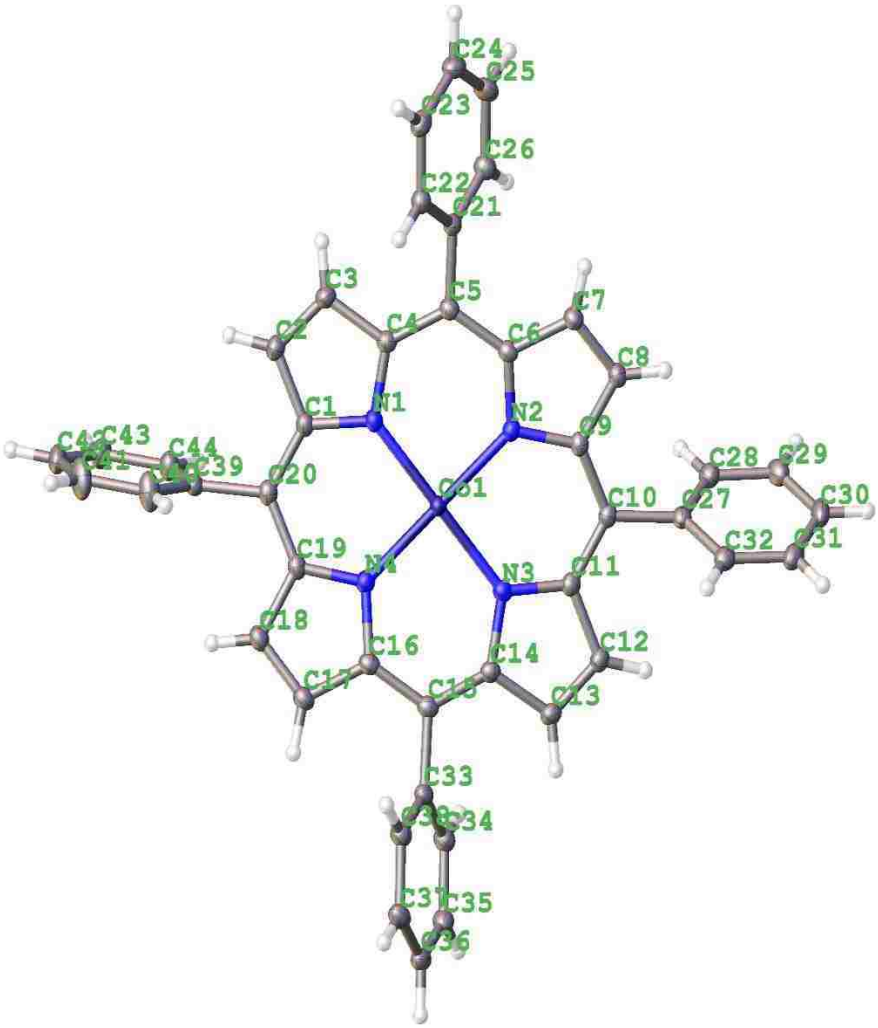

Figure 3-5. X-ray crystal structure of $Co^{I}(TPP)^{-}$

Table 3-2. Crystal data and structure refinement for $[Co^{I}(TPP)]^{-}$

Empirical formula	$C_{68}H_{69}N_6O_6ClKCo$
Formula weight	1199.77
Temperature/K	99.8(4)
Crystal system	monoclinic
Space group	$P2_1/n$
a/Å	13.94900(8)
b/Å	23.85506(15)
c/Å	17.81921(13)
α/°	90.00
β/°	97.4309(6)
γ/°	90.00
Volume/Å^3	5879.62(6)
Z	4
ρ_{calc}g/cm^3	1.355
μ/mm^{-1}	3.814
F(000)	2520.0
Crystal size/mm^3	0.3794 × 0.0955 × 0.0814
Radiation	CuKα (λ = 1.54184)
2Θ range for data collection/°	6.22 to 147.4
Index ranges	$-17 \leq h \leq 17$, $-29 \leq k \leq 29$, $-20 \leq l \leq 21$
Reflections collected	56801
Independent reflections	11735 [R_{int} = 0.0324, R_{sigma} = 0.0216]
Data/restraints/parameters	11735/0/749
Goodness-of-fit on F^2	1.024
Final R indexes [I>=2σ (I)]	R_1 = 0.0295, wR_2 = 0.0769
Final R indexes [all data]	R_1 = 0.0320, wR_2 = 0.0787
Largest diff. peak/hole / e Å^{-3}	0.28/-0.45

Table 3-3. Comparison of selected distance (Å) and angles (deg) in $[Co^{I}(TPP)]^{-}$

Atom	Atom	Distance (A˚)	Atom	Atom	Atom	Angle/˚
Co1	**N1**	**1.9494(11)**	**N1**	**Co1**	**N2**	**89.76(5)**
Co1	**N2**	**1.9527(11)**	**N1**	**Co1**	**N3**	**178.60(4)**
Co1	**N3**	**1.9504(11)**	**N1**	**Co1**	**N4**	**90.11(5)**
Co1	**N4**	**1.9511(11)**	**N3**	**Co1**	**N2**	**90.27(5)**
N1	**C1**	**1.3932(16)**	**N3**	**Co1**	**N4**	**89.89(5)**
N1	**C4**	**1.3910(17)**	**N4**	**Co1**	**N2**	**178.57(5)**
N2	**C6**	**1.3960(17)**	**C1**	**N1**	**Co1**	**127.55(9)**
N2	**C9**	**1.3909(16)**	**C4**	**N1**	**Co1**	**128.11(9)**
N3	**C11**	**1.3951(16)**	**C4**	**N1**	**C1**	**104.27(10)**
N3	**C14**	**1.3938(17)**	**C6**	**N2**	**Co1**	**128.05(8)**
N4	**C16**	**1.3950(18)**	**C9**	**N2**	**Co1**	**127.78(9)**
N4	**C19**	**1.3929(16)**	**C9**	**N2**	**C6**	**103.96(10)**
C1	**C2**	**1.4347(19)**	**C11**	**N3**	**Co1**	**127.34(9)**
C1	**C20**	**1.3851(19)**	**C14**	**N3**	**Co1**	**128.26(9)**
C2	**C3**	**1.351(2)**	**C14**	**N3**	**C11**	**104.26(10)**
C3	**C4**	**1.4363(18)**	**C16**	**N4**	**Co1**	**128.17(9)**
C4	**C5**	**1.3884(18)**	**C19**	**N4**	**Co1**	**127.85(9)**
C5	**C6**	**1.3893(18)**	**C19**	**N4**	**C16**	**103.96(11)**
C5	**C21**	**1.4926(18)**	**N1**	**C1**	**C2**	**110.73(11)**
C6	**C7**	**1.4302(18)**	**C20**	**C1**	**N1**	**125.46(12)**
C7	**C8**	**1.3511(19)**	**C20**	**C1**	**C2**	**123.70(12)**
C8	**C9**	**1.4318(18)**	**C3**	**C2**	**C1**	**107.11(12)**
C9	**C10**	**1.3887(18)**	**C2**	**C3**	**C4**	**107.19(12)**
C10	**C11**	**1.3842(19)**	**N1**	**C4**	**C3**	**110.67(11)**
C10	**C27**	**1.4970(17)**	**C5**	**C4**	**N1**	**125.44(12)**
C11	**C12**	**1.4306(18)**	**C5**	**C4**	**C3**	**123.85(12)**

3-3. UV-visible and infrared spectrum of cobalt(II) porphinone

The UV-visible spectra of the free base porphinone H_2OEPone and Co^{II}OEPone are shown in Figure 3-6. The UV-visible absorption spectrum of Co^{II}OEPone was consistent with the result obtained by Tutunea and Ryan[36], which confirms the successful insertion of the cobalt atom. For a better understanding of the starting porphinone (H_2OEPone) and the metal insertion product (Co^{II}OEPone), the UV-visible absorption data of both spectra are summarized in Table 3-4.

Comparing the UV-visible spectrum of the starting material, H_2OEPone, and the product Co^{II}OEPone, we observe that the Soret band shifted from 406 nm to 374 nm and 416 nm, while Q bands at 506, 548 nm disappeared, the 584 nm band shifted to 574 nm, and the 642 nm band shifted to 622 nm.

Table 3-4. The UV-visible absorption spectral data of porphinone and the cobalt porphinone complexes

Compounds	Solvent	B bands (nm)	Q bands (nm)	Reference
H_2OEPone	Chlorobenzene	406	506, 548, 584,642	this work
Co^{II}OEPone	Chlorobenzene	374,416	574,622	this work
Co^{II}OEPone	THF	374,412	618	36

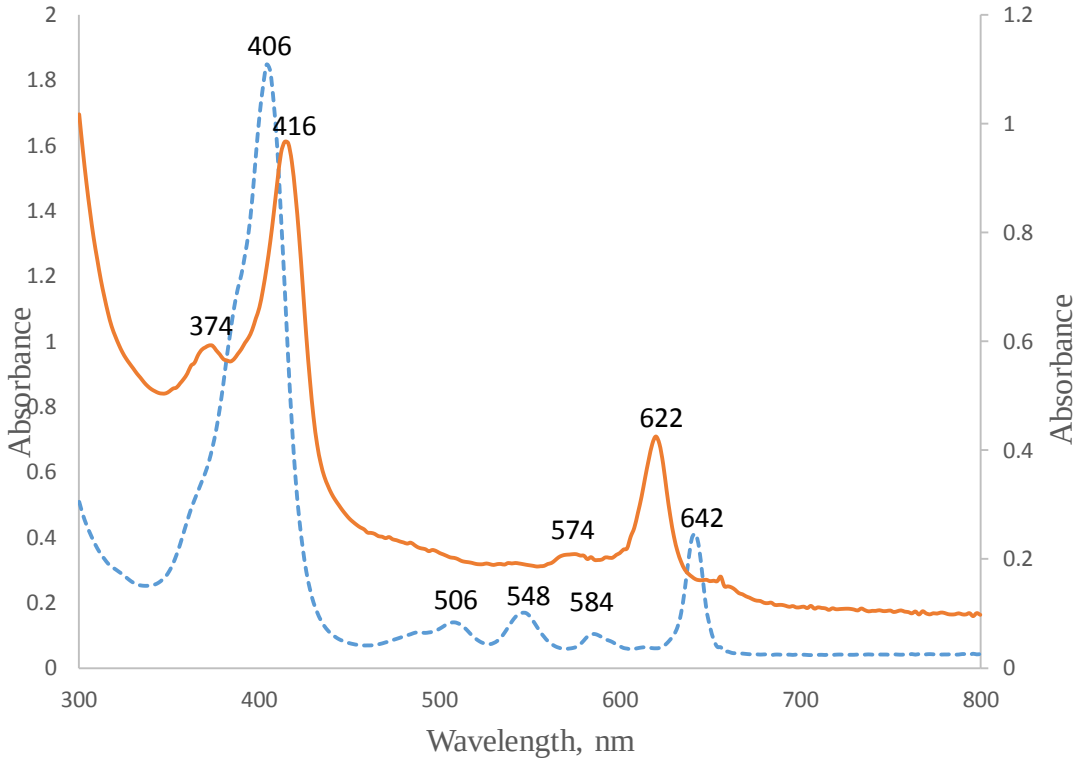

Figure 3-6. UV-visible spectra of H_2OEPone (dash line) and Co^{II}OEPone (solid line) in chlorobenzene solution

The FT-IR spectra of the starting material H_2OEPone and product Co^{II}OEPone are shown in Figure 3-7. The vibrations are summarized in Table 3-5.

Table 3-5. Infrared spectroscopic data of free base porphinone and cobalt porphinone complexes

Compound	Method	υ_{CO} (cm^{-1})	Other bands (cm^{-1})	References
H_2OEPone	KBr matrix	1716	1585, 1548	this work
Co^{II}OEPone	KBr matrix	1713	1595, 1562	this work
Co^{II}OEPone	THF	1709	1591, 1566	36

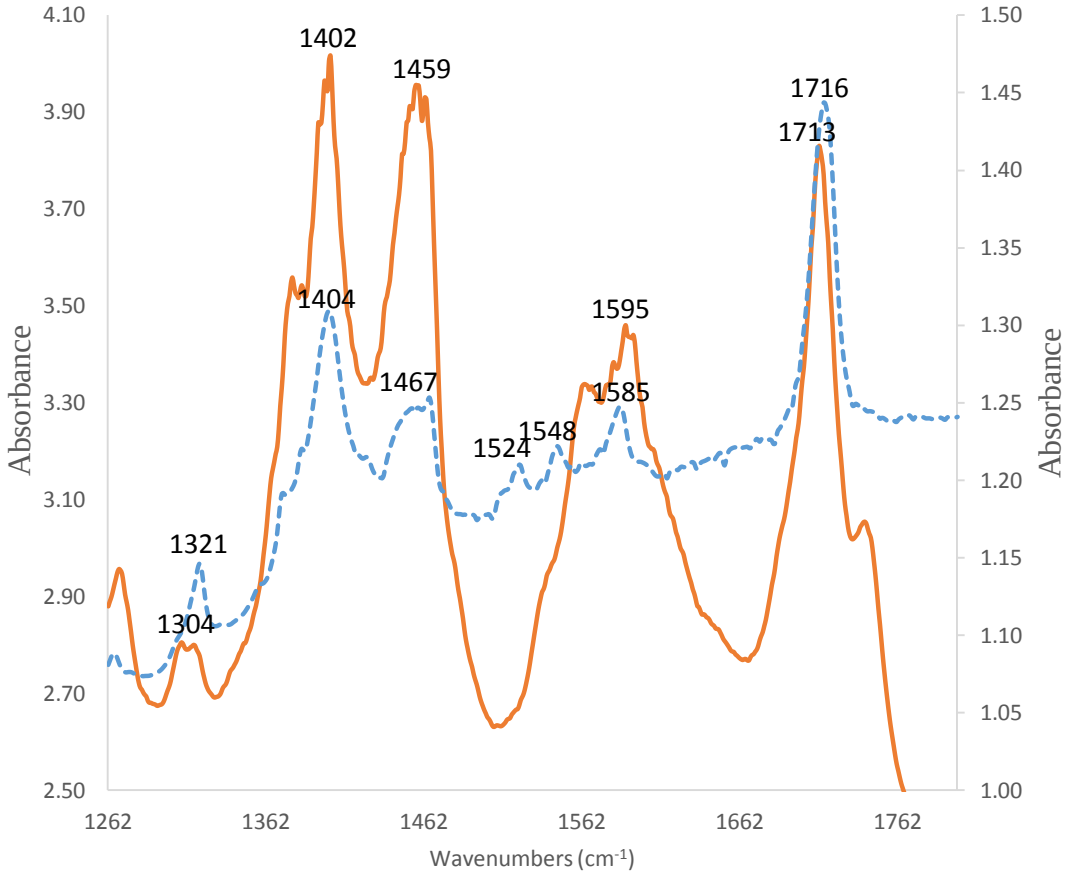

Figure 3-7. FT-IR spectra of the free base porphinone (dash line) and Co^{II}OEPone (solid line) in KBr matrix

From Table 3-5, we can see the infrared spectrum of Co^{II}OEPone was consistent with the results by Tutunea and Ryan[36]. Comparing this infrared spectrum with the one by Tutunea and Ryan[36], the υ_{CO} band was about 4 cm^{-1} higher. We found that when the cobalt was inserted into H_2OPEone, the υ_{CO} position did not change much (1716 cm^{-1} to 1713 cm^{-1}). Other bands changed from 1585 cm^{-1} to 1595 cm^{-1} and 1548 cm^{-1} to 1562 cm^{-1}. These results indicated that the insertion of cobalt into H_2OEPone is successful.

3-4. UV-visible and infrared spectrum of one electron reduced cobalt porphinone complex

Reduction of Co(II) octaethylporphinone was done with excess amount of 222 cryptated potassium-2-methyl-2-propanethiolate in chlorobenzene yielded a reduced product of Co(I) octaethylporphinone derivative of [Co(OEPone)] [K-222 cryptand] in Figure 3-8.

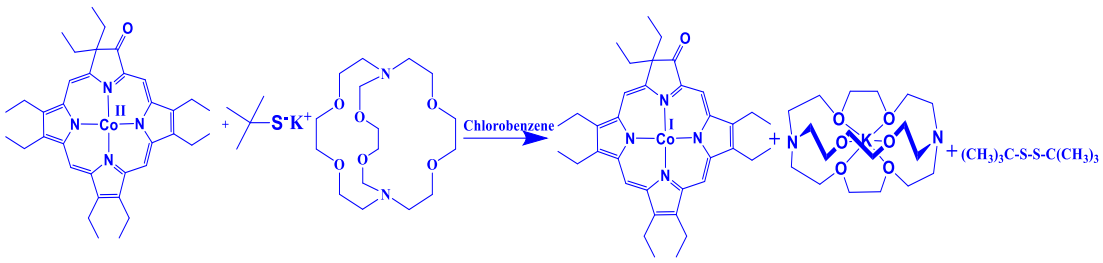

Figure 3-8. Scheme of the reduction of Co^{II}OEPone with 2.2.2 cryptated potassium-2-methyl-2-propane- thiolate

The UV-visible absorption spectra of the starting material Co^{II}OEPone and its reduction product of Co^{I}(OEPone)- with potassium 222-crypatand as a counter ion are shown in Figure 3-9. The UV-visible absorption spectrum of reduction product was compared to that reduction product that obtained in OTTLE cell spectroelectrochemistry by Tutunea and Ryan36. The absorption spectral data are summarized in Table 3-6.

Table 3-6. UV-visible absorption spectral data of cobalt porphinone complexes

Compound	Solvent	B bands (nm)	Q bands (nm)	References
Co^{II}OEPone	Chlorobenzene	374, 416	574, 622	this work
Co^{II}OEPone	THF	374, 412	606	36
$[Co^{I}(OEPone)]^{-}$	Chlorobenzene	362 416, 460	526, 612, 638	this work
$[Co^{I}(OEPone)]^{-}$	THF	354, 412	510, 606	36

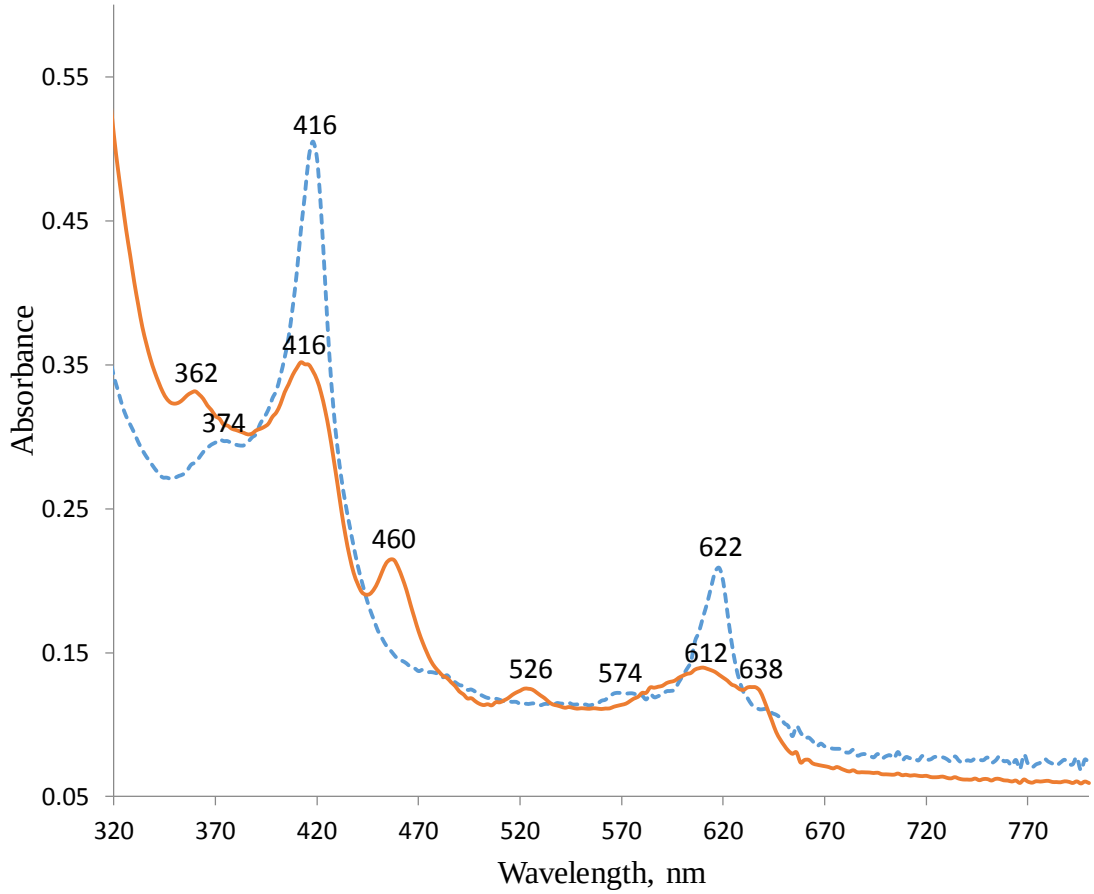

Figure 3-9. UV-visible spectra of the starting material Co^{II}OEPone (dash line) and reduction product $Co^{I}(OEPone)^{-}$ (solid line) in chlorobenzene solution

From the Table 3-6, the reduction of Co^{II}OEPone resulted in the molar absorptivity of the Soret band to decrease, the bands at 374 nm changed to 362 nm while the band at 416 nm did not shift but became weaker. There was a new band formed at 460 nm. At this moment we do not know the origin of this band but it did not appear in the spectroelectrochemical reduction[36]. In the reduction product $Co^{I}(OEPone)^{-}$ in the Q band region a new band appeared at 526 nm while 622 nm band from starting material split in two bands at 612 nm and 638 nm . While the reduction product UV-visible spectrum is fairly consistent, it does show significant differences with the results obtained by spectroelectrochemistry by Tutunea and Ryan[36].

The infrared spectra of the starting material Co^{II}OEPone and the reduction product $Co^{I}(OEPone)^{-}$ are shown in Figure 3-10. Tutunea and Ryan[36] examined the reduction of cobalt porphinone and cobalt porphinediones complex using infrared spectroelectrochemistry.

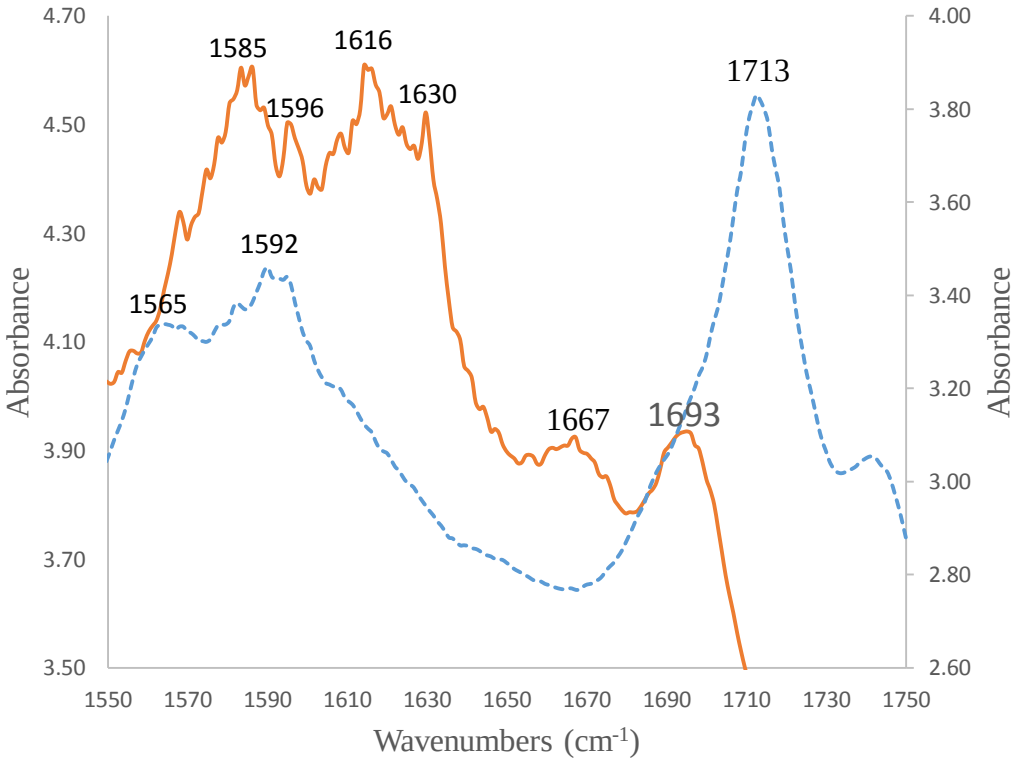

Figure 3-10. Infrared spectra of starting material Co^{II}OEPone (dash line) and reduction product $Co^{I}(OEPone)^{-}$ (solid line) in KBr matrix

For better comparison the infrared spectra of the starting material Co^{II}OEPone and the product $Co^{I}(OEPone)^{-}$ with our results, the results obtained by spectroelectrochemistry[36] and some predicted values by DFT calculations, the infrared data are summarized in Table 3-7.

Table 3-7. The infrared spectral data of cobalt and iron porphinone complexes

Compound	Method	υCO (cm-1)	Other bands (cm-1)	References
Co^{II}OEPone	KBr matrix	1713	1592, 1565	this work
Co^{II}(OEPone)	THF	1709	1589, 1562	36
Co^{II}(OEPone)	DFT	1700	…	36
$Co^{I}(OEPone)^-$	KBr matrix	1667	1693, 1616, 1596, 1585	this work
$Co^{I}(OEPone)^-$	THF	1674	1616,, 1593,1578	36
$Co^{I}(OEPone)^-$	DFT	1666	…..	36
$Fe^{I}(OEPone)^-$	DFT	1643	……	36

From Table 3-7, the carbonyl band for starting material Co^{II}OEPone was observed at 1713 cm^{-1}. Upon reduction the band shifted to 1667 cm^{-1} which was close to the values of 1709 cm^{-1} and 1674 cm^{-1} by spectroelectrochemistry[36]. The υ_{CO} band down shifted by 46 cm^{-1}. In the case of spectroelectrochemistry this shift was 33 cm^{-1}. Our research group performed some DFT calculations for Co^{II}OEPone and its reduction product, the υ_{CO} values are 1700 cm^{-1} and 1666 cm^{-1}, a downshift of 34 cm^{-1}. These frequency values are consistent with our results.

In addition to υ_{CO} bands, bands at 1693, 1616, 1596, 1585 cm^{-1} are observed. These values are consistent with results obtained by spectroelectrochemistry except the band at 1693 cm^{-1}. This band may be due to the same species which led to the absorption peak at 460 nm. At this moment we don't know the origin this bands.

3-5. Synthesis and one electron reduction of manganese(III) octaethylporphyrin chloride

Manganese(III) octaethylporphyrin was prepared from free base octaethylporphyrin. The UV-visible spectra of product $Mn^{III}OEPCl$ and H_2OEP are shown in Figure 3-11. The UV-visible spectrum of $Mn^{III}OEPCl$ are consistent with the absorption spectrum obtained by Dolphin[80] and Scheidt[72]. In comparing the spectra of H_2OEP with $Mn^{III}OEPCl$, the Soret band at 398 nm disappeared and a new split Soret band formed at 360 and 466 nm. In the Q-band region 498, 530, 568 and 620 nm bands disappeared and new bands appeared at 556 and 588 nm. From the analysis of UV-visible absorption spectra, we can see that the metal insertion of 'Mn-Cl' was successful.

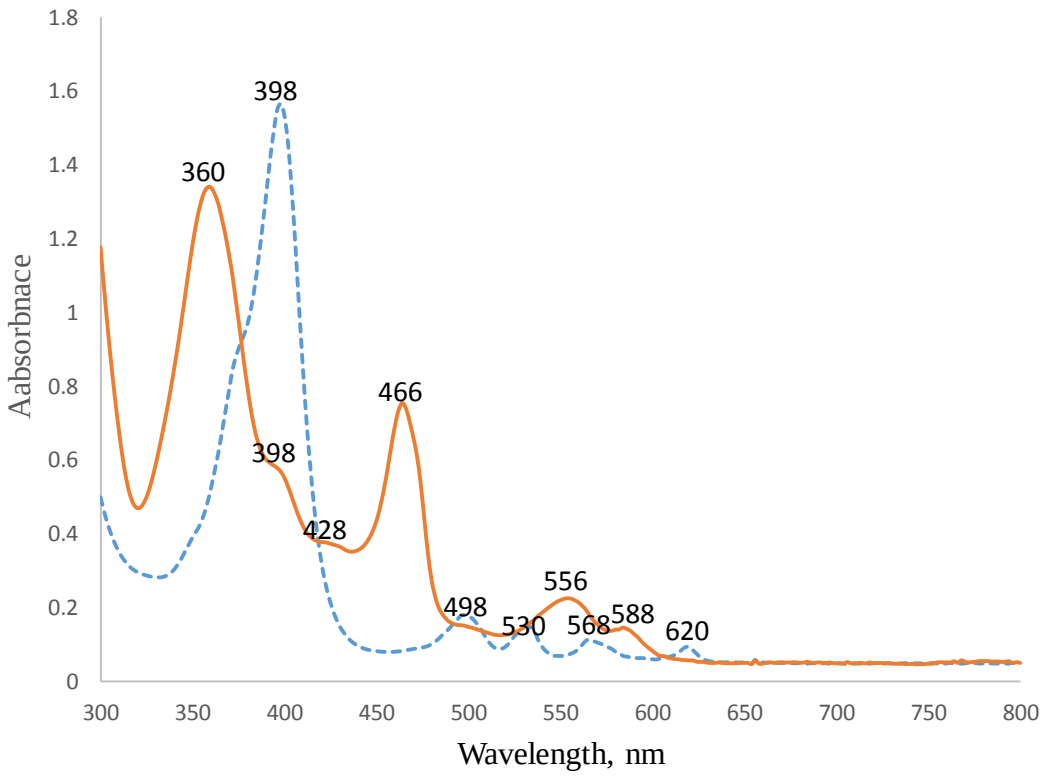

Figure 3-11. The UV-visible absorption spectra of starting material H_2OEP (dash line) and product $Mn^{III}OEPCl$ (solid line) in THF solution

The one electron reduction of Mn(III)OEPCl was carried out with tetrabutylammonium borohydride in a THF solution. The results are showed below. The UV-visible spectra of starting material Mn^{III}OEPCl and its reduction product Mn^{II}OEP shown in Figure 3-12. The absorption spectrum of reduction product Mn^{II}OEP was compared with the electrochemical reduction spectrum of Mn^{III}OEPCl which have done by Tutunea[41]. The data are summarized in Table 3-8.

Table 3-8. The UV-visible spectral data of manganese octaethylporphyrin complexes

Compound	Soret bands (nm)	Q bands (nm)	References
Mn^{III}OEPCl	360, 428, 466	556, 588	this work
Mn^{III}OEPCl	358, 424, 471	558, 589	72
Mn^{II}OEP	346, 418	540, 582	this work
Mn^{II}OEP	418	544	41

Generally, manganese(III) porphyrin complexes usually exhibit multiple Soret bands which arise from the interaction of the manganese orbitals and the porphyrin π*-orbital. Porphyrin (π) - metal (dπ) charge-transfer transitions are similar to porphyrin (π- π*) transitions. When the π-d charge-transfer and the π- π* Soret transitions occur at equivalent energies, they produce a split Soret. The band at 600 nm is assigned to a charge-transfer transition π-dπ, the band at 550 nm is due to the ligand transitions π- π* and it can be related to a usual Q band[81].

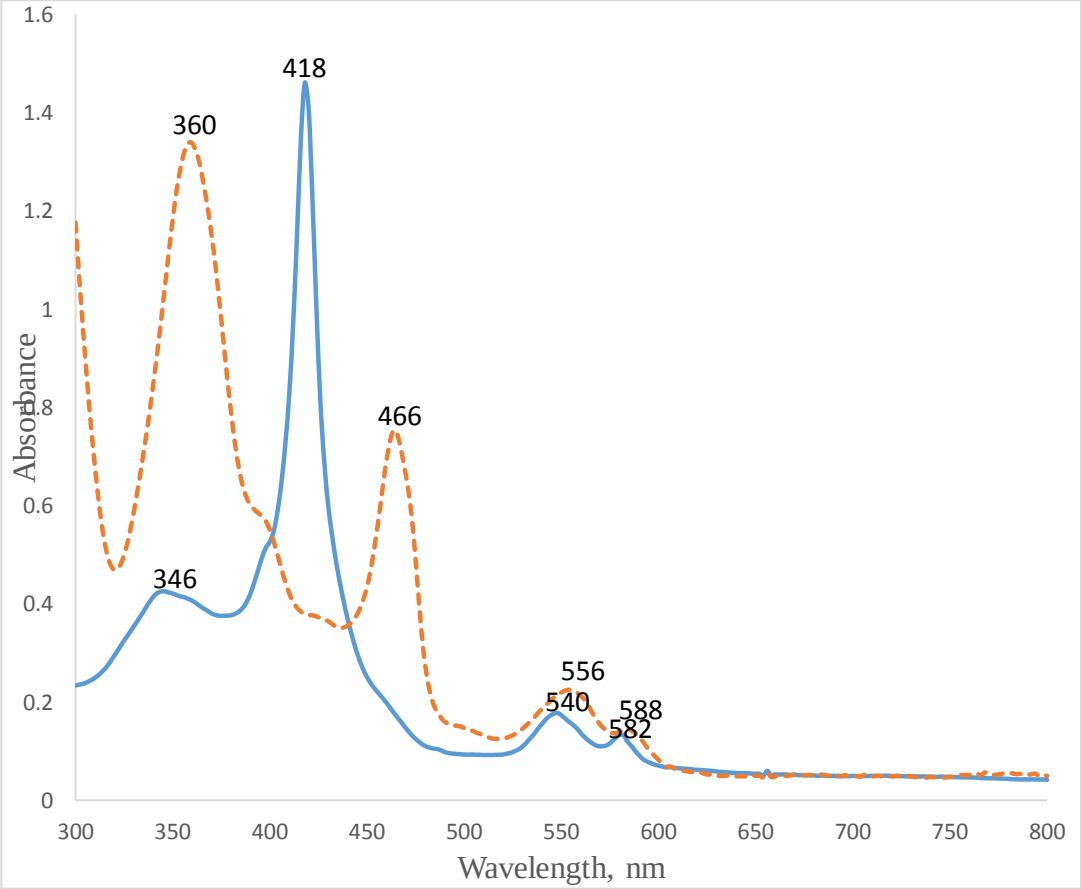

Figure 3-12. The UV-visible absorption spectra of starting material $Mn^{III}OEPCl$ (dash line) and reduction product $Mn^{II}OEP$ (solid line) in THF solution

In the one electron reduction of $Mn^{III}OEPCl$, the split-Soret bands at 360 nm and 466 nm disappeared and a new strong absorption Soret band formed at 418 nm. This strong Soret band generally indicates a Mn(II) species. Along with 418 nm band there was a new band formed at 346 nm, which was not observe by spectroelectrochemical reduction. In the Q-band region, bands at 556 nm and 588 nm were blue shifted to 540 nm and 582 nm. These results are consistent with spectroelectrochemical reduction[41], indicating that $Mn^{II}OEP$ had been formed.

3-6. One electron reduction of manganese octaethylporphyrin perchlorate

The UV-visible spectra of the starting material [Mn^{III}(OEP)($OClO_3$)] and its reduction product Mn^{II}OEP are shown in Figure 3-13. The absorption spectrum of the starting material [Mn^{III}(OEP)($OClO_3$)] was consistent with the work done by Scheidt[72] which shown λ_{max} (wavelength/nm) are 372, 434, 475 and 551, which indicated that we prepared [Mn^{III}(OEP)($OClO_3$)].

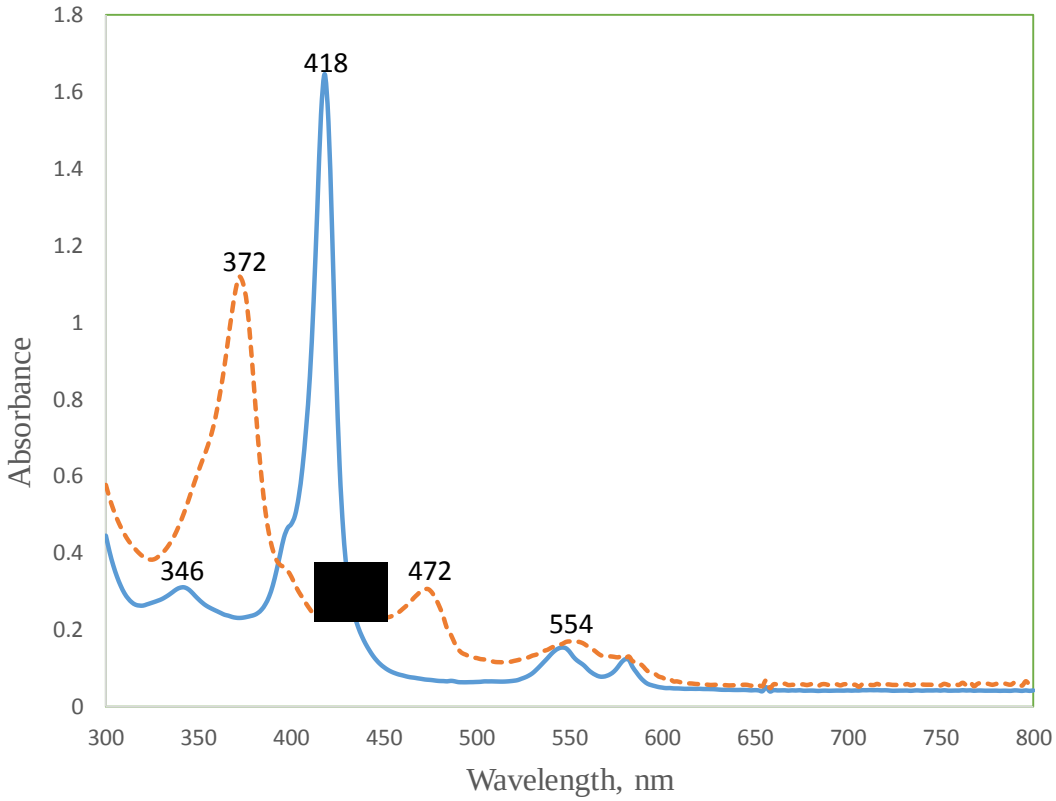

Figure 3-13. The UV-visible spectra of [Mn^{III}(OEP)($OClO_3$)] (dash line) and Mn^{II}OEP (solid line) in THF solution

Our reduction product has the absorption bands (wavelength/nm) at 346,418, 540 and 582. These values are identical to the reduction spectra obtained from $Mn^{III}OEPCl$. This is an indication that both reduction products are $Mn^{II}OEP$ and that a chloride ion had not coordinated with Mn. Both reduction spectra are shown in Figure 3-14.

Table 3-9. UV-visible absorption spectral data of manganese octaethylporphyrin complexes

Compound	Soret bands (nm)	Q bands (nm)	References
$Mn^{III}OEPCl$	360, 428, 466	556, 588	this work
$[Mn^{III}(OEP)(OClO_3)]$	372, 434, 472	554	this work
$Mn^{II}OEP$ [A]	346, 418	540, 582	this work
$Mn^{II}OEP$ [B]	346, 418	540, 582	this work

[A] Reduction product obtained from starting material $Mn^{III}OEPCl$
[B] Reduction product obtained from starting material $[Mn^{III}(OEP)(OClO_3)]$

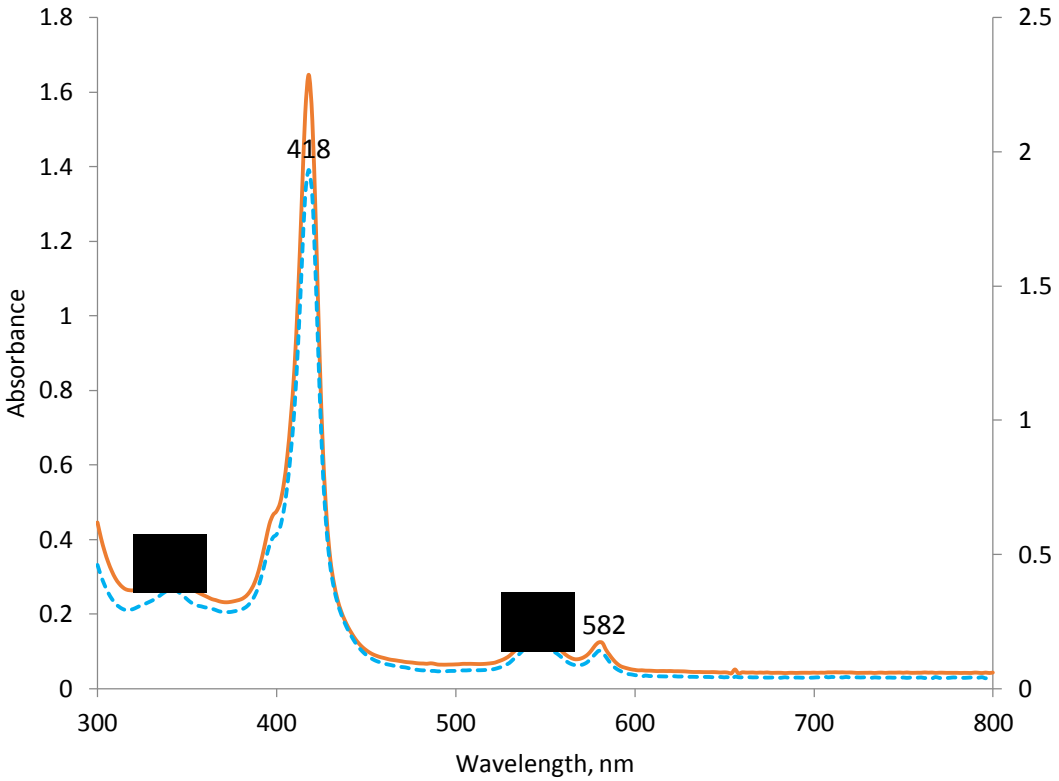

Figure 3-14. UV-visible spectra of reduction products $Mn^{II}OEP$ from the starting material $[Mn^{III}(OEP)(OClO_3)]$ (solid line) and $Mn^{III}OEPCl$ (dash line) in THF solution

3-7. X-ray crystallographic studies of $Mn^{III}OEPCl$

X-ray crystal structure analysis of manganese(III) octaethylporphyrin chloride was performed and crystallographic parameters are summarized in Table 3-12. $Mn^{III}OEPCl$ crystals are dark-red prisms and good diffraction were observed. The X-ray crystal structure of $Mn^{III}OEPCl$ is shown in Figure 3-15.

The metal Mn(III) ion has a square-pyramidal geometry with four pyrrole nitrogen and axial chloride ion. The Mn(III) ion is displaced from mean plane of N atoms by 0.273(2) Å. Coordination of all N atoms is symmetrical. Eight ethyl groups are alternatively rotated cis and trans relatively to the planes of the adjacent 5-membered rings. The

average bond distance between metal manganese and four pyrrole nitrogens is 2.017 Å. The distance between manganese and axial chloride ion is 2.391 Å and average bond angle between $(Np\text{-}Mn\text{-}Np)_{avg}$ is 109.69˚ (deg).

Table 3-10. Comparison of selected bond lengths in manganese and iron complexes

Bond (Å)	$Mn^{III}OEPCl$	$Mn^{III}TPPCl$[51]	$Fe^{III}TPPCl$[82]
M-Np	2.017	2.009	2.049
C_a-C_b	1.443	1.433	1.429
C_b-C_b	1.361	1.356	1.38
C_a-C_m	1.381	1.394	1.399

From the Table 3-10, the average M-Np bond length is more in $Fe^{III}TPPCl$ when compared to $Mn^{III}TPPCl$ and $Mn^{III}OEPCl$, C_a-C_b bond lengths increase, and the Ca-Cm bond lengths are shorter in Mn^{III} OEPCl.

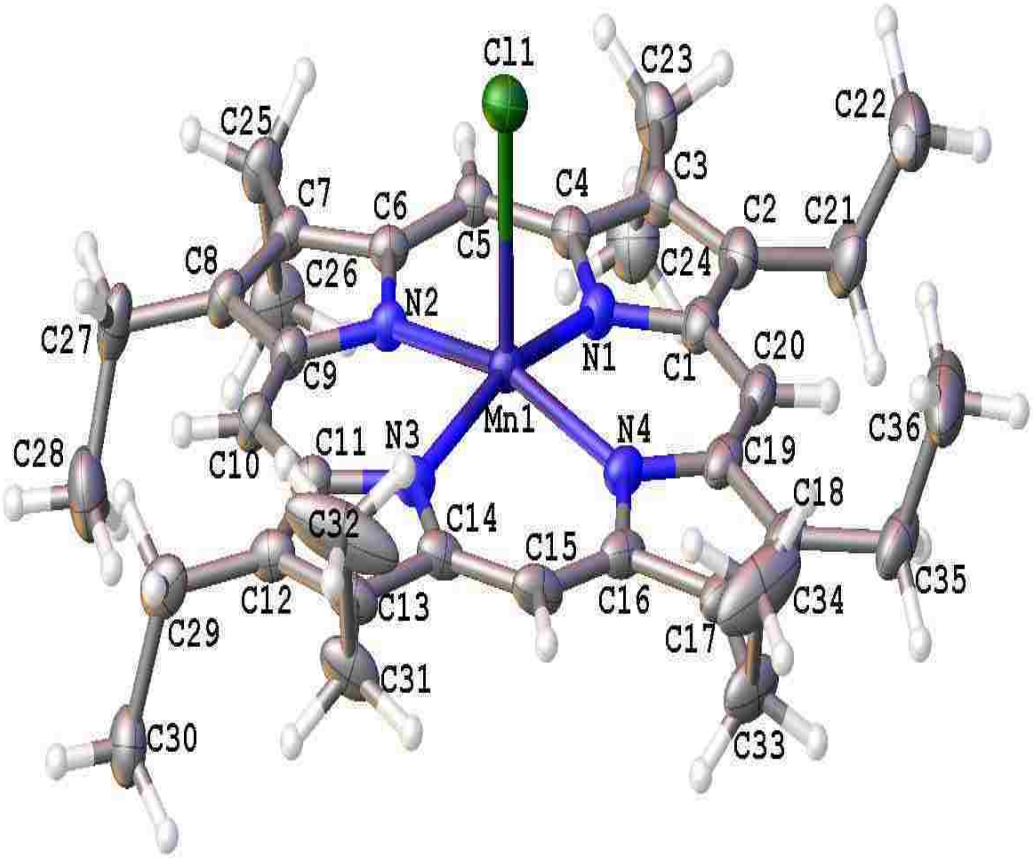

Figure 3-15. X-ray structure of the Mn^{III}OEPCl

Table 3-11. Crystal data and structure refinement for $Mn^{III}OEPCl$

Empirical formula	$C_{36}H_{44}N_4ClMn$
Formula weight	623.14
Temperature/K	99.95(10)
Crystal system	monoclinic
Space group	$P2_1/c$
a/Å	12.5986(2)
b/Å	13.3031(2)
c/Å	19.7951(3)
α/°	90.00
β/°	103.8886(18)
γ/°	90.00
Volume/$Å^3$	3220.64(10)
Z	4
$\rho_{calc}mg/mm^3$	1.285
m/mm^{-1}	0.524
F(000)	1320.0
Crystal size/mm^3	0.9455 × 0.0755 × 0.0572
Radiation	Mo Kα (λ = 0.7107)
2Θ range for data collection	5.62 to 58.92°
Index ranges	$-17 \leq h \leq 16$, $-18 \leq k \leq 17$, $-27 \leq l \leq 24$
Reflections collected	30331
Independent reflections	8016[R(int) = 0.0344]
Data/restraints/parameters	8016/0/387
Goodness-of-fit on F^2	1.049
Final R indexes [I>=2σ (I)]	$R_1 = 0.0472$, $wR_2 = 0.1162$
Final R indexes [all data]	$R_1 = 0.0624$, $wR_2 = 0.1273$
Largest diff. peak/hole / e $Å^{-3}$	0.99/-0.54

Table 3-12. Comparison of selected bond distances (Å) and bond angles (deg) in Mn^{III}OEPCl

Atom	Atom	Length/Å	Atom	Atom	Atom	Angle/°
Mn1	Cl1	2.3915(6)	N1	Mn1	Cl1	96.25(5)
Mn1	N1	2.0171(17)	N1	Mn1	N3	164.98(7)
Mn1	N2	2.0131(17)	N1	Mn1	N4	89.23(7)
Mn1	N3	2.0186(17)	N2	Mn1	Cl1	94.60(5)
Mn1	N4	2.0173(17)	N2	Mn1	N1	88.70(7)
N1	C1	1.372(3)	N2	Mn1	N3	89.21(7)
N1	C4	1.386(3)	N2	Mn1	N4	163.87(7)
N2	C6	1.382(2)	N3	Mn1	Cl1	98.75(5)
N2	C9	1.376(3)	N4	Mn1	Cl1	101.52(5)
N3	C11	1.376(3)	N4	Mn1	N3	88.65(7)
N3	C14	1.382(2)	C1	N1	Mn1	127.29(14)
N4	C16	1.389(3)	C1	N1	C4	105.48(17)
N4	C19	1.374(3)	C4	N1	Mn1	126.81(14)
C1	C2	1.443(3)	C6	N2	Mn1	127.13(14)
C1	C20	1.391(3)	C9	N2	Mn1	127.11(13)
C2	C3	1.364(3)	C9	N2	C6	105.47(16)
C2	C21	1.503(3)	C11	N3	Mn1	126.90(13)
C3	C4	1.441(3)	C11	N3	C14	105.28(17)
C3	C23	1.504(3)	C14	N3	Mn1	127.28(15)
C4	C5	1.380(3)	C16	N4	Mn1	127.02(15)
C5	C6	1.381(3)	C19	N4	Mn1	126.89(14)
C6	C7	1.441(3)	C19	N4	C16	105.86(17)
C7	C8	1.361(3)	N1	C1	C2	110.53(19)
C7	C25	1.500(3)	N1	C1	C20	124.6(2)
C8	C9	1.444(3)	C20	C1	C2	124.8(2)

3-8. UV-visible spectra of the manganese(II) tetraphenylporphyrin complex

The UV-visible spectra of the starting material $Mn^{III}TPPCl$ and the one electron reduction product $Mn^{II}TPPCl^-$ are shown in Figure 3-16. To better analyze the product that we obtained from $Mn^{III}TPPCl$ reduction, we compared our UV-visible absorption peaks with what have been obtained by Schultz[83] by spectroelectrochemistry. Our results are consistent with them.

As we have seen in $Mn^{III}OEPCl$, split-Soret bands were observed in $Mn^{III}TPPCl$. Upon reduction a sharp Soret band was observed at 434nm and the two Soret bands at 376 nm and 478 nm disappeared. In the Q-band region the bands decreased from 582 nm to 568 nm, 620 nm to 606 nm and the band at 532 disappeared. By seeing the changes in UV-visible absorption spectra, we can assume that a one electron reduction occurred. Absorption spectral data of $Mn^{III}OEPCl$ and $Mn^{III}TPPCl$ and their reduction products $Mn^{II}OEP$ and $Mn^{II}TPPCl^-$ are summarized in Table 3-13.

Table 3-13. The UV-visible absorption spectral data of manganese porphyrin complexes

Compound	Soret bands	Q bands	References
$Mn^{III}OEPCl$	360, 428, 466	556, 588	this work
$Mn^{III}TPPCl$	376, 402, 478	582, 620	this work
$Mn^{II}OEP$	346, 418	540, 582	this work
$Mn^{II}TPPCl^-$	410, 434	568, 606	this work

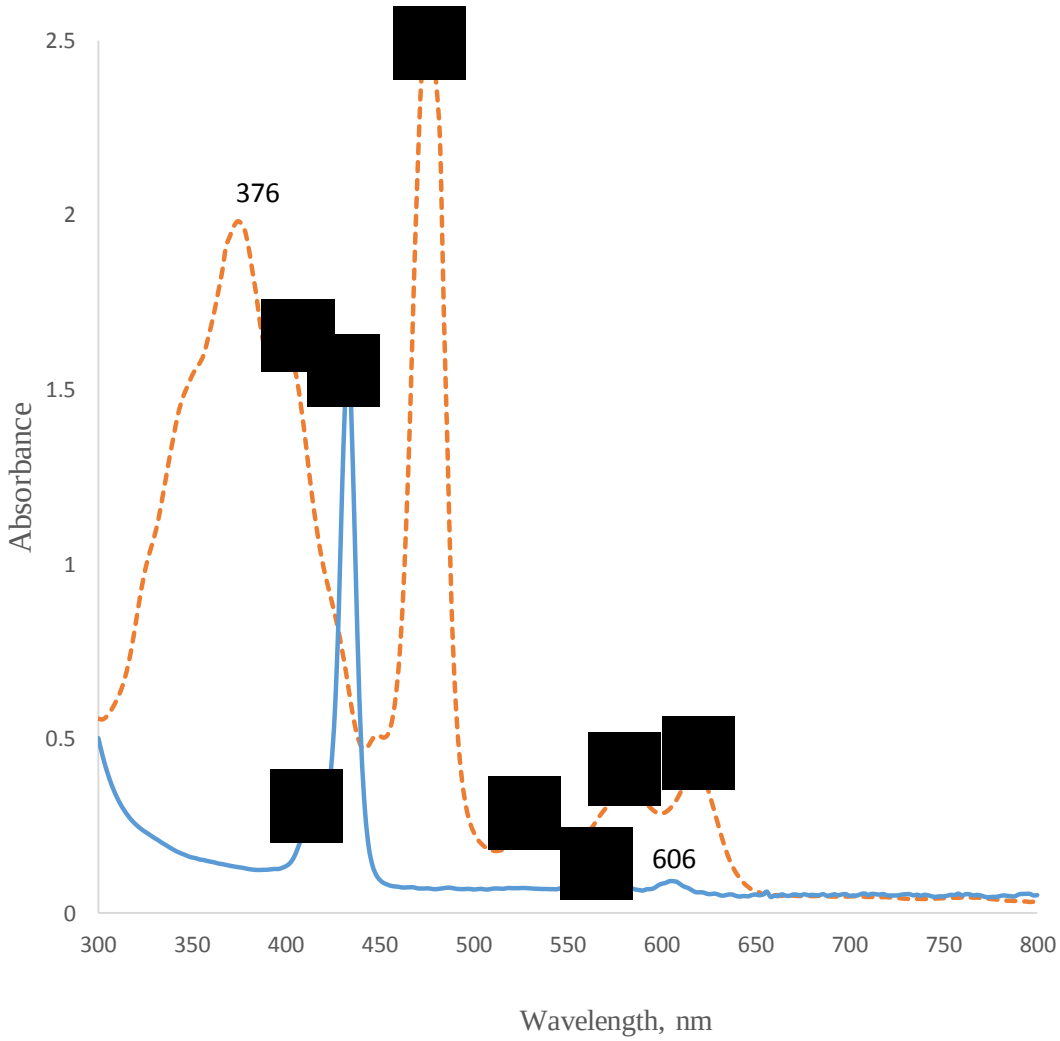

Figure 3-16. UV-visible absorption spectra of starting material $Mn^{III}TPPCl$ (dash line) and one electron reduction product $Mn^{II}TPP$ (solid line) in THF solution

3-9. One electron reduction of the manganese(III) tetraphenylporphyrin perchlorate complex

The UV-visible spectra of starting material [Mn^{III}(TPP)($OClO_3$)] and reduction product Mn^{II}TPP are shown in Figure 3-17. The absorption spectrum of the starting material [Mn^{III}(TPP)($OClO_3$)] is consistent with the work done by Zhi and Li[22] which showed λ_{max} (wavelength/nm) at 385, 403, 477, 510, 568 and 601.

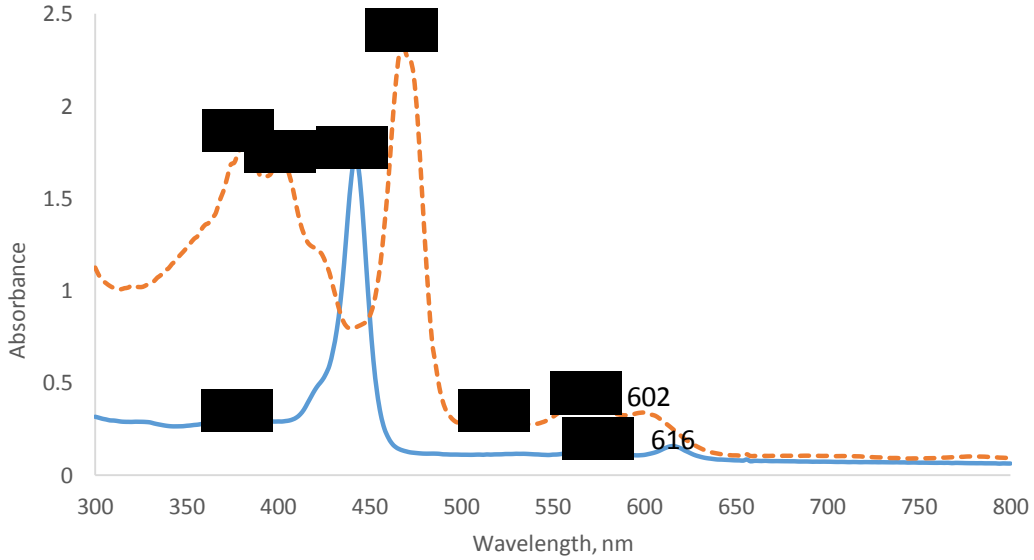

Figure 3-17. The UV-visible spectra of [Mn^{III}(TPP)($OClO_3$)] (dash line) and Mn^{II}TPP (solid line) in THF solution

Table 3-14. UV-visible absorption spectral data of manganese tetraphenylporphyrin complexes

Compound	Solvent	B bands (nm)	Q bands (nm)	Reference
$Mn^{III}TPPCl$	THF	376, 402, 476	532, 582, 620	this work
$Mn^{III}TPPCl$		374, 395, 473	525, 577, 616	22
$Mn^{III}TPPOClO_3$	THF	385, 404, 468	518, 570, 602	this work
$Mn^{III}TPPOClO_3$		385, 403, 477	510, 568, 601	22
$[Mn^{II}TPPCl]^-$ (from MnTPPCl)	THF	410, 434	568, 606	22
$Mn^{II}TPP$ from ($MnTPPOClO_3$)	THF	378, 442	576, 616	this work

From Figure 3-17 the reduction product has absorption bands (wavelength/nm) at 378, 442, 576 and 616. These values are different from the reduction spectra obtained from $Mn^{III}TPPCl$. This is an indication that the reduction products are different. From $[Mn^{III}(TPP)(OClO_3)]$, $Mn^{II}TPP$ was obtained, while from $Mn^{III}TPPCl$, $[Mn^{II}TPPCl]^-$ was obtained. Both reduction spectra are shown in Figure 3-18.

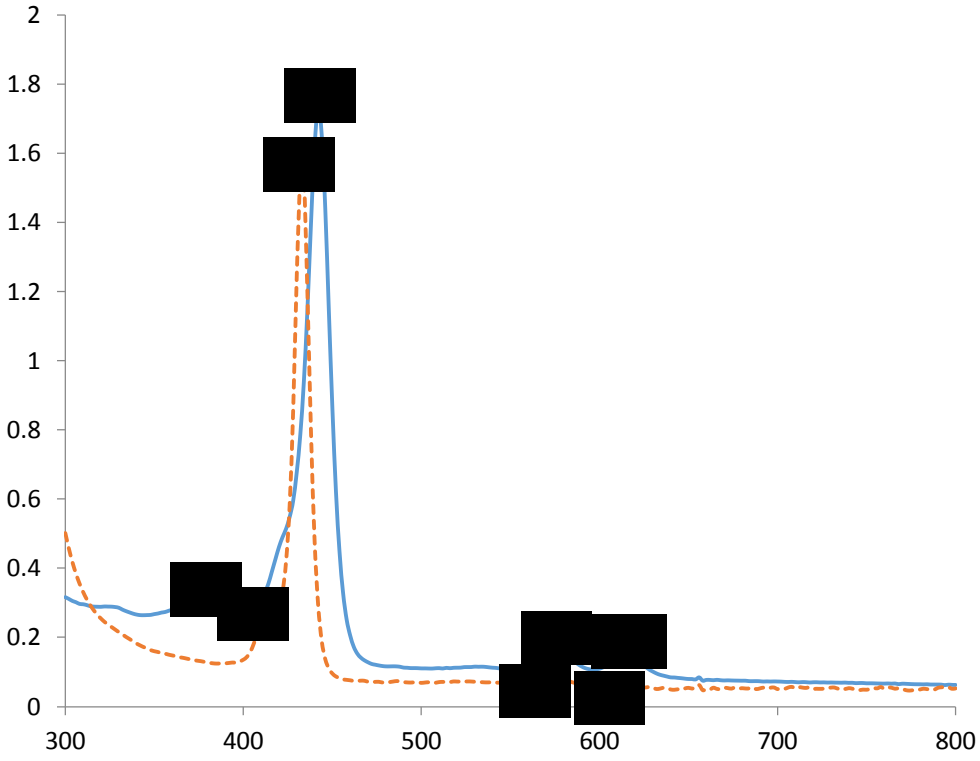

Figure 3-18. UV-visible spectra of $[Mn^{II}TPPCl]^-$ obtained from $Mn^{III}TPPCl$ (dash line) and $Mn^{II}TPP$ obtained from $Mn^{III}TPPOClO_3$ (solid line) in THF solution

3-10. X-ray crystallographic analysis of $[Mn^{II}TPPCl]^-$

X-ray crystallographic studies of $[Mn^{II}TPPCl]^-$ was performed and the crystallographic parameters are summarized in Table 3-17. The crystal was a dark-violet prism and good diffraction was observed. X-ray crystal structure of the Mn(II) tetraphenylporphyrin chloride anion and the tetrabutylammonium cation is shown in Figure 3-19.

Mn(II) ion has a square-pyramidal coordination, and was displaced from the mean plane of N atoms by 0.584(2) Å. Interestingly, only the lone pair of N3 is pointed toward Mn(II) ion. For other N atoms, their LPs are oriented below the coordination plane. This asymmetry may be a result of H-bond formation C-H…N3 with solvate chloroform molecule. Also, there are multiple C-H…Cl interactions.

Table 3-15 list of the average manganese-nitrogen bond lengths and manganese out-of-plane displacement for a number of Mn(II) and Mn(III) tetraphenylporphyrin complexes. The average bond distance of our reduced complex $[Mn^{II}TPPCl]^-$ between Mn-Np is 2.149 Å. The distance between Mn-Cl is 2.404 Å and the manganese displacement is 0.584 Å. When we compare our results with a low spin five coordinated $Mn^{II}TPP(NO)$, it has an average bond length between Mn-Np is 2.004 Å and a manganese displacement of 0.34 Å. In the case of the high spin five coordinated $Mn^{II}TPP$(1-methylimidazole), there is an average bond length between Mn-Np of 2.128 Å and a manganese displacement of 0.512 Å. Values for five coordinated $Mn^{III}TPPCl$ have an average bond length for Mn-Np of 2.009 Å and a manganese displacement of 0.27 Å. All of the above three complexes has smaller Mn-Np average bond length as compared to our reduced manganese complex.

Table 3-15. Comparison of metal-nitrogen bond distances in different manganese porphyrins

Compound	out-of-plane dist	Mn-N_{av} dist	Reference
$Mn^{II}TPP$ [a]	---	2.084	49
$Mn^{II}TPP(NO)$[b]	0.34	2.004	84
$Mn^{II}TPP(1\text{-}MeIm)$	0.512	2.128	84
$Mn^{II}TPP(Cl)^-$	0.584	2.149	this work
$Mn^{II}TPP(Cl)^-$	0.641	2.16	83
$Mn^{III}TPPCl$	0.27	2.009	83

[a] Four coordinated [b] Low spin five coordinated

When comparing our reduced complex, $Mn^{II}TPP(Cl)^-$, with a similar complex $Mn^{II}TPP(Cl)^-$ with potassium cryptated cation as a counter ion synthesized by Valentine[49], our complex has a smaller Mn-Np distances (2.15 Å) and the manganese displacement is longer (0.641 Å). This may be due to the effect of the different counter ion.

The average Mn-Np distance and Mn out-of-plane displacement for $Mn^{III}TPPCl$ are 2.009 Å and 0.27 Å. These are significantly smaller than those of $Mn^{II}TPP(Cl)^-$. This is quite expected because the $Mn^{III}TPPCl$ complex has d^4 complex which has vacant d_{x2-y2} orbital. Even though $Mn^{II}(TPP)Cl^-$ is isoelectronic with the $Fe^{III}TPP(Cl)$ complex, the latter complex has an average bond length for Fe-Np of 2.049 Å and an iron displacement of 0.383 Å. The longer metal-nitrogen bond length and metal out-of displacement of our complex, $Mn^{II}TPP(Cl)^-$ reflects a larger ionic radius.

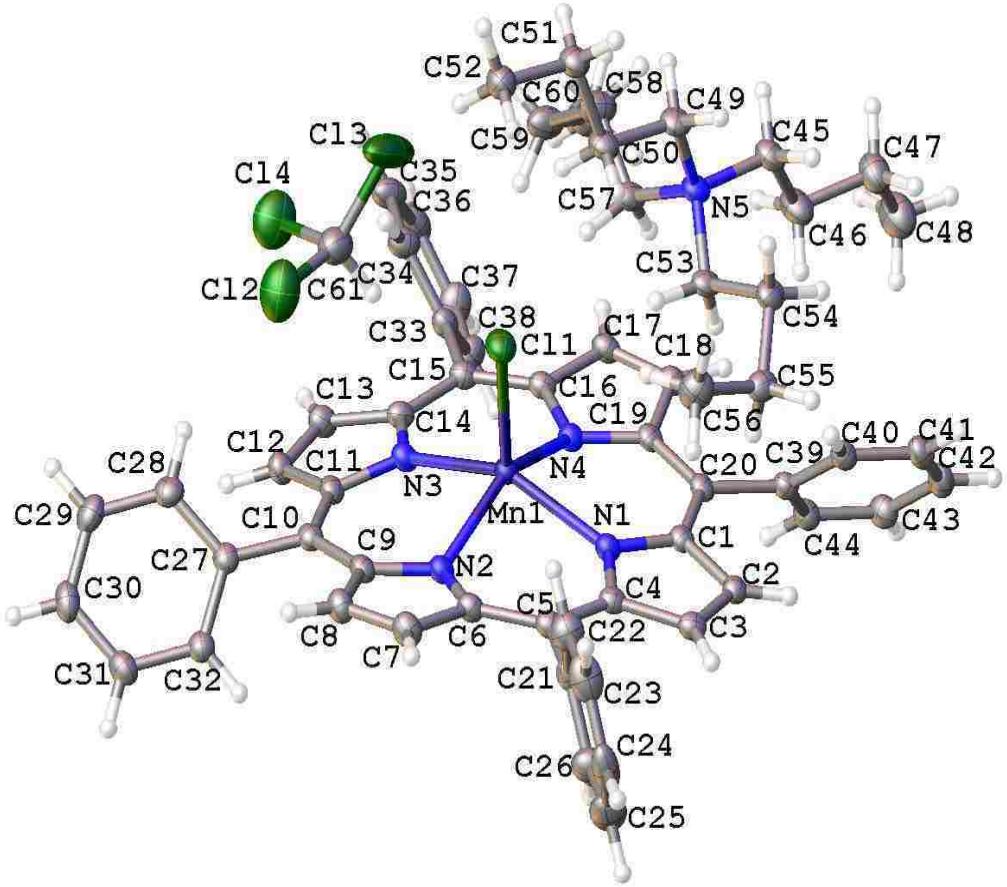

Figure 3-19. X-ray crystal structure of (NBu_4) ($Mn^{II}TPPCl$).$CHCl_3$

Table 3-16. Crystal data and structure refinement for (NBu_4) $(Mn^{II}TPPCl).CHCl_3$

Empirical formula	$C_{61}H_{65}N_5Cl_4Mn$
Formula weight	1064.92
Temperature/K	100.00(10)
Crystal system	monoclinic
Space group	$P2_1/n$
a/Å	14.30337(14)
b/Å	16.70252(12)
c/Å	22.9736(2)
α/°	90.00
β/°	90.8763(8)
γ/°	90.00
Volume/Å^3	5487.80(9)
Z	4
ρ_{calc}mg/mm^3	1.289
m/mm^{-1}	4.078
F(000)	2236.0
Crystal size/mm^3	0.7840 × 0.2072 × 0.1025
Radiation	Cu Kα (λ = 1.5418)
2Θ range for data collection	6.54 to 147.9°
Index ranges	$-17 \leq h \leq 17$, $-20 \leq k \leq 20$, $-28 \leq l \leq 28$
Reflections collected	49735
Independent reflections	10915[R(int) = 0.0408]
Data/restraints/parameters	10915/0/644
Goodness-of-fit on F^2	1.045
Final R indexes [I>=2σ (I)]	R_1 = 0.0528, wR_2 = 0.1464
Final R indexes [all data]	R_1 = 0.0569, wR_2 = 0.1509
Largest diff. peak/hole / e Å^{-3}	1.75/-1.18

Table 3-17. Comparison of selected distance (Å) and angles (deg) in (NBu_4)($Mn^{II}TPPCl$).$CHCl_3$

Atom	Atom	Length/Å	Atom	Atom	Atom	Angle/°
Mn1	Cl1	2.4037(7)	N1	Mn1	Cl1	106.28(5)
Mn1	N1	2.157(2)	N2	Mn1	Cl1	100.66(5)
Mn1	N2	2.1433(19)	N2	Mn1	N1	86.23(7)
Mn1	N3	2.150(2)	N2	Mn1	N3	85.72(7)
Mn1	N4	2.1452(19)	N2	Mn1	N4	148.06(7)
N1	C1	1.374(3)	N3	Mn1	Cl1	104.78(6)
N1	C4	1.373(3)	N3	Mn1	N1	148.84(7)
N2	C6	1.375(3)	N4	Mn1	Cl1	111.29(6)
N2	C9	1.367(3)	N4	Mn1	N1	84.91(7)
N3	C11	1.370(3)	N4	Mn1	N3	86.19(7)
N3	C14	1.371(3)	C1	N1	Mn1	127.70(15)
N4	C16	1.375(3)	C4	N1	Mn1	123.93(16)
N4	C19	1.373(3)	C4	N1	C1	106.96(19)
C1	C2	1.450(3)	C6	N2	Mn1	121.01(15)
C1	C20	1.411(3)	C9	N2	Mn1	124.05(15)
C2	C3	1.358(3)	C9	N2	C6	107.17(19)
C3	C4	1.443(3)	C11	N3	Mn1	126.98(15)
C4	C5	1.411(3)	C11	N3	C14	107.04(19)
C5	C6	1.408(4)	C14	N3	Mn1	125.98(16)
C5	C21	1.500(3)	C16	N4	Mn1	123.94(16)
C6	C7	1.443(3)	C19	N4	Mn1	125.89(15)
C7	C8	1.356(4)	C19	N4	C16	107.14(19)
C8	C9	1.450(3)	N1	C1	C2	109.31(19)
C9	C10	1.417(3)	N1	C1	C20	124.9(2)

3-11. UV-visible and infrared spectra of manganese(III) porphinone chloride

The UV-visible absorption spectra of H_2OEPone and Mn^{III}(OEPone)Cl are shown in Figure 3-20. The absorption spectrum of Mn^{III}(OEPone)Cl is consistent with the results obtained by our research group previously41. This confirmed that the insertion of '-Mn^{III}Cl' was successful. The starting material H_2OEPone and metal inserted product Mn^{III}(OEPone)Cl UV-visible absorption spectral data are summarized in Table 3-18.

Table 3-18. The UV-visible absorption spectral data of porphinone and the manganese(III) porphinone complexes

Compounds (solution)	B bands (nm)	Q bands (nm)	Reference
H_2OEPone (THF)	404	510, 548, 588, 642	this work
Mn^{III}(OEPone)Cl (THF)	362, 402, 432, 470	644	this work
Mn^{III}(OEPone)Cl (THF)	364, 478	642	41

In comparing the UV-visible absorption spectrum of the starting material H_2OEPone with the product Mn^{III}(OEPone)Cl, a split-Soret band appeared at 362 nm and 470 nm , along with weaker bands at 402 nm and 432 nm. On the Q band region, the bands at 510, 548, 588 nm were bleached and the 642 nm band shifted to 644 nm. A split-Soret band is generally indicative of the formation of a Mn(III) porphyrin.

The FT-IR spectra of H_2OEPone and Mn^{III}(OEPone)Cl are shown in Figure 3-21 and the vibrations are summarized in Table 3-19. From the Table 3-19, the Mn^{III}(OEPone)Cl that we have obtained is consistent with the spectrum obtained by Tutunea[41].

Table 3-19. The infrared spectroscopic data of porphinone and the manganese porphinone complexes

Compound	Method	υ_{CO} (cm^{-1})	Other bands (cm^{-1})	References
H_2OEPone	KBr matrix	1716	1585, 1548	this work
Mn^{III}OEPoneCl	KBr matrix	1714	1578, 1541	this work
Mn^{III}OEPoneCl	THF solution	1721	1578, 1542	41

The υ_{CO} band for Mn^{III}(OEPone)Cl is observed at 1714 cm^{-1}, which is 7 cm^{-1} lower than that obtained by spectroelectrochemistry[41]. For other bands 1578 and 1542 cm^{-1} are similar to 1578 and 1541 cm^{-1}. By seeing the changes in both UV-visible and infrared spectroscopy, we can conclude that the insertion of '-Mn^{III}Cl' to free base porphyrin was successful.

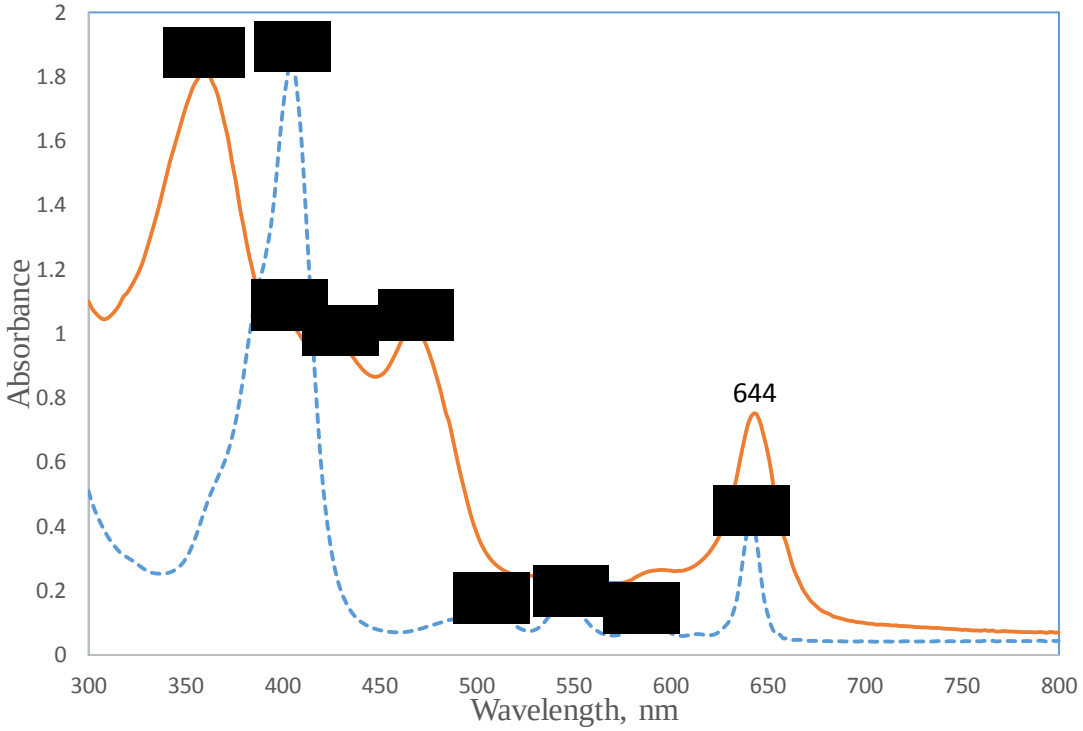

Figure 3-20. UV-visible spectra of H_2OEPone (dash line) and Mn^{III}(OEPone)Cl (solid line) in THF solution

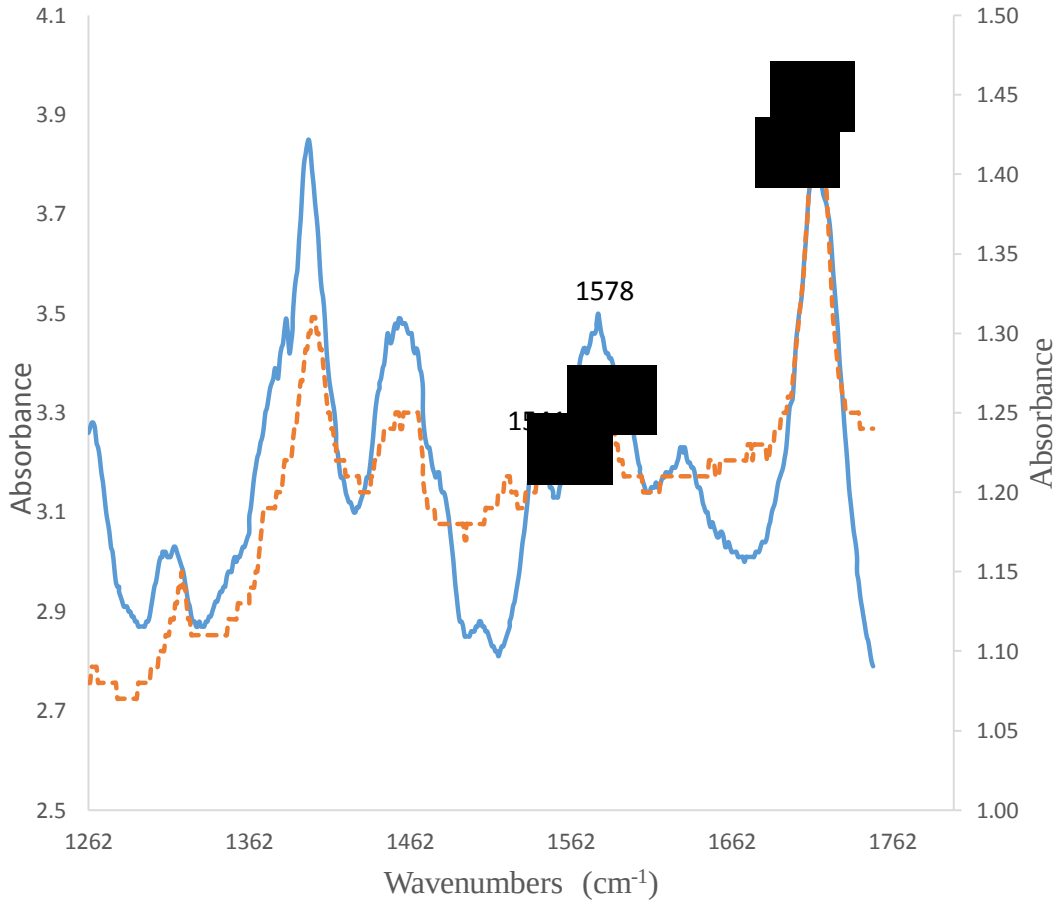

Figure 3-21. FT-IR spectra of H_2OEPone (dash line) and Mn^{III}(OEPone)Cl (solid line) in KBr matrix

3-12. UV-visible and infrared spectra of the Mn(II) porphinone complex

The UV-visible absorption spectra of Mn^{III}(OEPone)Cl and its reduced product Mn^{II}(OEPone) are shown in Figure 3-22. The absorption spectrum of our reduced product was compared to that obtained by OTTLE spectroelectrochemistry[41]. The results are qualitatively consistent. The UV-visible spectral data are summarized in Table 3-20.

Table 3-20. The UV-visible absorption spectral data of manganese porphyrin complexes

Compounds	Solvent	B bands (nm)	Q bands (nm)	Reference
Mn^{III}(OEPone)Cl	THF	362, 402, 432, 470	644	this work
Mn^{III}(OEPone)Cl	THF with 0.1 M TBAP	364, 478	642	41
Mn^{II}(OEPone)	THF	338,430	576, 622	this work
Mn^{II}(OEPone)	THF with 0.1 M TBAP	440	624	41

In the one electron reduction of Mn^{III}(OEPone)Cl complex, the split Soret bands at 362 and 470 nm disappeared, the Soret band was observed at 430 nm and a small band at 338 nm. In the Q band region, the band at 644 nm shifted to 622 nm. Similar results were observed in the electrochemical reduction. No broad band at 600-800 nm were seen in the visible region. This may suggest that the reduction occurred at the metal center, with back bonding of the metal d-π orbital to the porphyrin π^* orbital.

The infrared spectra of Mn^{III}(OEPone)Cl and the reduction product Mn^{II}(OEPone) are shown in Figure 3-23. The carbonyl vibration for the starting material Mn^{III}(OEPone)Cl is at 1714 cm^{-1}, with additional bands observed at 1632 and 1578 cm^{-1}. Upon a one

electron reduction, the carbonyl vibration band shifted to 1699 cm^{-1}. Other bands shifted from 1578 cm^{-1} to 1567 cm^{-1}.

Table 3-21. The infrared spectral data of manganese and iron porphinone complexes

Compound	Method	υ_{CO} (cm^{-1})	Other bands (cm^{-1})	References
Mn^{III}OEPoneCl	KBr matrix	1714	1632, 1578	this work
Mn^{III}OEPoneCl	THF	1721	1578	41
Mn^{III}OEPoneCl	DFT	1716	…	41
Mn^{II}OEPone	KBr matrix	1699	1602, 1567	this work
Mn^{II}OEPone	THF	1706	1545	41
Mn^{II}OEPone	DFT	1709	…..	41
$[Fe^{I}(OEPone)]^{-}$	DFT	1643	……	36

From the Table 3-21, upon reduction, υ_{CO} downshifted by 15 cm^{-1}. For the electrochemical reduction this shift was 15cm^{-1}, and the DFT calculation was 7 cm^{-1}. This shift in carbonyl is similar to shifts seen in the Fe^{III}OEPoneCl reduction (16 cm^{-1}) where the carbonyl vibration was weakened due to metal d- π back bonding to porphyrin π^* orbital. This suggests that the reduction occurred at a metal center.

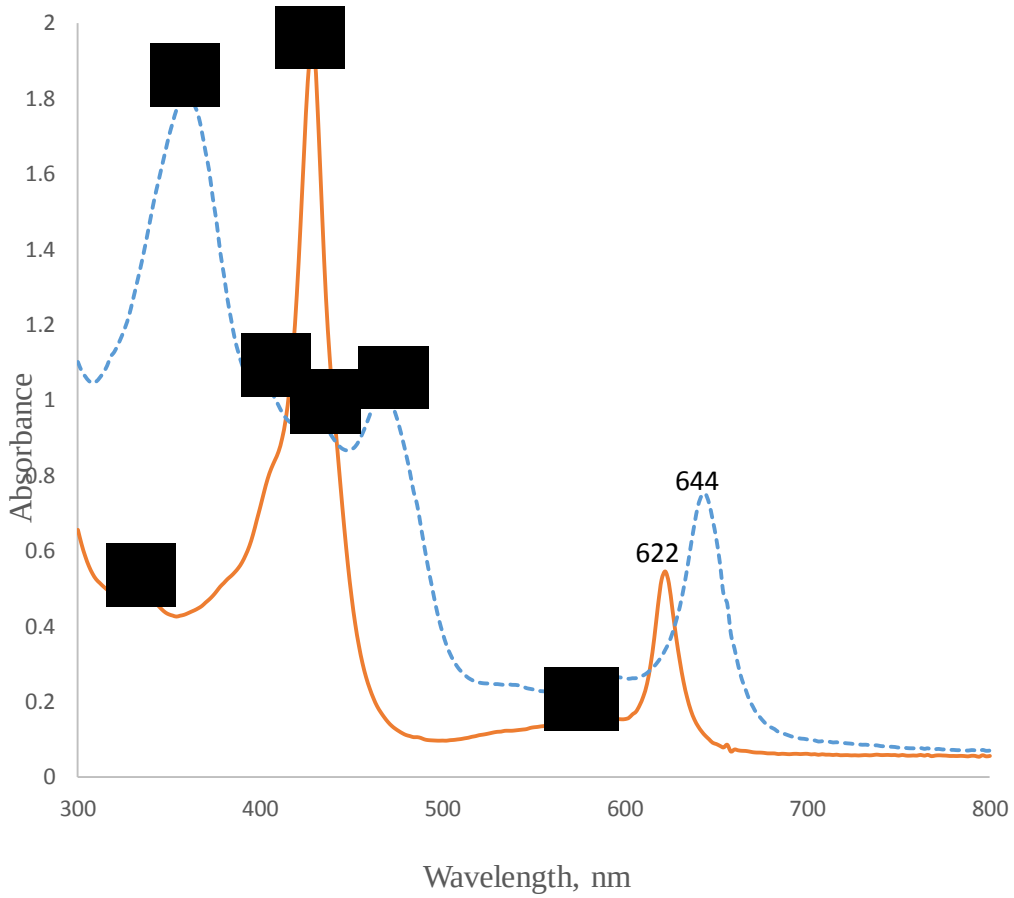

Figure 3-22. UV-visible spectra of starting material Mn^{III}OEPoneCl (dash line) and reduction product Mn^{II}OEPone (solid line) in THF solution

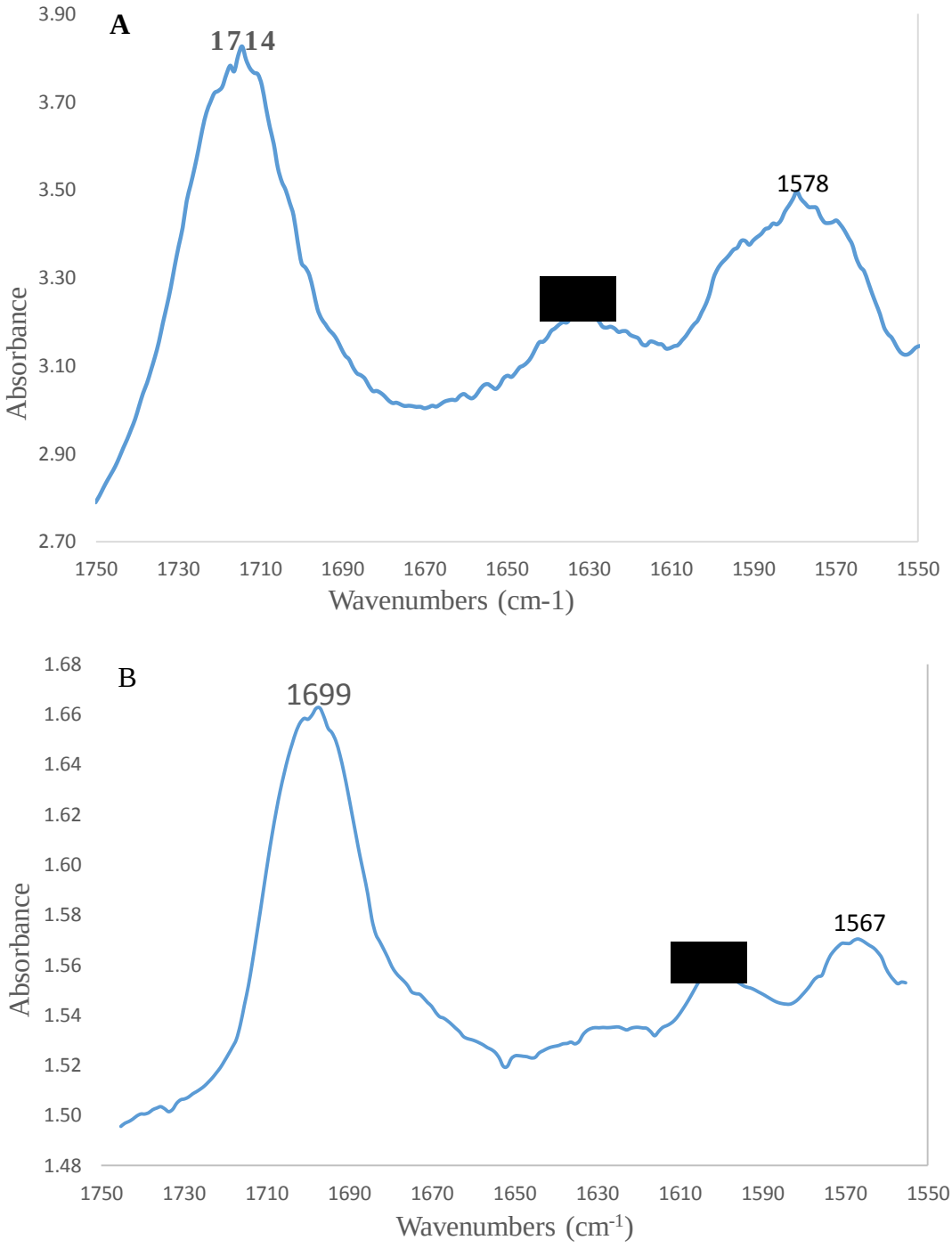

Figure 3-23. **A** FT-IR spectra of starting material Mn^{III}OEPoneCl **B** FT-IR spectrum of reduction product Mn^{II}OEPone in KBr Spectrum

3-13. UV-visible and infrared spectrum of iron tetraphenylporphyrin nitrosyl and their reduction products

The UV-visible spectra of Fe^{III}TPPCl and its nitrosyl product Fe^{II}(TPP)(NO) are shown in Figure 3-24. The UV-visible absorption spectrum of Fe^{II}(TPP)(NO) was consistent with the results obtained by Kadish[85], which showed that the insertion of '-NO' was successful. For a better understanding of the starting material Fe^{III}TPPCl and product Fe^{II}(TPP)(NO), the UV-visible absorption data are summarized in Table 3-22 below.

Table 3-22. The absorption spectral data of iron porphyrin and iron porphyrin nitrosyl complexes

Compound	B bands (nm)	Q bands (nm)	Solvent	Reference
Fe^{III}TPPCl	372, 420	510, 582, 696	THF	this work
Fe^{II}(TPP)(NO)	414	538, 610	THF	this work
Fe^{II}(TPP)(NO)	408	536, 607	THF	70
Fe^{II}(TPP)(NO)	410	540, 610	PhCN	85

Comparing the UV-visible spectrum of the starting material Fe^{III}TPPCl with Fe^{II}(TPP)(NO), the Soret band shifted from 420 nm to 414 nm and band at 372 nm disappeared, in the Q-band region 510, 582 and 696 nm disappeared and new bands formed at 538 and 610 nm.

The FT-IR spectrum of Fe^{II}(TPP)(NO) is shown in Figure 3-25. The shoulder peak at 1677 cm^{-1} represents υ_{NO} frequency, which is compatible with the reported value 1676 cm^{-1} by Yoshimura[91] and significantly lower than which is obtained by resonance Raman

spectroscopy[70] at 1681 cm^{-1}. A strong band was observed at 1699 cm^{-1}. However the origin of this band has not yet identified. The band does shift with ^{15}N substitution. Thus, it must be a N-atom vibration. From the UV-visible and infrared spectra insertion of "NO" is still successful.

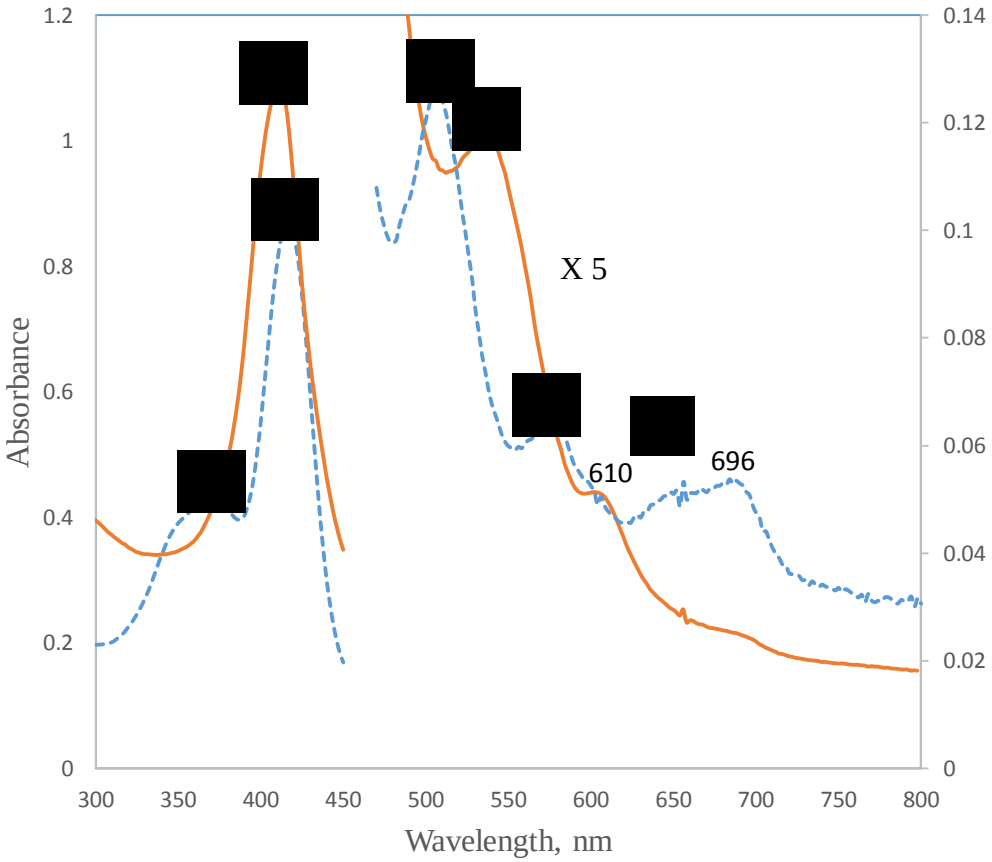

Figure 3-24. The UV-visible absorption spectra of Fe^{III}TPPCl (dash line) and Fe^{II}(TPP)(NO) (solid line) in THF solution

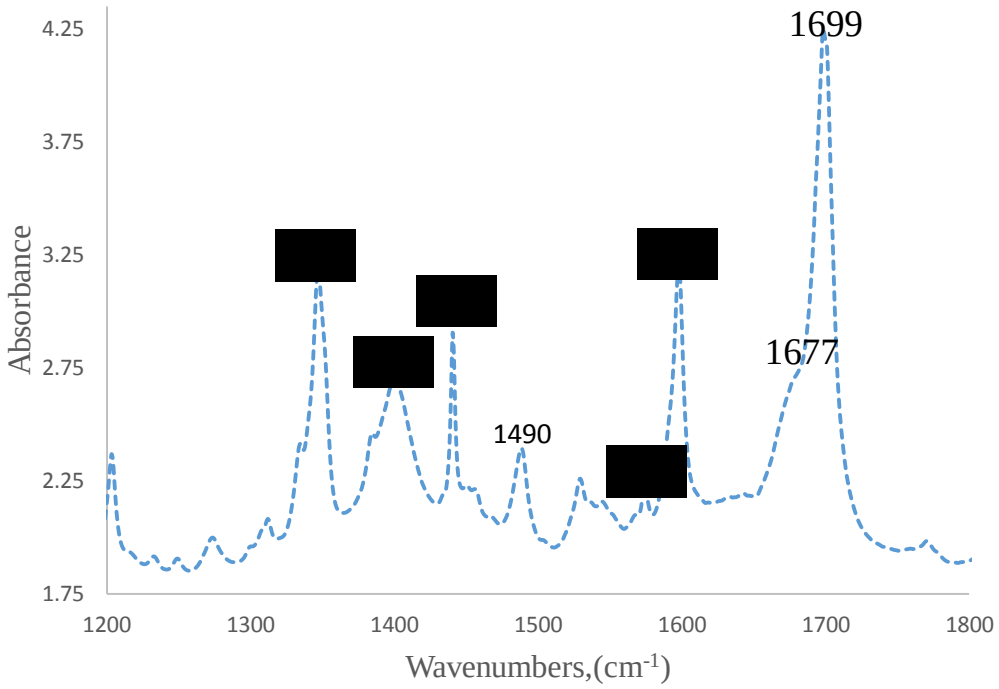

Figure 3-25. Infrared spectrum of the Fe^{II}(TPP)(NO) in KBr matrix

We synthesized ^{15}N isotopic labeled compound as Fe^{II}(TPP)(^{15}NO) with the ^{15}N hydroxyl amine hydrochloride. Upon isotopic substitution, υ_{NO} frequency shifted from 1677 cm^{-1} to 1649 cm^{-1}, which is significantly closer to literature value of 1645 $cm^{-1}$by Yoshimura[91] and 1647 cm^{-1} by resonance Raman spectroscopy[70]. In addition unknown intense band was observed at 1668 cm^{-1}. However this isotopic substitution did not give any changes in UV-visible spectrum. The shift in wave number of 28 cm^{-1} for υ_{NO} upon isotopic substitution of the nitrogen is within the range predicted on the basis of mass change. The infrared spectra of Fe^{II}(TPP)(NO) and Fe^{II}(TPP)(^{15}NO) are shown in Figure 3-26.

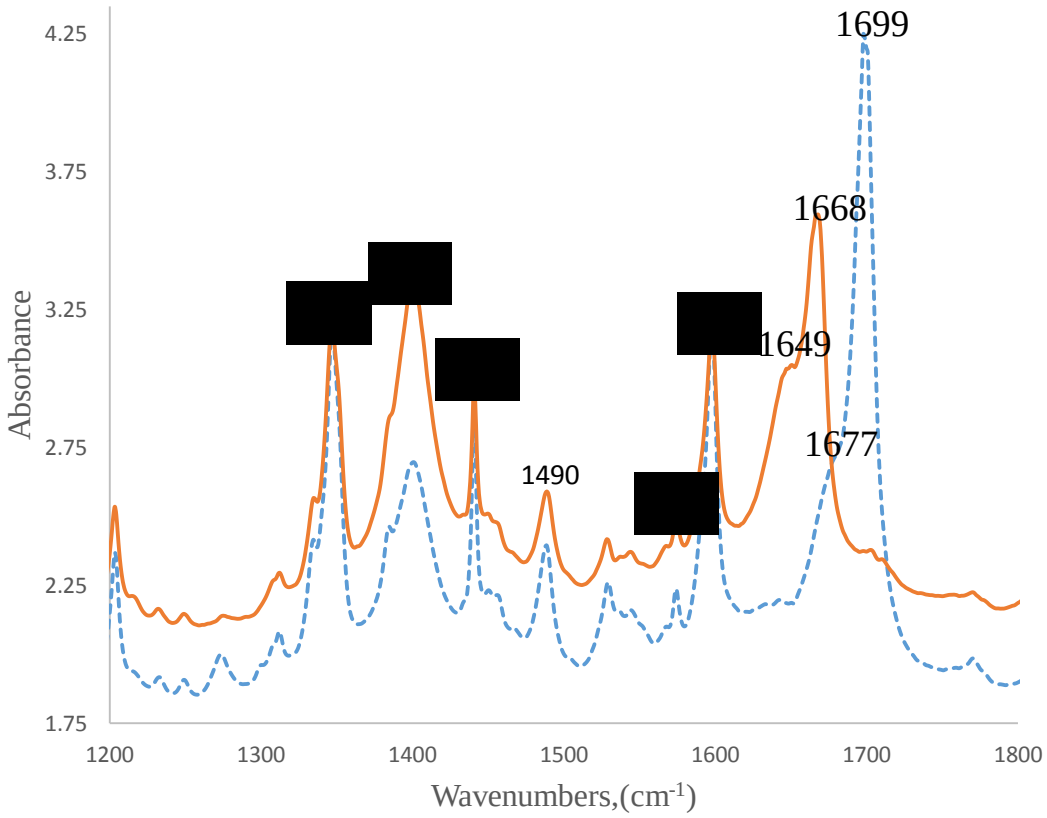

Figure 3-26. FTIR spectra of the $Fe^{II}TPP^{14}NO$ (dash line) and $Fe^{II}TPP^{15}NO$ (solid line) in KBr matrix

The UV-visible spectra of $Fe^{II}TPP^{14}NO$ and its one electron reduction product, $Fe^{II}(TPP)(NO)^{-}$ are shown in Figure 3-27. The absorption was compared to that obtained by Liu[70] who performed the reduction in spectroelectrochemistry and sodium anthracenide. The UV-visible spectral data were summarized in Table 3-23.

Table 3-23. The UV-visible spectral data of iron nitrosyl complexes

Compound	B bands (nm)	Q bands (nm)	Method	Reference
$Fe^{II}(TPP)(NO)$	414	538, 610		this work
$Fe^{II}(TPP)(NO)$	408	536, 607		70
$Fe^{II}(TPP)(NO)^{-}$	414	516, 618	$(TBA)(BH_4)$	this work
$Fe^{II}(TPP)(NO)^{-}$	408	516, 614	OTTLE	70
$Fe^{II}(TPP)(NO)^{-}$	406	513, 614	Na An	70

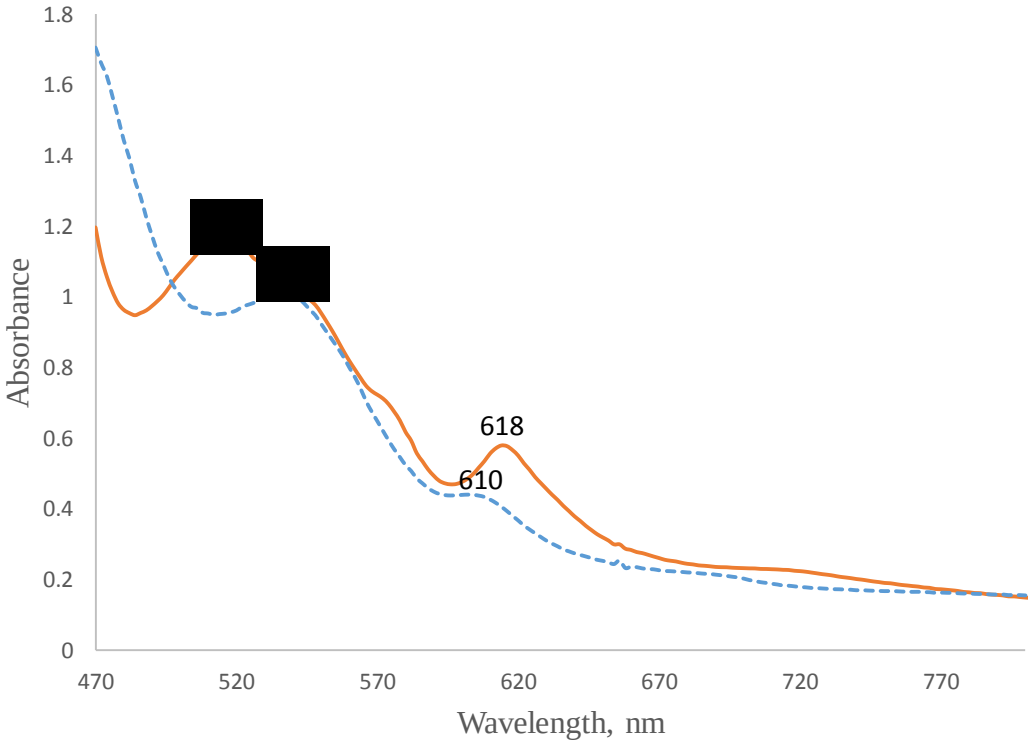

Figure 3-27. UV-visible spectra of $Fe^{II}(TPP)(NO)$ (dash line) and $Fe^{II}(TPP)(NO)^{-}$ (solid line) in THF solution

The first electron reduction of Fe^{II}(TPP)(NO) led the new bands that were appeared at 516 nm and 618 nm, while maintaining the consistency in the Soret region. These observations are compatible with previously reported data in spectroelectrochemistry[70]. These observations conclude the possibility of one electron reduction at the Fe-NO moiety, rather than at the porphyrin ring.

The infrared spectra of Fe^{II}(TPP)(NO) and its reduced product Fe^{II}(TPP)$(NO)^-$ are shown in Figure 3-28. Upon one electron reduction, υ_{NO}- (1488 cm^{-1}) and υ_{NO} (1677 cm^{-1}) bands were observed. This changing wave length by 189 cm^{-1} indicates the partial reduction of the υ_{NO} group, these results are qualitatively consistent with reduction occurred in spectroelectrochemical reduction and analyzed by resonance Raman spectroscopy[70] (decrease of 185 cm^{-1}). However in UV-visible spectrum the clear reduction of υ_{NO} to υ_{NO}^- was observed. This leads to contradiction between partial reduction and existence of borohydride at 1485 cm^{-1} in the system ($TBABH_4$ infrared frequencies are 1485, 1473, 1464, 1397 $cm^{-1}$and 1380 cm^{-1}).

The infrared spectra of Fe^{II}(TPP)(^{15}NO) and its one electron reduced product Fe^{II}(TPP)$(^{15}NO)^-$ are shown in Figure 3-29. Upon one electron reduction υ_{NO}- was observed at 1469 cm^{-1} (decrease of 180 cm^{-1}), which is significantly higher than with obtained in spectroelectrochemistry, and characterized by resonance Raman spectroscopy[70] (decrease of 172 cm^{-1}, from 1647 cm^{-1} to 1475 cm^{-1}). The reduced υ_{NO} frequency band was overlapped with borohydride band at 1464 cm^{-1}. From the UV-visible and infrared spectra the reduction of υ_{NO} to υ_{NO}- was observed. One electron reduction of Fe^{II}(TPP)(^{14}NO) and Fe^{II}(TPP)(^{15}NO), leads to disappearance of an unknown intense bands at 1699 cm^{-1} and 1668 cm^{-1}. From the studies on Fe(P)(NO) by

resonance Raman spectroscopy, the one electron reduction of Fe(P)(NO) generated a low-spin ferrous complex that led to a significant weakening of the NO bond.

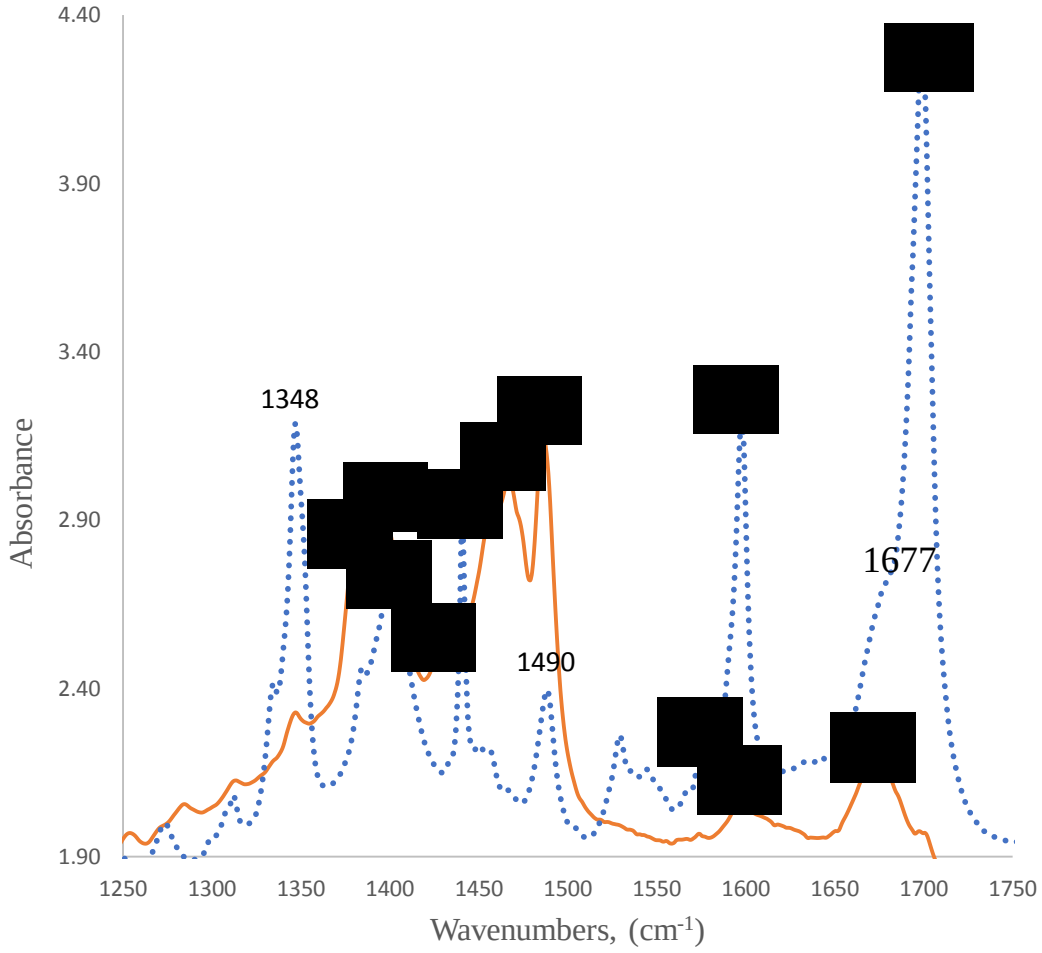

Figure 3-28. Infrared spectra of the Fe(TPP)(NO) (dash line) and reduction product $Fe(TPP)(NO)^-$ (solid line) in KBr matrix

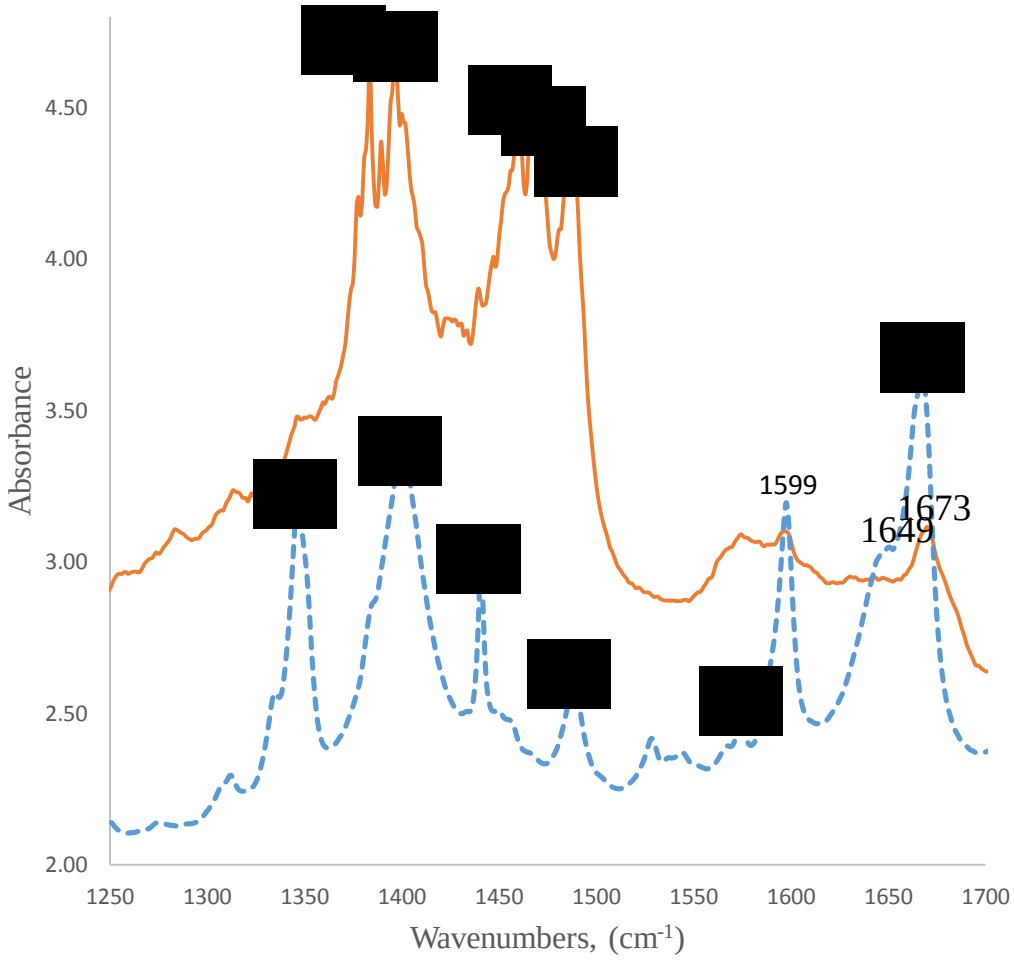

Figure 3-29. FTIR spectra of Fe(TPP)(^{15}NO) (dash line) and reduction product Fe(TPP)(^{15}NO)$^{-}$ (solid line) in KBr matrix

3-14. UV-visible and infrared spectra of iron octaethylporphyrin nitrosyl and their reduction products

The UV-visible spectra of the starting material Fe^{III}OEPCl and its nitrosyl product Fe^{II}(OEP)(NO) are shown in Figure 3-30. To better analyze the product that we obtained, we compared our UV-visible absorption peaks with what have been done by Kadish[85] in Table 3-24.

Table 3-24. The UV-visible spectral data of iron octaethylporphyrin nitrosyl complexes

Compound	B bands (nm)	Q bands (nm)	Solvent	Reference
Fe^{III}OEPCl	376	506, 534, 584, 638	THF	this work
Fe^{II}(OEP)(NO)	388, 478	528, 560	THF	this work
Fe^{II}(OEP)(NO)	389, 477	541, 555	THF	70
Fe^{II}(OEP)(NO)	394, 481	530, 552	PhCN	85

From the Table 3-24, we can see the UV-visible spectrum of the Fe^{II}(OEP)(NO) are consistent with that obtained by Liu[70] and Kadish[85]. Comparing the absorption spectrum of the starting material Fe^{III}OEPCl with the nitrosyl product Fe^{II}(OEP)(NO) that we obtained, the Soret band shifted from 376 nm to 388 nm and new small Soret band appeared at 478 nm, while in the Q band region bands at 528 nm and 560 nm appeared and bands at 506, 534, 584 and 638 nm disappeared. The ^{15}N isotopic substitution of Fe^{II}(OEP)(^{15}NO) has the same UV-visible spectra like Fe^{II}(OEP)(NO).

The FT-IR spectrum of the Fe^{II}(OEP)(NO) is shown in Figure 3-31. The υ_{NO} frequency value is 1663 cm^{-1}. This value is consistent with υ_{NO} frequency values of 1670 cm^{-1} obtained by Liu[85]. In Fe^{II}(OEP)(^{15}NO), the υ_{NO} band shifted to 1632 cm^{-1} upon isotopic substitution. Other bands were unchanged.

From the UV-visible absorption and infrared spectrum the insertion of '-NO' and isotopic labeling ^{15}N may be successful.

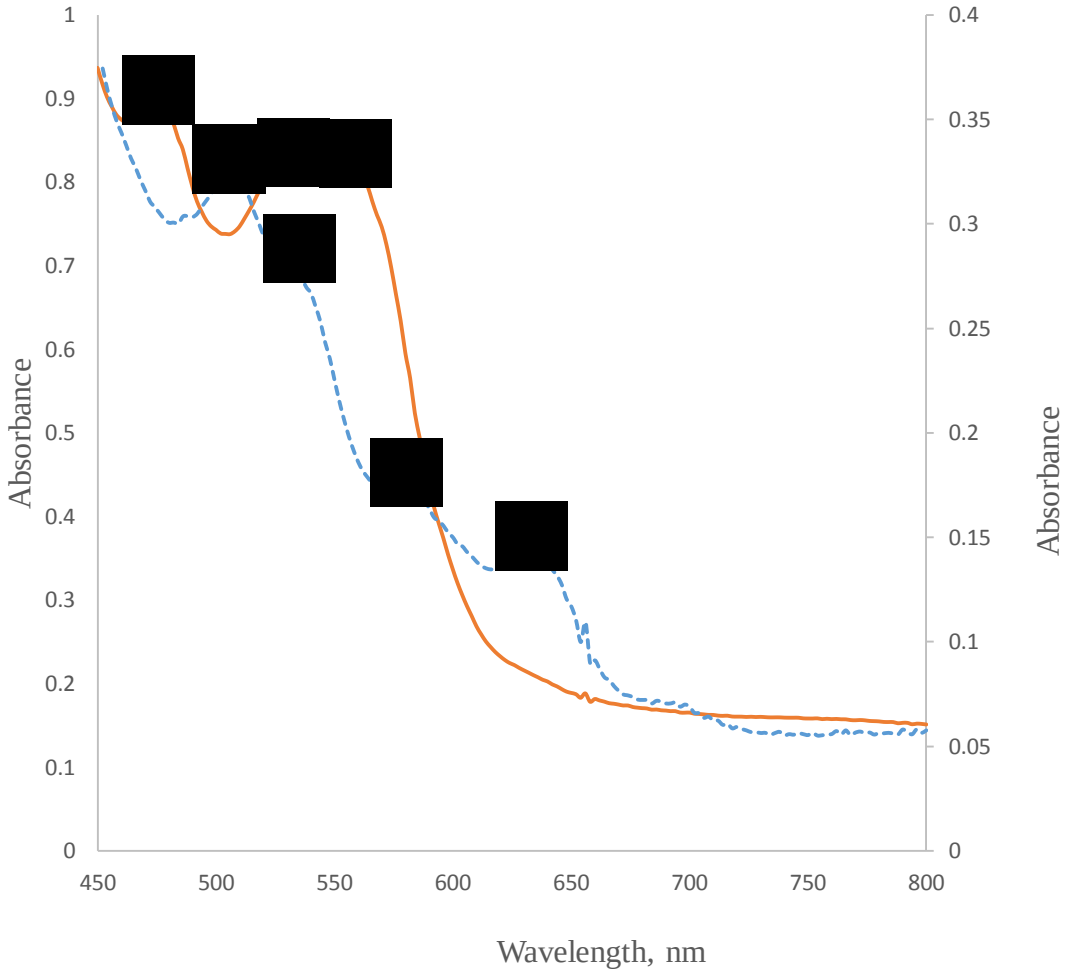

Figure 3-30. The UV-visible spectra of Fe^{III}OEPCl (dash line) and its nitrosyl product Fe^{II}(OEP)(NO) (solid line) in THF solution

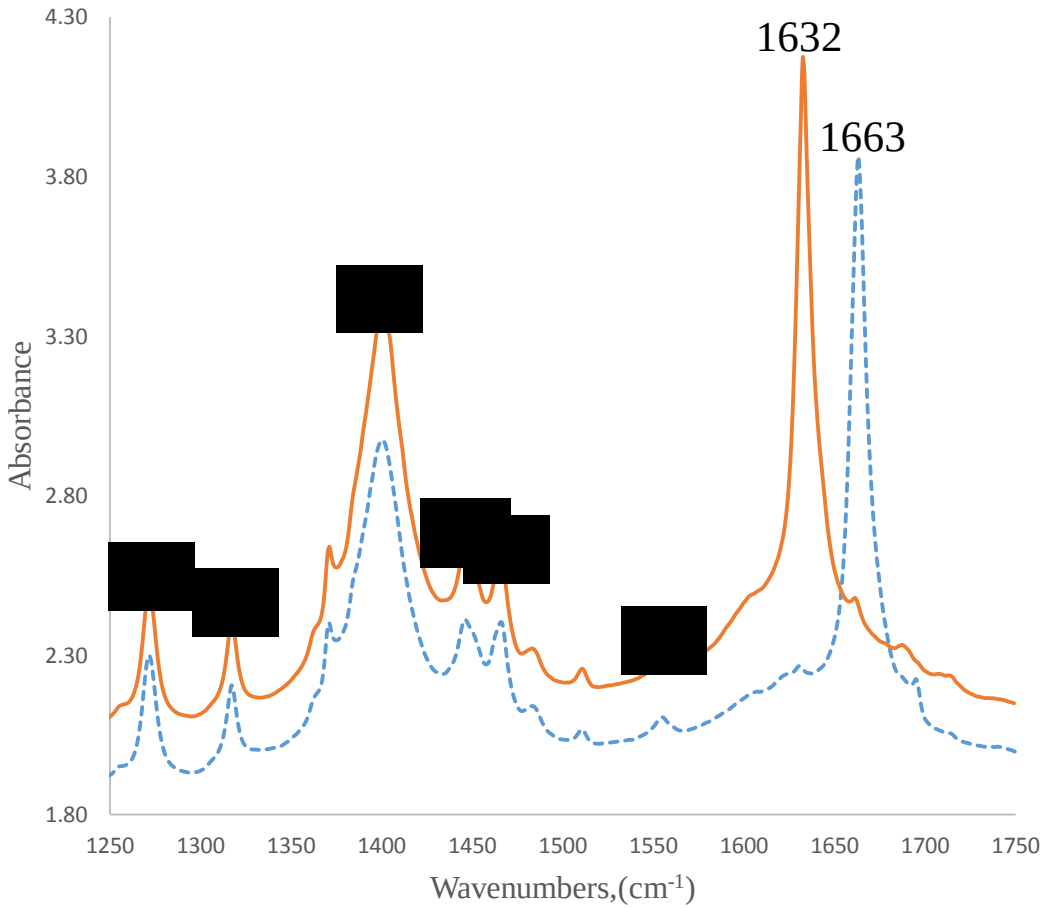

Figure 3-31. Infrared spectra of the $Fe^{II}(OEP)(^{14}NO)$ (dash line) and $Fe^{II}(OEP)(^{15}NO)$ (solid line) in KBr matrix

The UV-visible spectra of $Fe^{II}(OEP)(NO)$ and its one electron reduction product, $Fe^{II}(OEP)(NO)^-$ are shown in Figure 3-32. The absorption spectra were compared to that obtained by the reduction in spectroelectrochemistry[71]. The UV-visble spectra were summarized in Table 3-25. The one electron reduction of $Fe^{II}(OEP)(NO)$ led to a new band which appeared at 538 nm, while there was change in the Soret band region. The change in the Q band region and no change in observed in the Soret band with the addition of one electron suggest that the reduction occurs the Fe-NO moiety.

Table 3-25. The UV-visble spectral data of iron octaethylporphyrin nitrosyl complexes

Compound	B bands (nm)	Q bands (nm)	Solvent	Reference
Fe^{II}(OEP)(NO)	388, 478	528, 560	THF	this work
Fe^{II}(OEP)(NO)	389, 477	541, 555	THF	71
Fe^{II}(OEP)$(NO)^-$	388	538	THF	this work
Fe^{II}(OEP)$(NO)^-$	389	541	THF	71

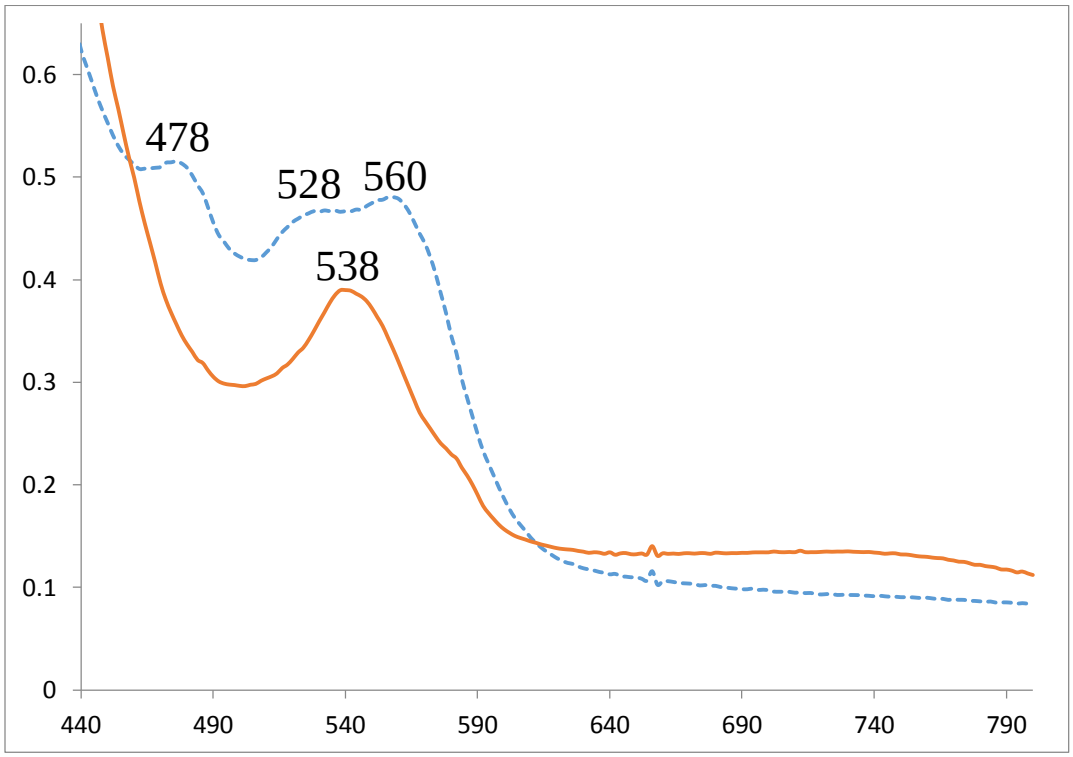

Figure 3-32: UV-Visible spectra of Fe(OEP)(NO) (dash line) and reduction product Fe(OEP)(NO^-) (solid line) in THF solution

3-15. Conclusion

From the X-ray crystal structure of $[Co^{I}TPP]^{-}$, the average distance between Co-Np is 1.951 Å. When they are compared with the known Ni(II) porphyrin structures, $(N\text{-}C_{\alpha})_{av}$ average bond distances of Co(I) porphyrin appears somewhat lengthened. These small changes are most probable due to enhanced-back donation of the electron- rich Co(I) center toward porphyrin π system. The infrared spectroscopy of Co-OEPone shows a red shift of in carbonyl band of 46 cm^{-1} which was slightly higher to the carbonyl shift recorded for Fe-OEPone (32 cm^{-1}). These shifts are thought to be due to a metal centered reduction. Therefore the carbonyl vibration was weakened due to increased electron density on the porphyrin ring caused by back-bonding from metal to porphyrin.

The UV-visible spectra for the one electron reduction for Mn(III)OEPCl, Mn(III)OEP($OClO_3$), Mn(III)TPPCl, Mn(III)TPP($OClO_3$) and Mn(III)(OEPone)Cl showed a shift from a split Soret band corresponding to a Mn(III) state to a normal Soret band in the Mn(II) form. This indicated that the electron transfer process occurred at the metal center. From the UV-visible spectra, the reduction of both Mn(III)OEPCl and Mn(III)OEP($OClO_3$) gave Mn(II)OEP complexes that were not coordinated with chloride or perchlorate ions. In Mn(III)TPPCl and Mn(III)TPP($OClO_3$) the one electron reduction gave $[Mn(II)TPPCl]^{-}$ and Mn(II)TPP correspondingly. The carbonyl frequencies for Mn(III)OEPoneCl is the highest energy for the Mn(III) complexes studied (1714 cm^{-1}). Addition of a d-electron (dπ-π back bonding) shifted the carbonyl frequencies to a lower energy. The observed shift was 15 cm^{-1} for Mn(III)/Mn(II) reduction (16 cm^{-1} for Fe(III)/Fe(II)). A decrease in energy of 15-16 cm^{-1} after addition of electron is an indication of a metal centered process.

From the UV-visible and infrared spectroscopy the synthesis of iron nitrosyl products of Fe^{II}(TPP)(NO), Fe^{II}(OEP)(NO) and isotopic labeling products Fe^{II}(TPP)(^{15}NO) and Fe^{II}(OEP)(^{15}NO) was successful. The reduction of iron tetraphenyl porphyrin nitrosyl compounds was carried out by using tetrabutylammonium borohydride as a reducing agents. The UV-visible and infrared spectroscopy indicated that the reduction had occurred. Attempts are being made obtain the X-ray crystal structure of Fe^{II}(TPP)$(NO)^-$, but X-ray quality crystals have not yet been obtained. Fe^{II}(OEP)NO reduction was carried out by using potassium anthracenide, attempts are being made to obtain solid precipitate of Fe^{II}(OEP)$(NO)^-$ for characterization by infrared spectroscopy and X-ray crystallography.

From this work we have determined the $TBABH_4$ can reduce Mn(III)TPPCl, Mn(III)OEPCl, Mn(III)(OEPone)Cl, Mn(III)TPP($OClO_3$), Mn(III)OEP($OClO_3$), Fe(II)(TPP)(NO), and Fe(II)(TPP)(^{15}NO) but not Fe(II)(OEP)(NO), and Fe(II)(OEP)(^{15}NO). The $E_{1/2}$ of these complexes are summarized in Table 3-26.

Table 3-26. $E_{1/2}$ potentials of the different metalloporphyrins

Complex	$E_{1/2}$(V)	Reduced by BH_4^-	$E_{1/2}$(V) Ref
Mn(III)(TPP)Cl	-0.23	Yes	89
Mn(III)(OEP)Cl	-0.347	Yes	41
Mn(III)(OEPone)Cl	-0.141	Yes	41
Mn(III)(TPP)($OClO_3$)	-0.12	Yes	89
Fe(II)(TPP)(NO)	-0.88	Yes	71
Fe(II)(OEP)(NO)	-1.07	No	90

Thus, we can estimate the redox potential of BH_4^- ranging between -0.88 V to -1.07 V. This can be compared to the reported E^o for BH_4^- (-1.24 V vs. NHE).

REFERENCES:

1. Milgrom, L. R., The colors of life: an introduction to the chemistry of porphyrins and related compounds; New York: Oxford University Press, **1997**, Chapter 1.

2. Jackson, A. H.; Dolphin, D.; "*The porphyrins*"; Academic Press, New York, **1978**, Vol.1, p. 374.

3. Malent'eva, T. A. *Russ. Chem. Rev*. **1983**, *52*, 641-661.

4. Doddrell, D.; Caughey, W. S. *J. Am. Chem. Soc.* **1972**, *94*, 2510-2512.

5. Licoccia, S.; Paolesse, R. *Struct. Bond*. **1995**, *84*, 71-134.

6. Harrison, P. J.; Fookes, C. J. R.; Battersby, A. R. *J. Chem. Soc. Chem. Comm*. **1981**, 797-799.

7. Chang, C.K.; Sotiriou, C. *J. Heterocycl. Chem.* ***1985****, 22*, 1739-1741.

8. Van Caemelbecke, E.; Will, S.; Aurtet, M.; Adamian, V. A.; Lex. J.; Gisselbrecht, J. –P.; Gross, M.; Vogel, E.; Kadish, K. M. *Inorg. Chem*. **1996**, *35*, 184-192.

9. Vogel, E.; Will, S.; Schulze Tilling, A.; Neumann, L.; Lex, J.; Trautwein, A. X.; Weighardt, K. *Angew. Chem., Int. Ed. Eng*. **1994**, *33*, 731-1735.

10. Sayer, P.; Gouterman, M.; Connell, C.R. *J. Am. Chem. Soc*. **1977**, *99*, 1082-1087.

11. Felton, R.H.*"*The Porphyrins*"*, Dolphin, D., Ed. Academic Press: New York **1978**, Vol. 5, pp 81.

12. Cocolios, P.; Kadish, K. M. *Isr. J. Chem*. **1985**, *25*, 138-147.

13. Salehi, A; Oertling, W. A.; Babcock, G. T.; Chang, C. K. *J. Am. Chem. Soc*. **1986**, *108*, 5630-5631.

14. Fuhrhop, J. H.; Mauzerall, D. *J. Am. Chem. Soc*. **1968**, *91*, 4174-4181.

15. Fuhrhop, J. H. *Struct. Bonding*, **1974**, *18*, 1-67.

16. Shiomura E. T.; Phillippi H. M. Goff; Scholz W. F.; Reed A. C. *J. Am. Chem. Soc*. **1981**, *103*, 6778-6780.

17. Felton, R. H.; Dolphin, D.; Borg D. C.; Fajer, J. *J. Am. Chem. Soc*., **1969,** *91*, 196-198.

18. Palmer, G. *"The Porphirins"*, Ed. Davis Dolphin, Vol 4, *Academic Press, New York*, **1978**, p-313-354.

19. Chang, C. K.; Hanson, L. K.; Richardson, P. F.; Young. Y.; Fajer, J. *Proc. Natl. Acad. Sci. U.S.A.* **1981**, *78*, 2652-2656.

20. Buchler, J. W. In *Porphyrins and Metalloporphyrins*; Smith, K. M., Ed.; Elsevier Scientific Publishing Co.: Amsterdam, 1975; pp 157-231.

21. Stolzenberg, A. M.; Stershic, M.T. *J. Am. Chem. Soc*. **1988**, *110*, 6391-6402.

22. Zhi-Li L.; Xiang-Qin, L. *Acta Chim. Sinica* **1993**, *51*, 1099-1105.

23. Richardson, P. F.; Cheng, C.K.; Hanson, L.K.; Spaulding, L. D.; Fajer, J. *J. Phy. Chem*. **1979**, *83*, 3420-3424.

24. Barkigia, K. M.; Fajer, J.; Spaulding, L.D.; Williams, G. J. B. *J. Am. Chem. Soc.* **1981**, *103*, 176-181.

25. Smith, E. L.; Mervyn, L.; Muggleton, P. W., Johnson, A. W.; Shaw, N. *Ann. N. Y. Acad. Sci.* **1964**, *112*, 565-574.

26. Wagner, G. C.; Gunsalus, IC.; Wang, M. Y. R.; Hoffman, B. H. *J. Biol. Chem*. **1981**, *256*, 6266-6273.

27. Whitlock, H. W.; Bower, K. B. *Tetrahedron Lett*. **1965**, *52*, 4827-4831.

28. Collat, J. W.; Abbott, J. C. *J. Am. Chem. Soc*. **1964**, *86*, 2308-2309.

29. Busch, D. H.; Weber, J. H.; Williams, D. H.; Rose, N. J. *J. Am. Chem. Soc*. **1964**, *86*, 5161-5162.

30. Kobayashi, H.; Hara, T.; Kaizu, Y. *Bull. Chem. Soc. Jpn*. **1972**, *45*, 2148-2155.

31. Doppelt, P.; Fischer, J.; Weiss, R. *Inorg. Chem*. **1984**, *23*, 2958-2962.

32. Calvin, M. *Pure Appl. Chem*. **1965**, *15*, 1-19.

33. Clarke, D. A,; Dolphin, D.; Grigg, R.; Johnson, A. W.; Pinnock, H. A. *J. Chem. Soc*. **1968**, 881-885.

34. Cullen, D. L.; Meyer, E. F. *J. Am. Chem. Soc*. **1974**, *96*, 2095-2102.

35. Collins, D. M.; Hoard, J. L. *J. Am. Chem. Soc.* **1970**, *92*, 3761-3771.

36. Tutunea, F.; Ryan, M. D. *J. Electroanal. Chem*. **2012**, *670*, 16-22.

37. Wei, Zhongcheng. PhD thesis, Marquette University, **1998**.

38. Chang. C. K.; Sotiriou, C. *J. Org. Chem*. **1987**, *52*, 926-929.

39. Arraullo, C.; Kadish, K. M. *Inorg. Chem*. **1990**, *29*, 2749-2757.

40. Wei, Z.; Ryan, M. D. *Inorg. Chem*. **2010,** *49*, 6948-6954.

41. Tutunea, Florentina. PhD thesis, Marquette University, **2012**.

42. Kadish, K. M.; Kelly, S. *Inorg. Chem*. **1979**, *18*, 2968-2971.

43. Boucher, L. J. *J. Am. Chem. Soc*. **1970**, *92*, 2725-2730.

44. Zaleski, J. *J. Physiol. Chem*. **1904**, *43*, 11-17.

45. Taylor, J. F. *J. Biol. Chem*. **1940**, *135*, 569-595.

46. Boucher, L.J. *J. Am. Chem. Soc*.**1970**, *90*, 6640-6645.

47. Fuhrhop, J. H.; Kadish, K. M.; Davis, D. G. *J. Am. Chem. Soc*. **1973**, *95*, 5140-5147.

48. Morehouse, K.M.; Neta, P. *J. Phys. Chem*. **1984**, *88*, 1575-1579.

49. Vanatta, R. B.; Strouse, C. E.; Hanson, L.K.; Valentine, J. S. *J. Am. Chem. Soc*. **1987**, *109*, 1425-1434.

50. Kirner, J. F.; Reed. C. A.; Scheidt, W. R. *J. Am. Chem. Soc*. **1977**, *99*, 2557-2563.

51. Tulinsky, A.; Chen, B. M. L. *J. Am. Chem. Soc*. **1977**, *99*, 3647-3651.

52. Anderson, O. P.; Lavallee, D.K. *Inorg. Chem*. **1977**, *16*, 1634-1639.

53. Tagliateste, P.; Li, J.; Autret, M.; Van Caemelbecke, E.; Villard, A.; D'Souza, F.; Kadish, K. M. *Inorg. Chem*. **1996**, *35*, 5570.

54. Donohoe, R. J.; Atamian, M.; Bocian, D. F. *J. Am. Chem. Soc*. **1987**, *109*, 5593-5599.

55. Ozaki, Y.; Iriyama, K.; Ogoshi, H.; Ochiai, T.; Kitagawa, T. *J. Phy. Chem*. **1986**, *90*, 6105-6112.

56. Ozaki, Y.; Iriyama, K.; Ogoshi, H.; Ochiai, T.; Kitagawa, T. *J. Phy. Chem*. **1986**, *90*, 6113-6118.

57. Stlozenberg, A. M.; Strauss, S. H.; Holm, R. H. *J. Am. Chem. Soc*. **1981**, *103*, 4763-4778.

58. Strauss, S. H.; Holm, R. H. *Inorg. Chem*. **1982**, *21*, 863-868.

59. Hickman, D. L.; Shirazi, A.; Goff, H. M. *Inorg. Chem*. **1985**, *24*, 563-566.

60. Mashiko, T.; Reed, C. A.; Haller, K. J.; Scheidt, W. R. *Inorg. Chem*. **1984**, *23*, 3192-3196.

61. Reed, C. A. *Adv. Chem. Ser*. **1982**, *201*, 333-356.

62. Cole, J. A.; Ferguson, S. J. The Nitrogen and Sulfur Cycles, 42nd Symp. Society for General Microbiology, New York, Cambridge University Press, Cambridge, UK, **1988**.

63. Fewson, C. A.; Nicholas, D. J. *Nature*, **1961**, *190*, 2-7.

64. Christner, J. A.; Janick, P. A.; Seigel, L. M. E. *J. Biol. Chem*. **1983**, *258*, 11157-11164.

65. Liu, Y.; Ryan, M. D. *Inorg. Chim. Acta*. **1994**, *225*, 57-66.

66. Garber, E. A.; Hollocher, T. C. *J. Biol. Chem*. **1981**, *256*, 5459-5465.

67. Fujita, E.; Faler, J. *J. Am. Chem. Soc*. **1983**, *105*, 6743-6745.

68. Scheidt, W. R.; Frissse, M. E.; *J. Am. Chem. Soc*. **1975**, *97*, 17-21.

69. Olson, L.W.; Schaeper, D.; Lanson, D.; Kadish, K. M. *J. Am. Chem. Soc*. **1982**, *104*, 2042-2044.

70. Choi, I.; Liu, Y.; Ryan, M. D. *Inorg. Chem*. **1991**, *30*, 1832-1839.

71. Liu, Yanming. PhD thesis, Marquette University, **1991**.

72. Chneg, B.; Cukiernik, F.; Fries, H. P.; Marchon, J. C.; Scheidt, W. R. *Inorg. Chem*. **1995**, *34*, 4627-4639.

73. Collman, J.P.; Sorrell, T. N.; Dawson, J. H, Trudell, J. R.; Jerassi, C. D. *Proc. Nat. Acad. Sci. USA*. **1976**, *73*, 6-10.

74. Choi, I.; Liu, Y.; Ryan, M. D. *Inorg. Chem*. **1997**, *36*, 3113-3118.

75. Doppelt, P.; Fischer, J.; Weiss, R. *J. Am. Chem. Soc*. **1984**, *106*, 5188-5193.

76. Moras, D.; Weiss. R. *Acta Crystallogr., Sect. B; Struct. Crystallogr. Cryst. Chem.* **1973**, *29*, 396-399.

77. Scheidt, W. R. *J. Am. Chem. Soc*. **1974**, *96*, 84-89.

78. Stevens, E. D. *J. Am. Chem. Soc*. **1981**, *103*, 5087-5095.

79. Radonovich, L. j.; Bllom, A.; Hoard, J. L. *J. Am. Chem. Soc*. **1972**, *94*, 2073-2078.

80. Edwards, L.; Dolphin, D. H. *J. Mol. Spectrosc*. **1970**, *35*, 90-109.

81. Falk, J. E.; "Porphyrins and Metalloporphyrins" *Elsevier, New York, N. Y.*, **1964**.

82. Hoard, J. L.; Cohen, G. H.; Glick, M. D. *J. Am. Chem. Soc*. **1967**, *89*, 1992-1996.

83. Mu, H. X.; Schultz, F. A. *Inorg. Chem*. **1995**, *34*, 3835-3837.

84. Scheidt, W. R.; Hotano, K.; Rupprecht, G. A.; Piciulo, P. L. *Inorg. Chem.* ***1979***, *18*, 292-299.

85. Lancon, D.; Kadish, K. M. *J. Am. Chem. Soc*. **1983**, *105*, 5610-5617.

86. Closs, G. L.; Closs, L. E. *J. Am. Chem. Soc*. **1963**, *85*, 818-819.

87. Liu, Y.; DeSilva, C.; Ryan, M. D. *Inorg. Chim. Acta.* **1997**, *258*, 247-255.

88. Arnold, D. P.; Heath, G. A.; James, D. A. *New. J. Chem*. **1998**, *22*, 1377-1387.

89. Kelly, S. L.; Kadish, K. M. *Inorg. Chem.* **1982**, *21*, 3631-3639.

90. Lorenz, C. R.; Dewald, H. D.; Lemke, F. R. *J. Electroanal. Chem*. **1996**, *415*, 179-181.

91. Yoshimura, T. *Inorg. Chim. Acta.* **1984**, *83*, 17-21.